Universitetet i Stavanger

FACULTY OF SCIENCE AND TECHNOLOGY

MASTER'S THESIS

Study programme/specialisation: Offshore Technology- Marine and Subsea Technology	Spring semester, 2017 Open access
Author: Andrzej Koziel	…… (signature of author)
Programme coordinator: Professor Ove Tobias Gudmestad Supervisor(s): Professor Sverre Kristian Haver	
Title of master's thesis: **Assessing wave conditions in a Norwegian fjord**	
Credits: 30	
Keywords: SWAN, coastal waters, fjord conditions,	Number of pages: 93 Stavanger 13th of June 2017

Abstract

The focus of this thesis is to obtain an estimate of the significant wave height together with the corresponding peak period for the proposed bridge locations at Bjørnafjord. The task was conducted by modelling and calculations done in SWAN software. The methodology for transforming the NORA10 hindcast data into the design wave conditions for the 10^{-2} and 10^{-4} probability of exceedance was introduced for an offshore location. Furthermore a short description for the methods of transforming the metocean conditions to the fjord position were presented.

The theory on the different wave generation and dissipation mechanisms present in the coastal waters was described. The description introduced the influence of those physical phenomena on the wave spectrum. The implementation of the dissipation mechanisms in SWAN was described with respect to the models produced for this thesis.

As an introduction to modelling in the SWAN, the test case model analysis based on the master thesis by Engbretsen (2012) was performed.

Furthermore a series of simplified idealized models was prepared. The models are reflecting the real bathymetry features found in the Bjørnafjord and are the basis for the analysis of the fjord. The cases were modelled to consider the influence of the bottom topography on the wave field. A number of sensitivity studies was executed to investigate the influence of the different coastal effects on the total sea characteristics.

Finally the Bjørnafjord wave model was created. Real bathymetry data was modelled based on the maps acquired from Kystverket. The inputs in regard to the wind and incoming wave conditions were based on the reports by SINTEFF - Stefanakos (2015) and NORCONSULT - Lothe (2015). A number of cases with different environmental conditions was analysed. Sensitivity study in regard to the dominating dissipation mechanisms was conducted. The obtained results were compared with the analyses done in the source reports of Stefanakos and Lothe.

Acknowledgement

My sincere gratitude goes to my project supervisor, Professor Sverre K. Haver, at the University of Stavanger, Norway, for his continual support and guidance.

Scope of work

MSc thesis 2017

Title: **Assessing wave conditions in a Norwegian fjord**

Student: **Andrzej Koziel**

The Norwegian Road Directorate aiming for a ferry – free highway from Stavanger to Trondheim. Such a highway will involve a number of fjord crossings. The primary solution for a ferry free fjord crossing is a tunnel under the fjord. For some fjords such a solution will not be the preferred solution due to the water depth at the crossing location. For such cases a bridge is to be preferred. If the width of the fjord is large a floating bridge solution may well be the preferred solution. As a consequence, wind and wave conditions at the bridge crossing location are needed.

The focus of this thesis is to discuss how wave conditions at target location can be established. This includes the locally generated wind sea and the long period ocean waves that propagated into the fjord. Furthermore, focus should be on relative importance of the various physical mechanisms regarding their impact on estimated wave conditions at target site.

Here we shall assume that the bridge will be designed similarly as offshore structures i.e. a limit state based design. This means we need to know the met-ocean conditions sufficient well to estimate characteristic loads corresponding to annual exceedance probabilities of 10^{-2} (ULS) and 10^{-4} (ALS), respectively. Met-ocean conditions should also be sufficient for possible estimating fatigue damage due to weather variability.

The necessary offshore met-ocean information will be given by the Norwegian hindcast data base, NORA10, giving weather characteristics every 3 hours from 1957 – 2014. In connection with this thesis, offshore wave conditions can be adopted from the master thesis prepared by Juliet Ebiose Ngbeken. Regarding local wind conditions, we may get some measurements from the Road Directorate or from the Norwegian Meteorological Institute.

As mentioned above, focus should be to understand and discuss the various physical mechanisms affecting the estimated wave conditions at target site. For this purpose, SWAN can be applied to an idealized fjord geometry.

Below is a possible division into sub-tasks. The candidate may well deviate from this if another schedule is found more convenient.

1. As an extended introduction to the MSc thesis, describe the work that needs to be done in order to present metocean design condition in a fjord – accounting both for local wind sea and

incoming offshore sea conditions.

2. The local wind sea shall be calculated using SWAN. At first, make yourself familiar with SWAN and do a validation of your familiarity by repeating: i) The model test case and ii) The Doggerbank case presented in the MSc of Espen Engebretsen. Verify that you obtain the same results as in that thesis. Do some sensitivity analysis for the Doggerbank case. What happen with increasing wind speed? What happen if bottom slope is reduced?

3. Introduce an idealized fjord geometry and investigate the relative importance of the physical mechanisms modelled by SWAN for various idealized fjord geometries. Discuss the results and comment on the relevance for real fjord case. This point is considered a very important part of the thesis.

4. Introduce realistic bottom topography for the fjord east of the bridge position. Calculate the wave field corresponding to a mean wind speed from east of 20m/s, 25m/s 30m/s and 35m/s. Present wave spectra at various positions and give corresponding significant wave height and spectral peak period. Do sensitivity studies which you consider important in view of point 3).

5. Specify offshore design wave conditions based on some reference. Discuss how can we estimate the corresponding conditions at fjord locations – including local wind effects and incoming swell. Discuss options and select your preferred approach. Use SWAN to transform open sea conditions to various positions along the fjord for 10^{-2} – and 10^{-4} – annual probability offshore sea conditions. Run at least one case with and without wind to investigate if wind input will affect the energy on long period peak periods.

6. Summarize your main findings in a conclusion chapter. Recommend further work based on your experience.

The candidate may of course select another scheme as the preferred approach for solving the requested problem.

The work may show to be more extensive than anticipated. Some topics may therefore be left out after discussion with the supervisor without any negative influence on the grading.

The candidate should in his report give a personal contribution to the solution of the problem formulated in this text. All assumptions and conclusions must be supported by mathematical models and/or references to physical effects in a logical manner. The candidate should apply all available sources to find relevant literature and information on the actual problem.

The report should be well organised and give a clear presentation of the work and all conclusions. It is important that the text is well written and that tables and figures are used to support the verbal presentation. The report should be complete, but still as short as possible.

The final report must contain this text, an acknowledgement, summary, main body, conclusions, suggestions for further work, symbol list, references and appendices. All figures, tables and equations

must be identified by numbers. References should be given by author and year in the text, and presented alphabetically in the reference list. The report must be submitted in two copies unless otherwise has been agreed with the supervisor.

The supervisor may require that the candidate should give a written plan that describes the progress of the work after having received this text. The plan may contain a table of content for the report and also assumed use of computer resources. As an indication such a plan should be available by early April.

From the report it should be possible to identify the work carried out by the candidate and what has been found in the available literature. It is important to give references to the original source for theories and experimental results.

The report must be signed by the candidate, include this text, appear as a paperback, and - if needed - have a separate enclosure (binder, diskette or CD-ROM) with additional material.

Supervisor: Sverre Haver, UIS.

Content

List of figures

List of tables

List of symbols

c_g	Wave group velocity
d	Water depth
f	Frequency
$f(x)$	Probability density function of stochastic variable x
g	Acceleration of gravity
h_0	Threshold level for the POT method
k	Wave number
m	Number of years
n	Spreading coefficient
$D(\theta)$	Directional function
E	Energy
$F(x)$	Cumulative probability distribution function of stochastic variable x
H	Wave height
H_{m0}	Significant wave height obtained from spectrum
H_s	Significant wave height obtained from time series
K_{ref}	Refraction coefficient
K_{sh}	Shoaling coefficient
L	Wave length
$N(\sigma, \theta)$	Action density Spectrum
$S(\omega)$	Wave spectral density
$S_{in}(f, \theta)$	Energy transfer
T	Period
T_p	Spectral peak period
Q_B	Fraction of breaking waves
α	Scale Weibull parameter
β	Shape Weibull parameter
λ	Longitude or wave length
φ	Latitude
ξ	Iribarren number
Φ	Standard normal cumulative distribution finction

List of abbreviations

SWAN	Simulating WAves Nearshore
ALS	Accidental Limit State
ULS	Ultimate Limit State
FLS	Fatigue Limit State
JONSWAP	Joint North Sea Wave Project
2D	Two dimensional
STWAVE	Steady State spectral Wave
POT	Peak Over Threshold
NORA10	Norwegian ReAnalysis 10km

1 Introduction

1.1 Background

The Norwegian public Roads Administration in years 2017- 2033 is developing a ferry-free route connection between Trondheim and Kristiansand. The goal of the project is to stream traffic, decreas the travel time between major cities and provide further development of the coastal area through better logistic connections. The existing motorway is divided by eight ferry crossing which are planned to be replaced by tunnels or bridges. Although the proposed crossings cover 37km of the roughly 1000km of the total length of the described E39 motorway section, the engineering challenges connected to the development provide a need for extensive research.

Figure 1-1 The E39 ferry-free motorway project. Vegdirektoratet (2015).

The fjords in question are characterized by unique topography features – large depth varying from 450m to 1250m, span of the single crossing varying from 2 to 9 km and steep shores. The following features combined with severe environmental conditions require numerous studies to be conducted in connection to the technical solutions and loading estimates.

There possible bridges technology considered for the fjord crossings are suspension bridge, floating bridge and the submerged tube bridge. The technology solutions for different types differ greatly in terms of execution costs, experience with the construction and the overall difficulty of the construction process. The suspension bridge is the most worldwide technical developed solution of the proposed set.

The bridge construction composes of the deck, pillars and the suspension cables. The deck of the bridge is suspended on cablese connected to the grirders anchored to the bridge pillars. The loading is transferred mainly by the cables witch permits small cross-sections of the bridge deck. The solution is particularly sensitive to wind loading and harmonic resonance.

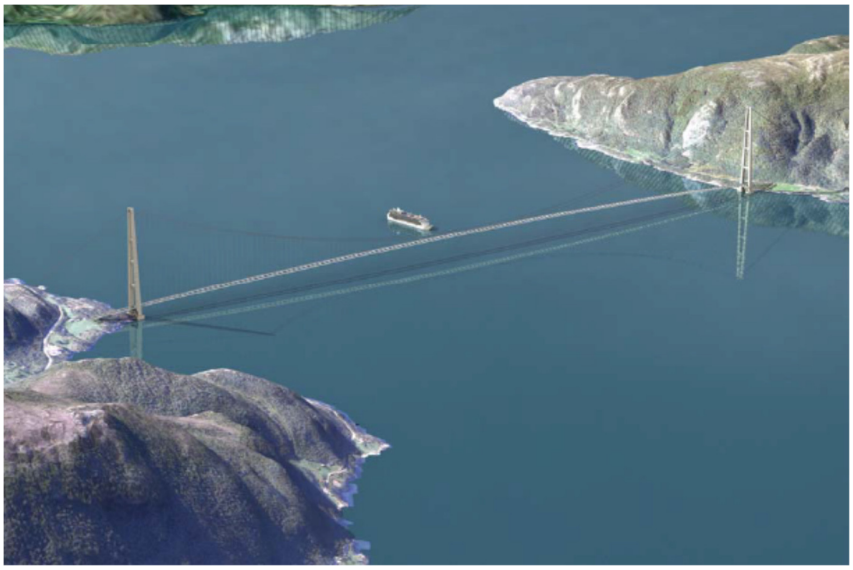

Figure 1-2 Suspension bridge. Ellevset (2011).

The floating bridge construction is based on a series of concrete pontoons, floating on the water surface, which transfer the vertical loading of the deck The horizontal forces are accommodated by the stiffness of the combined deck and pontoon cross-sections. The arched shape of the pontoon bridges proposed provide better accommodation to the wind and wave loads in deep water (loading is relatively lower near the shore due to refraction and water depth).

Figure 1-3 An existing floating bridge: the Nordhordlandsbru near Bergen. The nearest span constructed as a suspended bridge to enable ship traffic. Ellevset (2011).

The submerged floating bridge is based on a concept of buoyancy tunnels bellow the water line. The solution is executed with closed metal or concrete tubes which positive (combination of tube and bottom anchoring lines) or negative buoyancy (combination of the tube and pontoons). The solution provides lower environmental loading than in the pontoon bridge case but requires more studies with concerned to the safety of the construction and the tunnel travellers The submerged bridge is a relatively new technology which still requires extensive research.

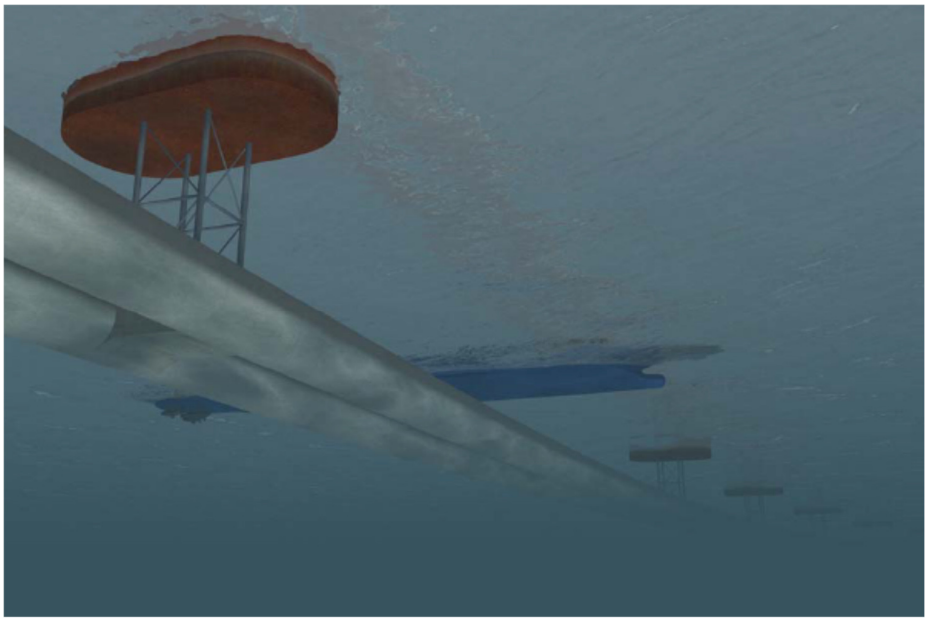

Figure 1-4 Submerged floating pipe bridge with negative buoyancy. Ellevset (2011)

Due to the necessity of providing an open traffic route for ship based transport for most of the fjords a combination of proposed solution can be a viable solution (ref **Figure 1-3**). The complexity of designing such a bridge will expand the time needed for engineering work.

Each bridge structure needs to be designed in the consideration to the Norwegian Standard building codes and NORSOK. Both standards adopt the limit state design approach in respect of the design environmental loading. Investigations of the wind, wave and current at the crossing location need to be conducted. The dominant loading in the fjord will be the result of surface waves from the local generated wind sea and the incoming ocean swells. The design wave conditions need to be established for the ultimate limit state (ULS) and the accidental limit state (ALS) cases.

Further investigation of the frequency of the incoming waves need to be conducted for establishing the risk of resonance induced loading in the structure. The local wind generates waves with the spectrum peak near the first order eigen frequency of the long span bridges. The swells provide waves higher peak frequency spectra which can correspond to the other eigen frequency modes. The proper analysis of the wave statistics data is also necessary for obtaining an accurate estimate of the structure's life span and the fatigue limit state (FLS).

The long term observations of wave and wind are conducted in the North Sea. The data gathered for a number of offshore locations provides the best base for the environmental loads estimation. The wave loading data in the coastal area, and especially in the fjords is rarely gathered or the time span for the observations is significantly shorter. The loads at the crossing positions need to be calculated based on the offshore data adopting proper transformation models that include the near shore effects.

1.2 Objectives

The main objective of the thesis is to obtain an estimate for the design wave conditions at the position for planned Bjørnafjord crossings. The wave conditions will provide basic input for the further concept and limit state structure design of the bridge.

The thesis will describe the process for estimating the met-ocean wave conditions based on the hindcast data, measured at the position outside of the fjord. The report will consider also the possible method of converting the obtained swell wave and wind conditions into met-ocean conditions in the position of the fjord crossing.

An introduction to the SWAN (Simulating WAves Nearshore) wave modelling will be conducted by recreating the model from the master thesis by Engebretsen (2012). The purpose of this exercise is to validate the knowledge of SWAN program as well as to set a base for the further investigation on the effects of different bathymetry.

Furthermore sensitivity analysis of the idealized fjord models will be conducted in SWAN program in the terms of the importance of various physical processes accompanying near shore, complex bathymetry conditions.

Finally the analysis of the Bjørnafjord SWAN model was conducted in the light of findings obtained during the sensitivity analysis of the idealized cases. The conditions at the position of the planned fjord crossing will be calculated based on the input provided by SINTEF, Stefanakos (2015), NORCONSULT, Lothe (2015) and the bathymetry based on the data from Kartverket.

2 Methodology for determining the 50-year sea state- input for further analysis with SWAN.

2.1 Gathered data.

For proper structural design of structures exposed to ocean loading a design wave condition has to be established. The estimation of the parameters is based on the measured data. Hindcast data of the significant wave height, corresponding spectral period and the accompanying wind conditions is available for the north sea. The NORA 10 database contain data gathered from 1st September 1957 is provided by the Norwegian meteorological institute. The dataset records observation with a 3 hour interval. The available data contains wind direction, wind speed, significant wave height and peak period of the total sea.

2.2 Estimation of the cumulative distribution.

The hindcast data is transformed into a probability distribution of the wave parameters. Two basic approaches are advised for calculating the distribution for design wave height DNV (2014):

-global model approach (initial distribution method)– utilizes all measured data from long series of subsequent observations.

-event model – utilizes only the observations chosen from the total data set that exceed some threshold level. The Peak Over Threshold (POT) or the storm analysis method can be used for the event model analysis.

The global model approach is preferred for obtaining sea parameters for locations where sever weather conditions are dominant in the long term approach. This methods allows better fitting of the tail behaviour for the calculated spectra as it utilizes more data. The event model provides good estimation of the wave distribution for areas with calm seas, where there might be only a few severe events.

The global model approach introduces, unless the data indicates otherwise, a 3-parameter Weibull initial distribution to be assumed as the marginal significant wave height distribution:

$$F_{H_s}(h) = 1 - \exp\left[-\left(\frac{h-\gamma}{\alpha}\right)^{\beta}\right] \quad (2\text{-}1)$$

where

α is the scale parameter,

β is the shape parameter and

γ is the location parameter.

The event model Peak Over Threshold approach uses a 2-parameter Weibull or an exponential distribution with the form of:

$$F_{H_s}(h) = -exp\left\{-\frac{h-h_0}{\theta}\right\} \quad (2\text{-}2)$$

where $\theta = E[H - h_0]$ and h_0 is the chosen threshold for the measured wave heights.

The POT model should be compared with a different approach for obtaining the distribution, because of the methods sensitivity to the chosen threshold value.

The 3 distributions mentioned above are usually fitted as set of extreme waves using various methods. The most common used are: the method of moments (MOM), the least square method (LS), the maximum likelihood methods (MLE).

2.3 The environmental contour concept

The environmental contour concept represents a rational procedure for defining an extreme sea state condition DNV (2014). The goal of the method is to obtain the H_{m0} and T_p parameters corresponding to m-year probability of return. The initial step for this method is to obtain a joint probability density function for H_{m0} and T_p:

$$f_{H_{m0}T_p}(H_{m0}, T_p) = f_{H_{m0}}(H_{m0}) f_{T_p|H_{m0}}(T_p|H_{m0}) \quad (2\text{-}3)$$

and transform it into a standard normalized U-space:

$$\Phi(u_1) = F_{H_s}(h_s) \quad (2\text{-}4)$$

$$\Phi(u_2) = F_{T_z|H_s}(t_z) \quad (2\text{-}5)$$

where Φ is the standard normal cumulative distribution function. In such proposed space the contours of constant probability of return lie on a circle defined by value β equal:

$$\sqrt{{u_1}^2 + {u_2}^2} = \beta = -\Phi^{-1}\left(\frac{1}{N_m}\right) \quad (2\text{-}6)$$

where

$$u_1 = \Phi^{-1}\left(F_{H_{m0}}(H_{m_0})\right) \quad (2\text{-}7)$$

$$u_2 = \Phi^{-1}\left(F_{T_p|H_{m0}}(T_p|H_{m0})\right) \quad (2\text{-}8)$$

and N_m is the estimated number of sea states durin m years. It is given by:

$$N_m = \frac{n_{obs} \cdot m[years]}{m_{obs}[years]} \quad (2\text{-}9)$$

where

n_{obs} is the number of observed sea states in the specified direction,

m_{obs} is the number of years data has been gathered for.

After transforming the contour line of constant probability of return from the Gaussian space to the physical space we obtain the following expressions:

$$H_{m0} = {F^{-1}}_{H_{m0}}(\Phi(u_1)) \quad (2\text{-}10)$$

$$T_p = {F^{-1}}_{T_p|H_{m0}}(\Phi(u_2)) \quad (2\text{-}11)$$

By plotting the corresponding values we obtain the m-year sea state parameters - they are determined from the peak of the contour.

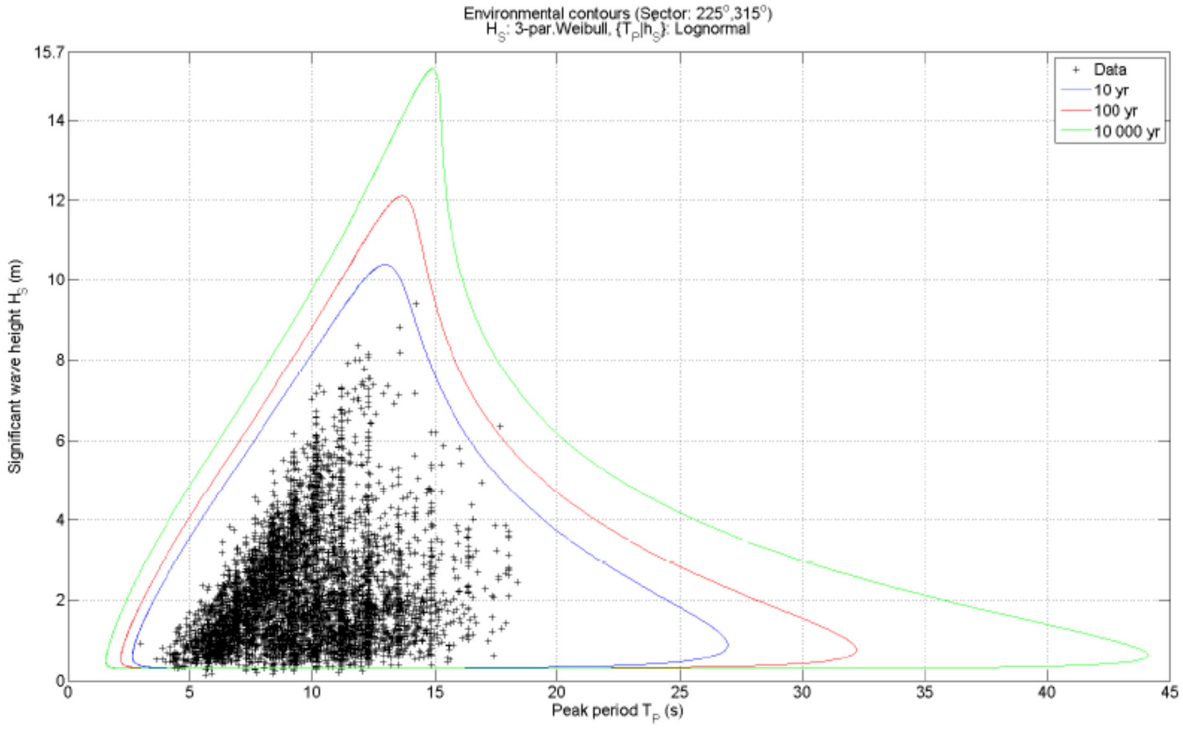

Figure 2-1 Enviromental contours of the significant wave heights and corresponding peak periods for the location outside of the Bjørnafjord (at the location 60N, 4.5E). Stefanakos (2015).

The NORA10 is gathered in the offshore area, to obtain the input parameters at the entrance of the fjord an additional analysis needs to be conducted. The analysis can be done with a computational model that considers nearshore effects like STWAVE, CGWAVE, WAM or SWAN model.

3 Introduction to estimation of fjord wave conditions.

3.1 Physical processes and theories relevant for estimation of nearshore wave conditions.

The wave spectrum in a fjord consist of a local wind sea and the incoming wave swells. Due to decreasing water depth, ocean waves reaching the coastal areas are affected in the terms of amplitude and propagation direction. This phenomenon is a result of various physical processes that need to be understood and taken into consideration for proper estimation of the design wave conditions in the fjord. The overview of the processes with the relative importance for different areas is shown in **Figure 3-1.**

Process	Oceanic waters	Coastal waters		
		Shelf seas	Nearshore	Harbour
Wind generation	●●●	●●●	●	○
Quadruplet wave–wave interactions	●●●	●●●	●	○
White-capping	●●●	●●●	●	○
Bottom friction	○	●●	●●	○
Current refraction / energy bunching	○/●	●	●●	○
Bottom refraction / shoaling	○	●●	●●●	●●
Breaking (depth-induced; surf)	○	●	●●●	○
Triad wave–wave interactions	○	○	●●	●
Reflection	○	○	●/●●	●●●
Diffraction	○	○	●	●●●

●●● = dominant, ●● = significant but not dominant, ● = of minor importance, ○ = negligible.

Figure 3-1 The relative importance of the various processes affecting the waves in oceanic and coastal waters, Holthuijsen (2007).

The diagram showing influence off the different source terms on the total energy spectrum is shown in **Figure 3 -2**.

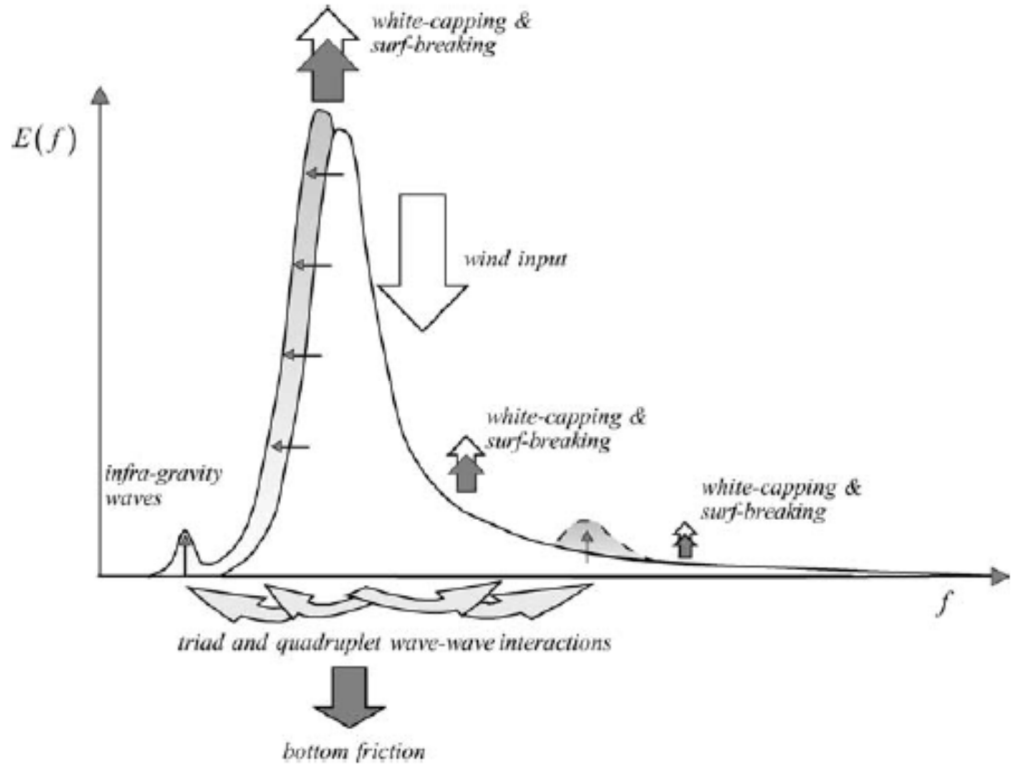

Figure 3-2 The summarized effect of the source terms on the incident wave spectrum. Holthuijsen (2007).

3.1.1 Wind generation

In the case of some pre-existing vertical water surface turbulence - this roughness- a kind of superposition of harmonic waves modify the airflow of the incoming wind blowing over the surface. The pressure at the water surface is modified by the airflow which as a consequence further increases further the wave growth.

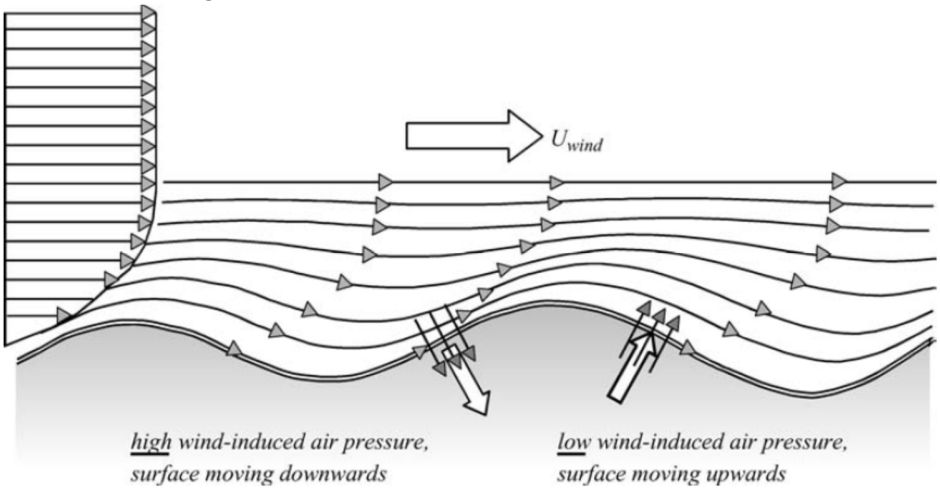

Figure 3-3 The wave-induced wind-pressure variation over a propagating harmonic wave. Holthuijsen (2007).

The transfer of energy for a constant wind is constant in time, which provides a linear correlation:

$$S_{in,1}(f,\theta) = \alpha \quad (3\text{-}1)$$

with $\alpha\left(f,\theta,\vec{U}_{wind}\right)$.

The air pressure on a wave crest is positive on windward side of the wave crest and negative on the other side (refer **Figure 3-1**). This pressure is dependent on the wave amplitude and results in further growth of wave steepness. It can be described by the exponential component:

$$S_{in,2}(f,\theta) = \beta E(f,\theta) \quad (3\text{-}2)$$

with $\beta \sim [U\ cos(\theta - \theta_{wind})/c]^2$. The total energy transfer is:

$$S_{in}(f,\theta) = \alpha + \beta E \quad (3\text{-}3)$$

The wind generated energy for a local wind sea comes in the peak and the far frequency side of the spectrum (refer **Figure 3-2**)

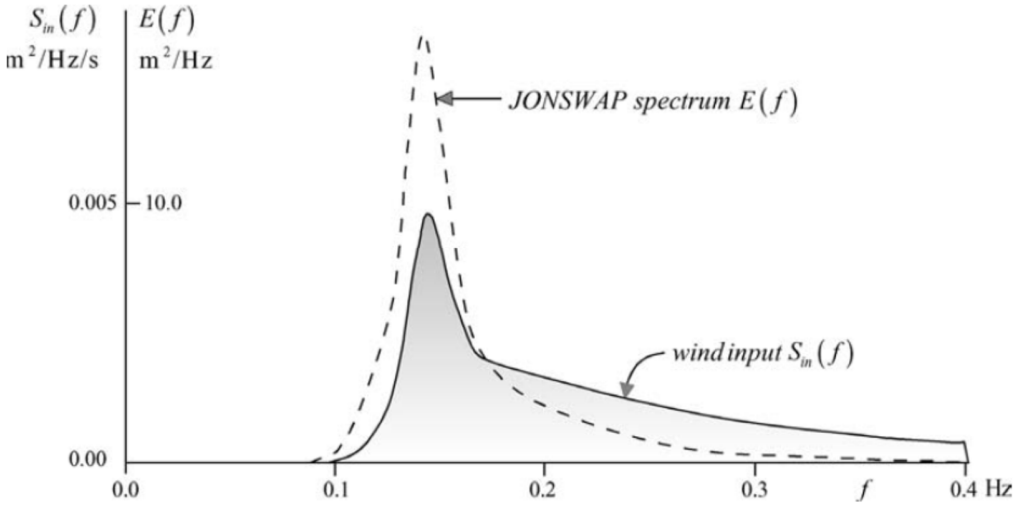

Figure 3-4 The wind input energy term, for a JONSWAP spectrum in deep water for H_{mo}=3.5m , T_p =7s and U_{10}= 20m/s. Holthuijsen (2007)

3.1.2 Wave propagation.

3.1.2.1 Shoaling.

Shoaling is the deformation of waves in the direction of propagation as the wave approaches shallow water, Holthuijsen (2007). For a harmonic wave approaching a gentle slope, due to the rule- that number of waves propagating through a fixed point in space is constant the wave frequency is constant. Through the dispersion relation it can be shown that while depth decreases the wave length and phase speed will decrease.

$$\omega^2 = gk\tanh(kd) \quad (3\text{-}4)$$

The description of the process can be illustrated by a normal wave incident (i.e., parallel bottom contours) under stationary conditions (see **Figure 3-5**.) The following conditions assume that the depth variation is considered slow enough that local water depth can be assumed as constant – this

assumptions also provides that the amplitude change is slow enough to locally approximate the incident with the linear wave theory. Under such conditions, in the absence of wave generation or dissipation, the wave energy leaving volume G through plane 2 is equal to the wave energy entering volume G through plane 1.

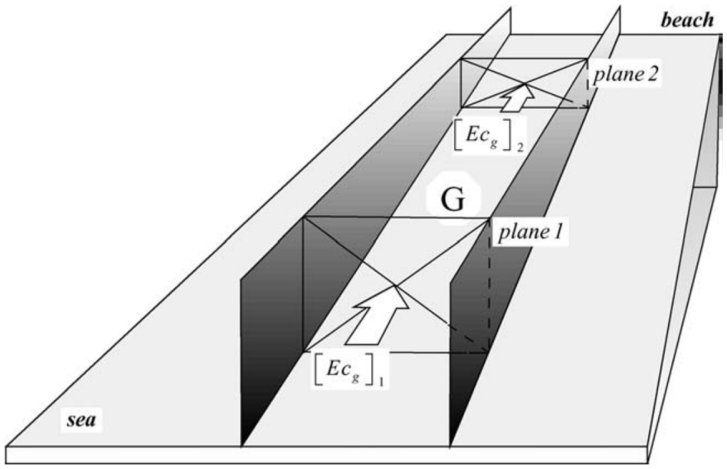

Figure 3-5 A wave approaching a straight coastline at normal incidence under stationary conditions. Holthuijsen (2007).

The conservation of energy is then:

$$P_1 b = P_2 b \;\rightarrow\; [Ec_g]_1 = [Ec_g]_2 \rightarrow \frac{1}{2}\rho g a_1^2 c_{g,1} = \frac{1}{2}\rho g a_2^2 c_{g,2} \;\rightarrow a_2 = \sqrt{\frac{c_{g,1}}{c_{g,2}}}\, a_1 \qquad (3\text{-}5)$$

After taking the under consideration the up wave boundary in deep water the equation describes the shoaling coefficient:

$$K_{sh} = \sqrt{\frac{c_{g,\infty}}{c_g}} \qquad (3\text{-}6)$$

The correlation shows that the wave group speed decreases when the wave approaches the shore. The wave amplitude although initially decreasing at the shore line approaches infinity. The breaking mechanism dissipates the waves before it happens (refer **Figure 3-6**).

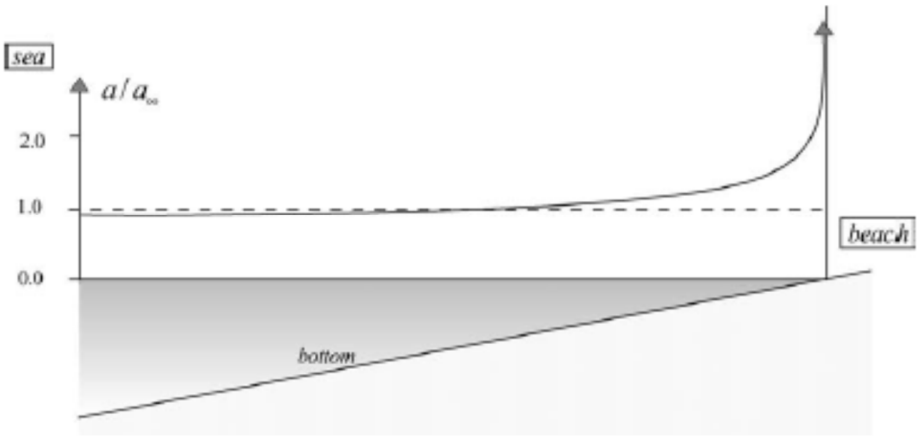

Figure 3-6 The amplitude evolution of a harmonic wave approaching the shore an normal incident under conditions that allow linear wave theory approximation. Holthuijsen (2007).

3.1.2.2 Refraction

With the oblique wave-shore incident (the propagation direction parallel to the depth contours) the wave will slowly shift the direction towards the region with the shallower water .i.e.. the shoreline.

The directional change is always towards the region with the lower propagation speed. The depth variation in this case leads to phase speed variation along the wave crest. This can be shown considering **Figure 3-5**.

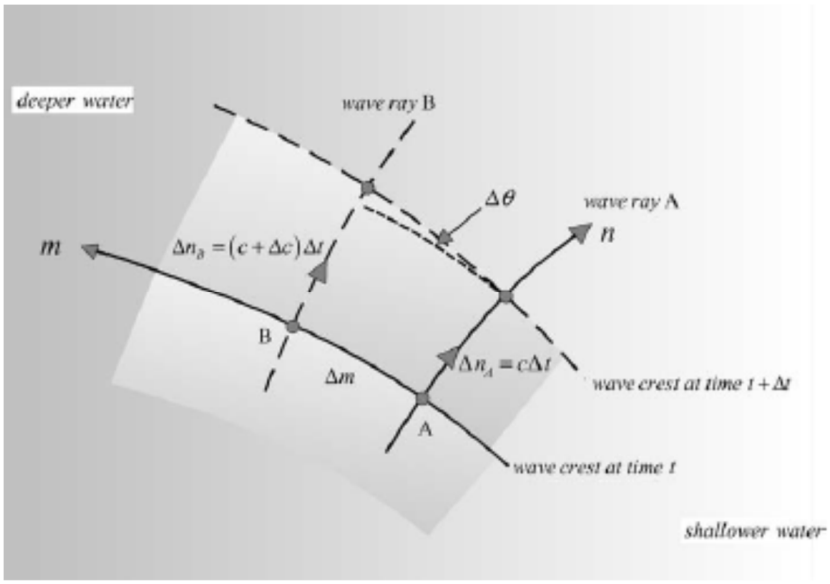

Figure 3-7 Turning of the wave crest towards the shallow water depth. Holthuijsen (2007).

For a line with equal phase velocity (in this case the wave crest) that travelled the distance $\Delta n_A = c\Delta t$ and $\Delta n_B = (c + \Delta c)\Delta t$ for point A and B respectively the directional turning rate becomes:

$$\frac{\Delta\theta}{\Delta n} = -\frac{\Delta c \Delta t}{\Delta m} \qquad (3\text{-}7)$$

For a infinitesimally small differences with the assumption of stationary variable depth and the absence of current the relation becomes:

$$\left(\frac{d\theta}{dn}\right) = -\frac{1}{c}\frac{\partial c}{\partial m} \quad (3\text{-}8)$$

For an oblique incident the following correlation becomes the Snel's Law:

$$\frac{sin\theta}{c} = constant \quad (3\text{-}9)$$

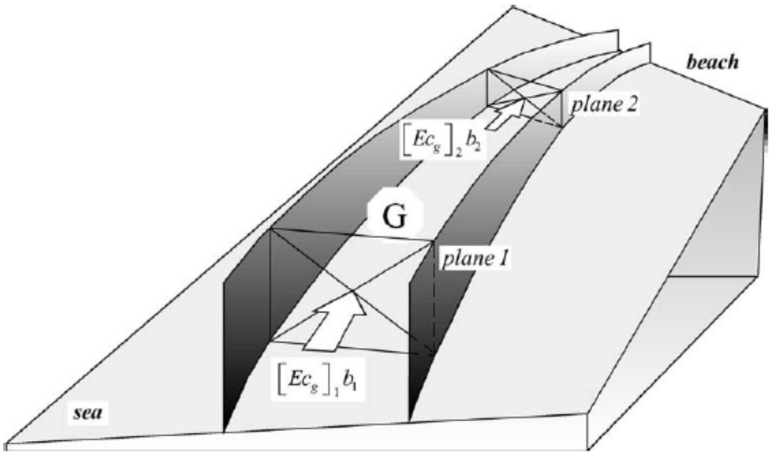

Figure 3-8 Under stationary conditions, in the absence of dissipation and generation the wave energy leaving volume G along two parallel wave rays, through plane 1 is equal to the energy entering through plane 1. Holthuijsen (2007).

The energy change due to refraction can be described based on the situation illustrated in **Figure 3-6**. In the following case (assuming the rate of depth variation allows the linear wave theory approximation) the conservation of energy is described as:

$$P_2 b_2 = P_1 b_1 \;\rightarrow\; \left[E c_g\right]_2 b_2 = \left[E c_g\right]_1 b_1 \;\rightarrow \frac{1}{2}\rho g a_2^2 c_{g,2} = \frac{1}{2}\rho g a_1^2 c_{g,1}\frac{b_1}{b_2} \quad (3\text{-}10)$$

After simplification:

$$a_2 = \sqrt{\frac{c_{g,1}}{c_{g,2}}}\sqrt{\frac{b_1}{b_2}}a_1 \quad (3\text{-}11)$$

After taking the under consideration the up wave boundary in deep water the equation describes the refraction coefficient:

$$K_{ref} = \sqrt{\frac{c_{g,\infty}}{c_g}} \quad (3\text{-}12)$$

3.1.2.3 Diffraction

Diffraction is the turning of waves towards areas with lower amplitudes due to amplitude changes along the wave crest. Diffraction is particularly strong along the geometric shadow line of obstacles such as islands, headlands and breakwaters, Holthuijsen (2007). With the diffraction effects accounted, for the

wave rays (lines orthogonal to the propagating wave crest) curve into the shadow area behind the obstacle (refer **Figure 3-9**).

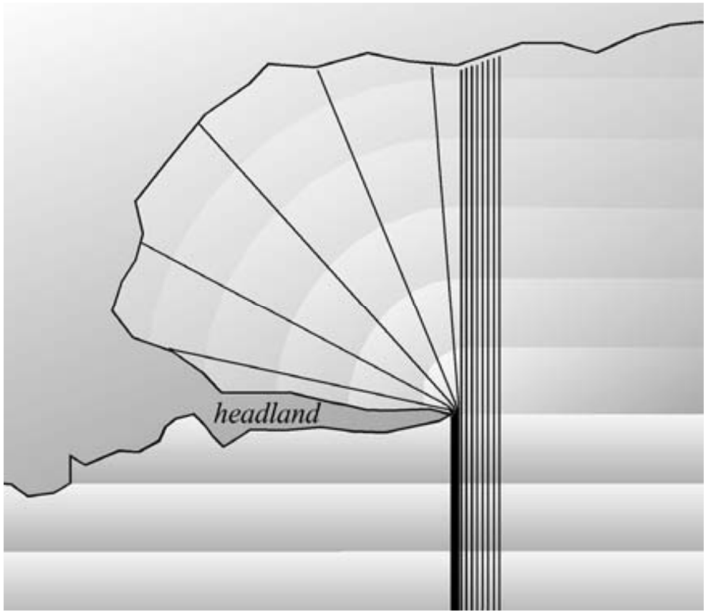

Figure 3-9 Diffraction of the wave rays due to occurrence of headland (assuming constant water depth- no refraction and no reflection - idealized case) Holthuijsen (2007).

The spatial turning rate is derived on the same basis as the refraction effects (refer **Equation 3.8**). The turning rate in time is:

$$c_{\theta,diff} = \frac{C_g}{2(1+\delta_a)} \frac{\partial \delta_a}{\partial m} \quad (3\text{-}13)$$

where

δ_a is the second order spatial derivative f the wave amplitude,

C_g -the group velocity with the effect off diffraction:

$$C_g = c_g(1+\delta_a)^{1/2} \quad (3\text{-}14)$$

Equation 3.9 is derived with the assumption of constant water depth. Such an ideal situation, with absence of water depth variations rarely occurs in real world applications. With a bottom slope near the obstacle the refraction needs to be accounted for separately.

3.1.2.4 Reflections

The coast topography is usually reflecting the waves in some degree. The reflection degree is varying based on the sloping of the shore and thus the angle of attack of the incoming wave. A vertical wall can reflect up to 100% of energy. The resulting wave field near the obstacle is a summation of the incoming wave and the reflected one. The coast line is however usually really intricate which results in a multidirectional reflection of the incoming wave spectrum.

Due to the nature of the fjords with a number of vertical rocky walls, reflection influence should be considered in the wave prediction for a local scale. The reason for that is found in the precise bathymetric and directional spectra wave input required for computation as well as a relatively high computational force required. The reflection is therefore often neglected for ocean scale applications.

Due to the scale of investigated area, precision of the bathymetric data and the input methodology for the reflection calculations required by SWAN (further explained in **Chapter 3.2.1**) the reflection influence for the modelling done was omitted.

3.1.2.5 Tides and currents

Time-varying water depths and ambient currents produced by tides, storm surges or river discharge may change the amplitude, frequency and direction of the incoming waves. Due to lack of data about the currents in the investigated fjord the influence of current on the design wave is neglected.

3.1.3 Dissipation

3.1.3.1 White-capping

White- capping is breaking due to wave steepness. The occurrence of white capping is not dependant directly of the water depth and thus they can occur in deep water conditions. In case of a shallow water normal beach incident -the steepness of the wave is increased due to shoaling and the white cap dissipation gain on importance. However in a more complicated bathymetry conditions diffraction and refraction can prevent energy bunching and diminish the white cap influence on the total dissipation.

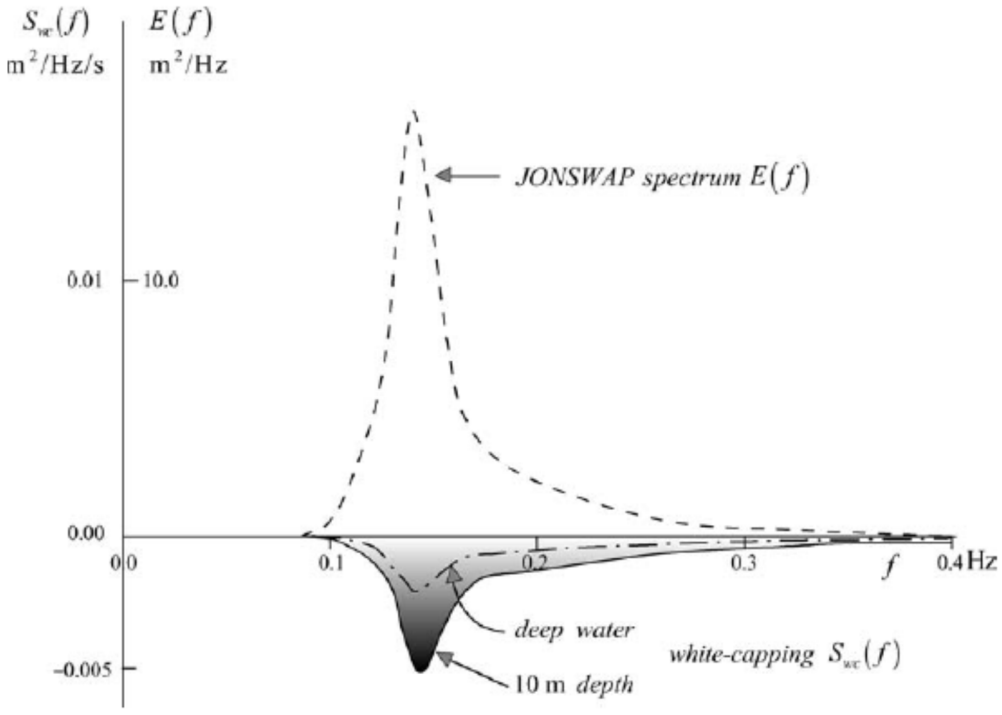

Figure 3-10 Impact of white-capping on a JONSWAP spectrum (H_s=3.5 m and T_p= 7s) for deep and shallow water conditions d=10m. Holthuijsen (2007)

3.1.3.2 Bottom friction

Bottom friction is a dissipation mechanism based on momentum transfer between waves and the thin turbulent boundary at the basin bottom. In the result of this transfer the orbital motions of water particles is transfer to the bottom particles. The effect is therefore dependant on the type of material of the bottom. The influence seems to be biggest for loose bottom material like sand.

The energy of the waves can be high enough to change the bottom form. The shift from a flat sandy bottom to a rippled bottom surface induces the shear stress. Due to increasing roughness, which as a results increases the bottom friction, dissipation of waves is quicker. The mentioned situation describes the complexity of the correlation between the friction and the incoming waves.

There are three basic formulation of the bottom friction influence on wave characteristics:

-the drag-law model developed by Collins, assuming one empirically obtained coefficient that allows to calculate a proper estimate of the shear bottom stress,

-the eddy-viscosity model developed by Madsen, based on the permanent flows over a turbulent-boundary-layer and,

-JONSWAP empirical model developed by Hasselmann, based on real observations of swell dissipation.

Effects of a JONSWAP modelled bottom friction on the wave spectrum is shown in **Figure 3-11**

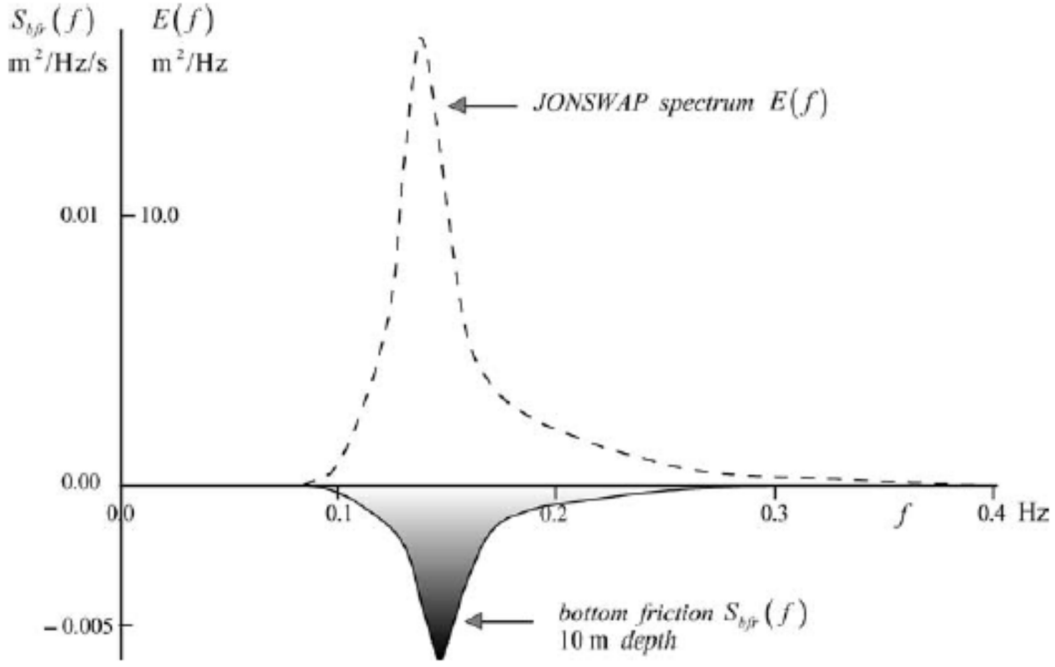

Figure 3-11 Impact of white-capping on a JONSWAP spectrum (H_s=3.5 m and T_p= 7s) for shallow water conditions d=10m. Holthuijsen (2007).

3.1.4 Depth-induced (surf-)breaking

The dissipation of energy due to surf breaking is proportional to the energy density:

$$S_{surf}(f,\theta) = \overline{D}_{surf} E(f,\theta)/m_0 \quad (3\text{-}15)$$

$$\overline{D}_{surf} = -\frac{1}{4}\alpha_{BJ} Q_B \overline{f_0} H_{max}^2 \quad (3\text{-}16)$$

where

α_{BJ} is the tuning coefficient based on observations (usually $\alpha_{BJ} \approx 1$)

Q_B is the fraction of breaking waves (wave breakers described closer in **Chapter 3.1.6**),

$\overline{f_0}$ is the mean zero-crossing frequency of the breaking waves,

H_{max} is the maximum wave height for the existing wave length.

The shape of the influence of surf breaking is identical to the shape of the wave spectrum.

The

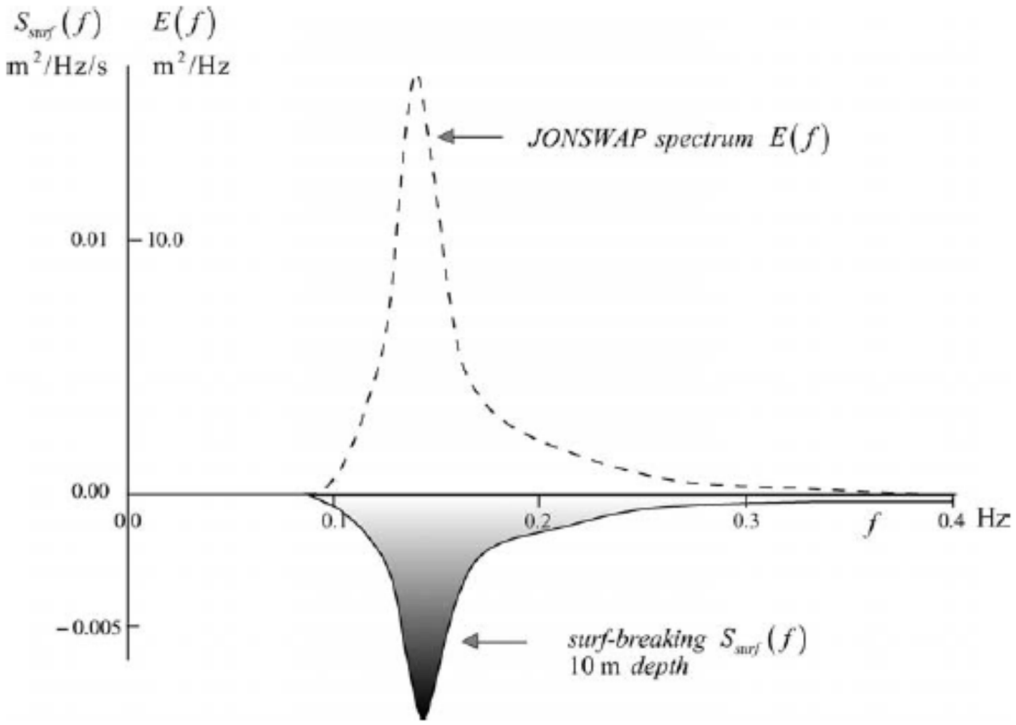

Figure 3-12 Impact of surf-breaking on a JONSWAP spectrum (H_s=3.5 m and T_p= 7s) for shallow water conditions d=10m, Holthuijsen (2007).

3.1.5 Nonlinear wave-wave interactions- quadruplet and triad wave-wave interactions

Quadruplet and triad wave-wave interactions are phenomena of transferring the energy amongst the waves. The transfer occurs due to resonance. The quadruplet interaction refers to a situation of four individual wave interaction and analogically triad interactions refer to three wave components interacting.

The quadruplet energy exchange is one of the dominant processes changing the spectrum in the deep water conditions. The total energy balance must become constant in the resonance exchange thus both the positive and negative influence of the quadruplets interaction on the spectrum. The low frequency amplification is usually dissipated quickly by white-capping with the high frequency components are smoothing the wind sea generated component. In shallow water the influence of quadruplets become even more intensified (refer **Figure 3-13**).

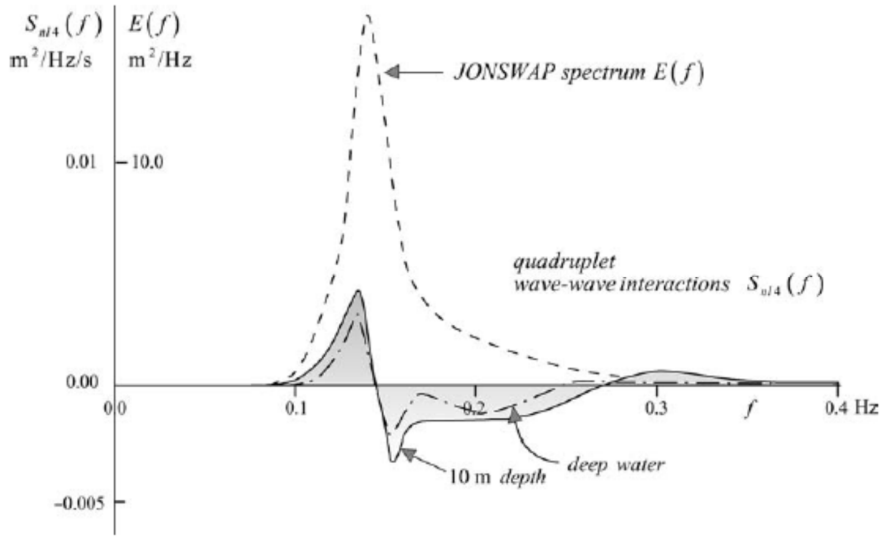

Figure 3-13 Quadruplet wave-wave interaction influence on a JONSWAP spectrum (H_s=3.5 m and T_p= 7s) for deep and shallow water conditions d=10m. Holthuijsen (2007).

The triad wave-wave interactions are not realisable for the deep water conditions. In extremely shallow water when the waves become non-dispersive a three wave component resonance is possible. In such conditions the triad interactions often generate a second peak at double the peak frequency (and sometimes also at higher peak multiplies).

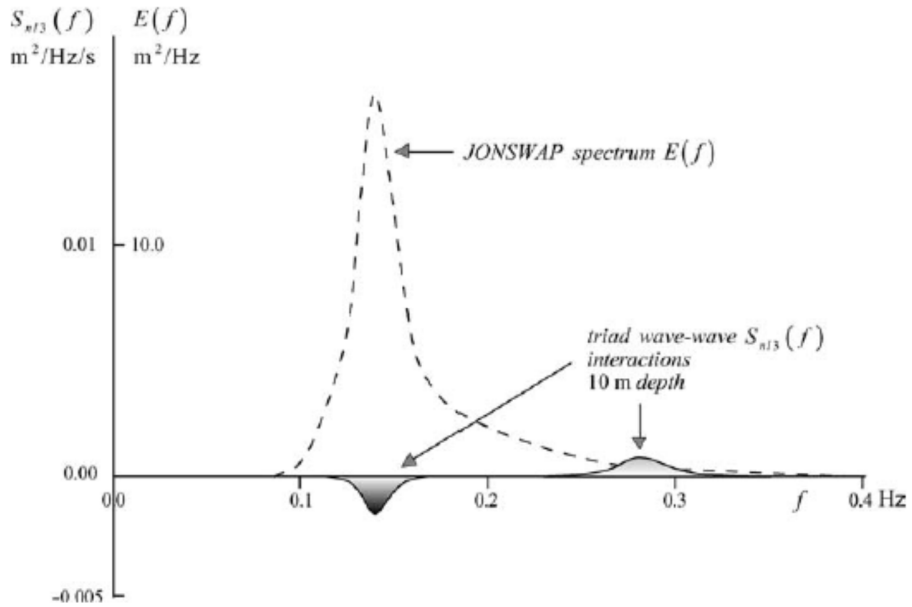

Figure 3-14 Quadruplet wave-wave interaction influence on a JONSWAP spectrum (Hs=3.5 m and Tp= 7s) for deep and shallow water conditions d=10m. Holthuijsen (2007).

3.1.6 Breaking waves

The wave breaking is one of the most nonlinear process affecting waves in the coastal area. The breaking is usually classified by according to visual recognition. The most common classification divides the breaking waves into three categories: spilling breakers, plunging breakers and surging breakers, Svendsen (2006). The mathematical description of breaking waves can be introduced with the Iribarren number (surf similarity parameter):

$$\xi_{br} = \frac{tan\alpha}{\sqrt{H_{br}/L_{\infty}}} \quad (3\text{-}17)$$

where H_{br} is the wave height at the anticipated point of breaking and L_{∞} is the deep water wave length. Replacing the breaking wave height with the deep water wave height:

$$\xi_{\infty} = \frac{tan\alpha}{\sqrt{H_{\infty}/L_{\infty}}} \quad (3\text{-}18)$$

The described parameter allows to determine the expected kind of barkers (assuming a flat beach).

Table 3-1 Breakers occurrence in respect to the Iribarren number. Holthuijsen (2007)

Type of breaker	Iribarren range for deep water	Iribarren range for shallow water
Spilling	If $\xi_{\infty} < 0.5$	If $\xi_{\infty} < 0.4$
Plunging	If $0.5 < \xi_{\infty} < 3.3$	If $0.4 < \xi_{\infty} < 2.0$
Surging	If $\xi_{\infty} > 3.3$	If $\xi_{\infty} > 2.0$

The Iribarren number characterises also the reflection of waves off the beach and run-up of the waves up a beach.

The shape of the different types of breakers are shown in Figures 3-14 through 3-16.

Figure 3-15 Spilling breakers. Svendsen (2006).

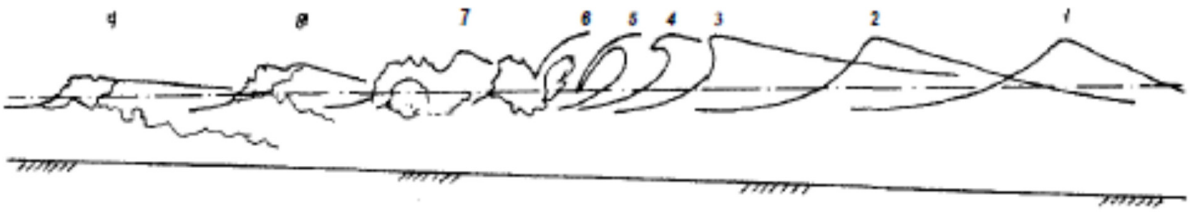

Figure 3-16 Plunging breakers. Svendsen (2006)

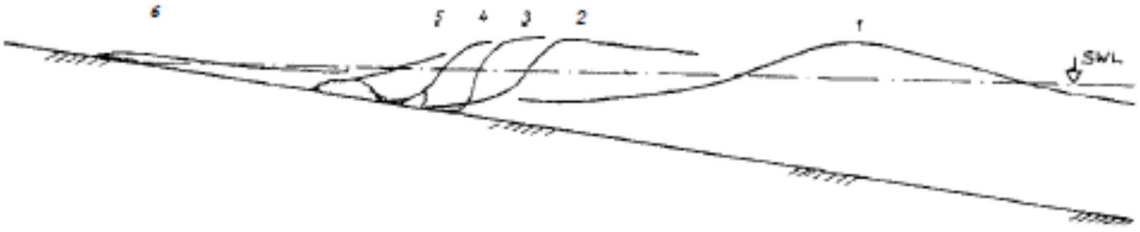

Figure 3-17 Surging breakers. Svendsen (2006)

3.2 Implementation of the theories of near shore wave energy dissipation in SWAN

3.2.1 The SWAN wave model basic assumptions

The SWAN model (Simulating WAves Near Shore) is a third-generation wave model developed at the Delft University of Technology. The Swan model accommodates for the following processes in the terms of sources and sinks: wind generation, wave propagation in time and space, bottom- and current-induced shoaling and refraction, diffraction (only an approximation) and reflection (approximation only for obstacles - not considered for bathymetry).

Dissipation processes included into the model are: white-capping, bottom friction dissipation, surf-breaking and nonlinear wave-wave interactions: quadruplet and triad wave-wave interactions.

The model can also introduce effects of wave damping due to vegetation (not included in this paper due to lacking data on the vegetation in the area), turbulent viscosity effects and dissipation due to effects of a fuzzy layer of bottom muds (in the case of Norwegian fjords the bottom is assumed fixed).

The SWAN model incorporates in some cases several underlaying theories in regard to one process which allows a more customized approach to the modelled problem (refer **Table 3-2**).

Table 3-2 Overview over physical processes and generation modes in SWAN (2015)

process	authors	generation mode		
		1st	2nd	3rd
Linear wind growth	Cavaleri and Malanotte-Rizzoli (1981) (modified)	×	×	
	Cavaleri and Malanotte-Rizzoli (1981)			×
Exponential wind growth	Snyder *et al.* (1981) (modified)	×	×	
	Snyder *et al.* (1981)			×
	Janssen (1989, 1991)			×
	Yan (1987) (modified)			×
Whitecapping	Holthuijsen and De Boer (1988)	×	×	
	Komen *et al.* (1984)			×
	Janssen (1991)			×
	Alves and Banner (2003)			×
Quadruplets	Hasselmann *et al.* (1985)			×
Triads	Eldeberky (1996)	×	×	×
Depth-induced breaking	Battjes and Janssen (1978)	×	×	×
Bottom friction	JONSWAP (1973)	×	×	×
	Collins (1972)	×	×	×
	Madsen *et al.* (1988)	×	×	×
Obstacle transmission	Seelig (1979), d'Angremond (1996)	×	×	×
Wave-induced set-up		×	×	×
Vegetation dissipation	Dalrymple (1984)	×	×	×
Mud dissipation	Ng (2000)	×	×	×
Turbulence dissipation		×	×	×

3.2.1.1 The action balance equation

SWAN model is based on the action balance equation (the calculation account for the wave-current interactions). For small scale computation (for Cartesian co-ordinates) the equation becomes:

$$\frac{\partial N(\sigma,\theta;x,y,t)}{\partial t}+\frac{\partial c_{g,x}N(\sigma,\theta;x,y,t)}{\partial x}+\frac{\partial c_{g,y}N(\sigma,\theta;x,y,t)}{\partial y}+\frac{\partial c_{\theta}N(\sigma,\theta;x,y,t)}{\partial \theta}+\frac{\partial c_{\sigma}N(\sigma,\theta;x,y,t)}{\partial \sigma}=\frac{\partial S(\sigma,\theta;x,y,t)}{\sigma} \quad (3\text{-}19)$$

The $S(\sigma,\theta)$ component is the source term of energy density. It represents the effects of generation, nonlinear wave-wave interactions and dissipation. The $N(\sigma,\theta)$ term represents the action density spectrum.

In the equation the firs term (from the left side) accounts for the nonstationary situations (change of rate of action in time).

The second and third terms account for the propagation of action in space (with $c_{g,x}$ and $c_{g,y}$ representing propagation velocities).

The fourth term represents the directional change in the action propagation – it accounts for depth and current induced refraction and diffraction.

The fifth term describes the variation in frequency induced by depth and current variation.

In the absence of ambient currents and assuming stationary runs (as in all situations considered in this paper) the equation becomes the energy balance equation with the action density replaced by the energy balance density.

$$\frac{\partial c_{g,x}E(\omega,\theta;x,y,t)}{\partial x}+\frac{\partial c_{g,y}E(\omega,\theta;x,y,t)}{\partial y}+\frac{\partial c_{\theta}E(\omega,\theta;x,y,t)}{\partial \theta}=S(\omega,\theta;x,y,t) \quad (3\text{-}20)$$

3.2.1.2 Input parameters

The following parameters need to be specified as an input for SWAN stationary analysis:

-computational grid,

-directional resolution and coverage,

-frequency resolution and range,

-bottom grid,

-boundary input – incoming wave spectrum at the boundary position,

-spreading coefficient,

-generation model,

-physical processes that should be enabled/disabled for the planed run,

-output parameters request and the location.

A short description of possibilities for the most important input categories for this thesis is provided bellow.

3.2.1.3 Computational an bottom grid.

The computational grid impute needs to be defined in respect to the problem coordinates where the size of the grid should be cover by the bathymetry grid (minimal requirement). The correlation between the computation grid and the input grids should secure that the energy spreading should cover the whole computational grid (for all possible situations). The advised range for cell size discretization lays between 50- 1000m for costal applications, SWAN (2015).

While modelling cases with open water boundaries, without any wave input - a sufficient enough size of the bottom grid should extend over the edge of the computational grid. This helps prevent the leakage through those boundaries due to refraction.

The cell size (in the geometric shadow of the obstacle position) in case of diffraction calculation should be in the range of 1/5 to 1/10 of the dominant wave length. This constrains can be worked over with nested runs or unstructured meshes.

SWAN allow description of the grid as a regular, curvilinear or unstructured (triangular mesh grid).

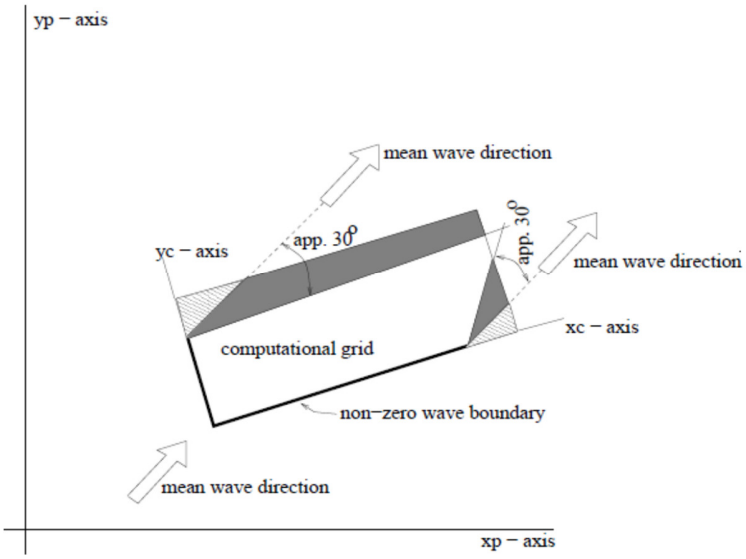

Figure 3-18 Cartesian computational grid for SWAN modelling. The grey area shows the common mistakes while modelling- insufficient input grid in respect to the spatial coverage required by the program, SWAN (2015)

A directional resolution needs to be chosen for the computation run. Advised values lay between 15° and 10° for wind sea and between 2° and 5° for swells. The directional range needs to cover the energy propagation area. A secure solution of 360° coverage can be adopted.

SWAN adopts a Cartesian coordinate system (with the orthogonal or nautical coordinate systems as an option) Cartesian system equal to the one found in SWAN (0 degrees in the positive x direction with the counter clockwise positive angle notation) was assumed for this paper.

3.2.1.4 Directional resolution and coverage

The minimum and the maximum frequencies recommended in SWAN (2011) should follows the correlation $\Delta f/f \approx 0.1$ where

$$\Delta f = \left(-1 + \left[\frac{f_{high}}{f_{flow}} \right]^{\frac{1}{[msc]}} \right) f \quad (3\text{-}21)$$

And $f_{flow} > 0.04\ Hz\ and\ f_{high} \leq\ 1Hz$. The f_{flow} should be below the minimum peak awaited as the result for the analysis.

3.2.1.5 Boundary input and spreading coefficient

The wave spectrum at the boundary is described as a two dimensional spectrum given by:

$$S(f, \theta) = S(f)D(\theta) \quad (3\text{-}22)$$

where $S(f)$ is the one dimensional spectrum (JONSWAP, Pierson-Moskowitz or a Gaussian-shaped), and $D(\theta)$ is the directionality function given by:

$$D(\theta) = Acos^{n}(\theta - \theta_p) for\ |\theta - \theta_p| \leq \frac{\pi}{2} \quad (3\text{-}23)$$

where
θ_p is the main wave propagation direction and
n is the spreading coefficient.
The spreading coefficient describes the range in which the waves can spread. Coefficient can be set for SWAN calculations as an integer within a range <2 ; 65>. The lower value corresponds to short crested waves like wind sea whereas the $n = 65$ is advised only for long crested oceanic swells.

3.2.1.6 Output parameters and locations

SWAN can produce output parameters for a specific chosen array of points, a curve (the points along the curve are calculated with the division given by the user) or a grid. The possibilities of the output grid design are similar to those for the bottom and computational grid.

The spatial resolution of the output grid must be sufficient to obtain relevant spatial precision. In the cases when the output grid does not follow the computational grid an bi-linear interpolation is used to calculate results. The obtained results can therefore be interpolated twice (data from the input grids interpolated to fit the computational grid and afterwards the results interpolated to the output grid resolution). This can sometimes result in a supposed loss of information about the bathymetry (refer **Chapter 5 and 6**).

3.2.1.7 Reflection, transition and absorption

Due to complexity of the process, high input precision requirements and a high computational power needed, SWAN dose not model the reflection for none of the input grids. The process is available for computation of separate elements modelled directly in the computational grid with the command "obstacle". The process is design to calculate the influence of linear objects such as dams, headlands and breakwater. The input requires description of the geometry (coordinates, slope) and the ratio for transition of energy through the barrier. Due to input work difficulties and the local scale (due to geometric requirements), this type of object modelling for reflection is omitted in this thesis.

The bottom grid assumes then no reflection and the dry land assumes total energy absorption. For a U-formed, steep cliff-shored fjord this assumption can provide some uncertainty with the results.

4 Recreation of constant slope experiment by Engbretsen

4.1 Introduction

An exercise of recreating the results of the test case (by Engbretsen (2012)after Svangstu 2011) investigation was conducted to familiarize with the SWAN program. The input data was obtained from the master thesis from the Norwegian University of Science and Technology in Trondheim. The obtained solution was compared with the results from Engbretsen report. The test case was conducted with the following input data.

Table 4-1 Model test setup values from Engbretsen (2012)

Significant wave height (m)	Peak period(s)	Maximum depth (m)	Minimum depth (m)	Horizontal length of tank (m)
10.5138	11.25	67.23	0	1377.187

The analysis was performed as a two dimensional stationary run for the full scale model with the swell input as long crested waves (spreading coefficient set to n=65). The incoming wave field was described as a JONSWAP spectrum with the peakedness coefficient of $\gamma = 3.3$. The default settings for the physical processes provided in the SWAN model were used for the investigation. Additionally the triad wave-wave interaction and dissipation through bottom friction where enabled due to the suspicion of the importance of the mentioned processes in the total energy loss. Due to long crest input an neglecting the effects of wind the quadruplets wave-wave interaction where omitted as recommended in SWAN (2015).

4.2 Computational grid and input grid

The computational grid created was a rectangular regular grid. The grid size was assumed as 1377,167m by 5000m with the beginning of the grid at point (0,0). The input grid for bathymetry was created with dimensions equal to the computational grid. The depth of the bathymetry was specified as 67.23m and 0 for the west and east boundaries of the computational grid respectively.

The bathymetry was assumed as a constant slope provided as one element (due to constant slope of the idealized case the bottom grid could be assumed as one element without loss of result precision), where the computational grid was divided into elements Δx= 20 by Δx= 50 m respectively based on the initial analysis performed by Engbretsen. The wave propagation was modelled perpendicular to the bottom slope (assumption of the lack of refraction and diffraction in the investigated case).

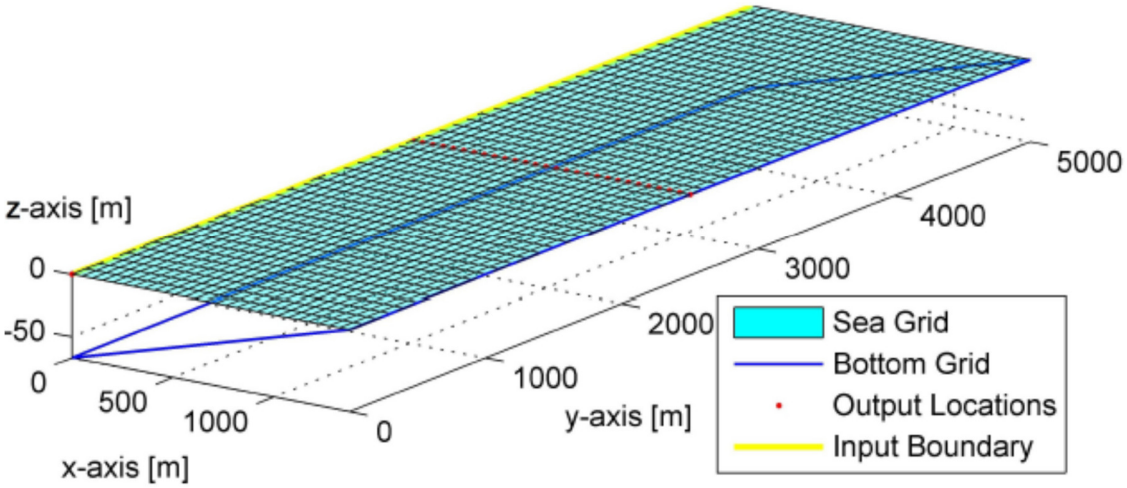

Figure 4-1 The graphic representation of the constant slope problem. Engbretsen (2012)

4.3 Frequency resolution

The minimum spectral frequency f_{low}, and the maximum spectral frequency, f_{high} were specified to be 0.0530Hz and 1Hz respectively for the test case.

The directional space was chosen to be 360° - providing coverage over the whole area. Directional resolution of 10° was assumed according to SWAN (2015) recommendations to use 15° ≤ Δθ ≥10° for wind sea and 5° ≤ Δθ ≥ 2° for swells.

4.4 Physical Processes

The default option for the near shore and dissipation physical processes were utilized in SWAN. The physical processes activated are: surf-breaking, white-capping and the dissipation by bottom friction. Due to lack of wind and a constant moderate depth variation the bottom friction is assumed the governing energy dissipation mechanism.

4.5 Output modelling

The analysis was focused on the spectral density and the significant wave height for the points set at the line parallel to the x-axis in the midpoint of the computational domain in respect to the y-axis. The significant wave height was investigated for the bottom depth varying from 67.23m to 15m. A sensitivity to analysis was performed for the influence of different dissipation processes on the result.

4.6 Comparison of the output from SWAN with Engbretsen result

The analysis of the described model was done in SWAN. The spectra at the output locations are shown in **Figure 4-2** (with the results obtained by Engebretsen shown in **Figure 4-3**).The results obtained were analogues to the ones obtained in the recreated analysis.

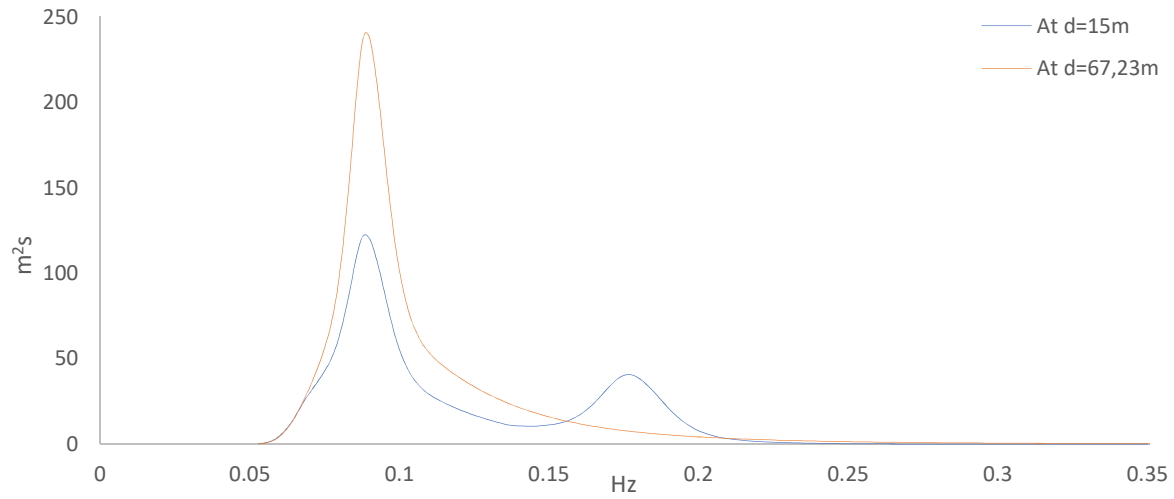

Figure 4-2 Spectrum output at the investigated locations for the test case.

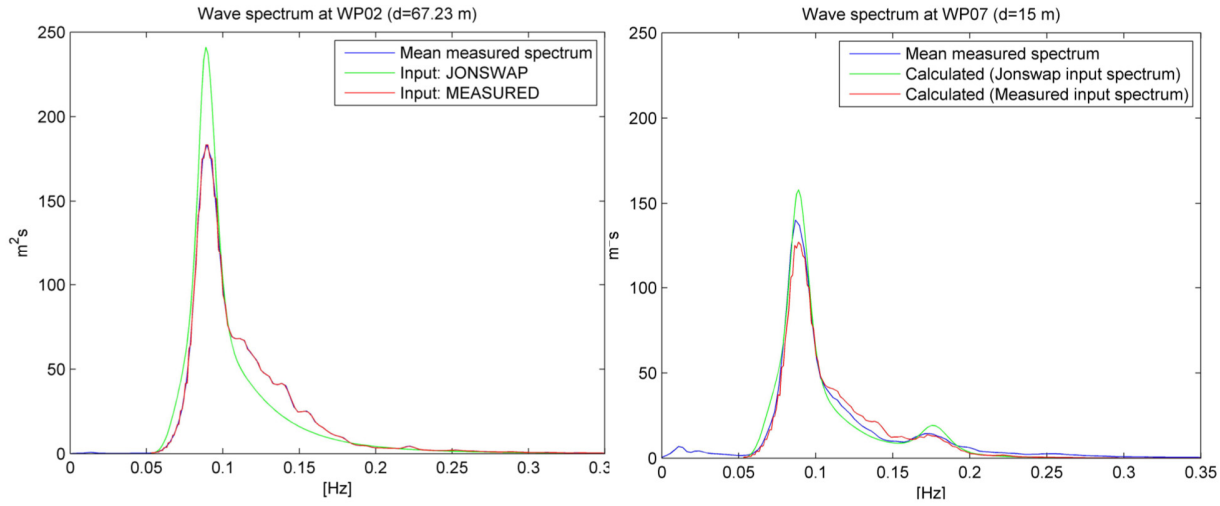

Figure 4-3 The results of the full scale model of the test case obtained by Engebretsen. On the left: spectrum at depth d=67.23m- input spectrum. On the right: the spectrum for d=15m. Engebretsen (2012)

Furthermore the sensitivity study of the influence of the different dissipation processes was conducted to familiarize with the input methods, parameters and commands for different mechanics available in SWAN. Results were presented for the significant wave height parameter relative to the dimensionless water depth. The value for H_s is given by:

$$H_s = 4\sqrt{\iint E(\omega,\theta)d\omega d\theta} \quad (4\text{-}1)$$

where $E(\omega,\theta)$ is the variance density spectrum dependant on ω – the absolute radian frequency.

The value for the dimensionless water depth is described as the water depth relative to the wave length d/L. The wave length for the linear wave theory (used in SWAN) is given by:

$$L = \frac{g}{2\pi} \cdot T^2 \cdot tanh(kd) \quad (4\text{-}2)$$

where k is wave number and T is the wave period. The wave length was calculated in SWAN as the peak wave length. The obtained results are shown in **Figure 4-4**.

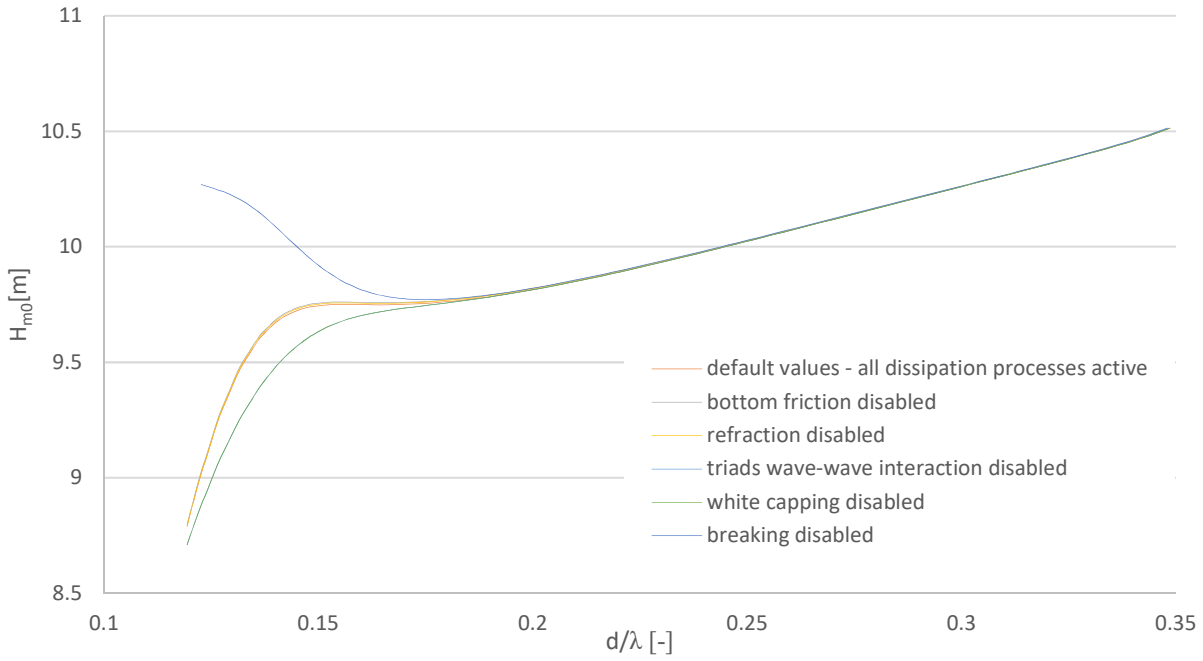

Figure 4-4 Sensitivity study for the influence of different processes for the significant wave height.

Whilst recreating the test case experiment special interest was set to the results regarding the refraction of the waves toward the open water boundaries parallel to the wave propagation (refer **Figure 4-5**). The figure shows the leakage of energy through the sides. The problem is a result of the methodology of inputting wave parameters in SWAN. The input in this case is set at the x=0 line but is only valid for the computational grid. The conditions outside of the grid (for y>500 and the negative values of y) dose not have a full directional coverage of the incoming wave. This solution provides lower energy density in those areas and cause the waves to refract in those directions.

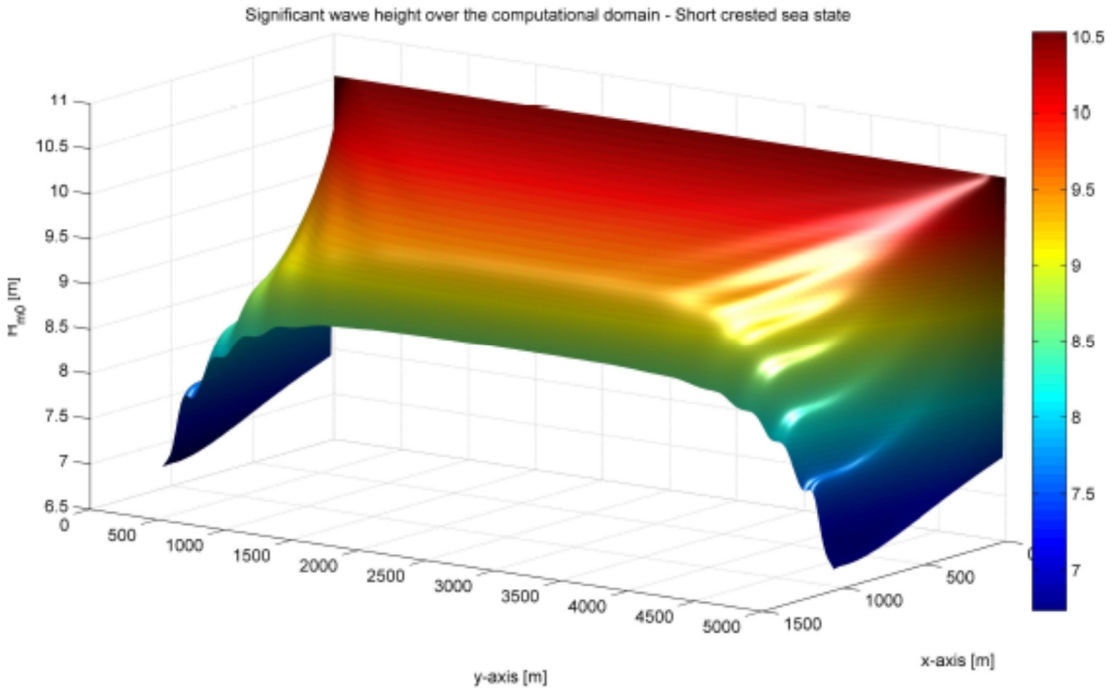

Figure 4-5 The significant wave height over the entire computational domain for the short crested test case Engebretsen (2012).

Although keeping this in mind and assuming a wide enough computational grid it is possible to obtain reliable wave characteristic near the midline of the model the solution is not applicable in constrained estuaries such as fjords (due to the fact that fjords have the width in the relative range of about 25 -300 wind sea wave length). Such a simplification in the model is not feasible for the a fjord model due to lack of reliable research connecting refraction in the open ocean conditions and refraction toward the sloped shore. Such transformations method, if devised, would be of a complex nature. Due to those facts a reliable bathymetry input for the sides of the fjords need to be modelled. The considerations mentioned above were the inspiration and the basis for the analysis in **Chapter 5**.

5 Idealized simple models for bathymetry sensitivity analysis

The Bjørnafjord (analysed further in **Chapter 6**) is a fjord characterized by a complex bathymetry. Two narrow, deep inlets (norther and southern) provide the connection of the fjord to the open ocean. The incoming waves come parallel to the inlets axis. Approximately in the middle of the length of both inlets a turn occurs which introduces a sudden decrease in the spectral energy. The eastern sector of the fjord is on the other hand shallower with a slow bottom slope. The compositions of different elements prevents an easy estimation of the degree of importance of a singular dissipation processes. Due to this complexity a series of three groups of idealized models with special bathymetry was introduced to properly estimate the energy evolution in the fjord.

5.1 Basic models assumptions

All computations where conducted as stationary runs in Cartesian coordinate system.

Due to similarities of the total dimensions (length, width, depth, longitudinal slope wave input) the computational domain was chosen to have the density of dx=50m and dy=50m based on chapter 6.1 of Juliet's Ngbeken (2016) thesis.

The minimum spectral frequency f_{low}, and the maximum spectral frequency, f_{high} were specified to be 0.0530Hz and 1Hz respectively for all models.

The directional space was chosen to be 360° - providing coverage over the whole area. Directional resolution of 10° chosen.

Each model where drawn as a series of surfaces with the incident of the surface resulting in a sharp "edgy" connection. Due to further discretization of the mesh the edge can transform into a radius of roughly one or two meters. Due to lack of data and the total scale of the models such geometric characteristics where neglected.

Because of the lack of information about the bottom material a JONSWAP bottom friction coefficient of $c_{fjon} = 0.019\ m^2 s^{-3}$ was assumed for calculations. The value is advised by SWAN (2015) for non-sandy bottoms.

No vegetation based dissipation was assumed for the model – this can be an underestimation as Bjørnafjord lays near the warm Gulf Stream which can result in intensive marine flora. This fact together with the arbitrary chosen bottom friction leads to uncertainties in the bottom friction dissipation. Thus this mechanism is not the most intensive dissipation model for costal area no further investigation was conducted.

The observed sloping of the side of Bjørnafjord (based on available bathymetry data)is in the range :

-most steep slope in the inlet – 1: 1.5 (Δd=400m for Δy=600m),

-least steep slope in the inlet – 1: 3 (Δd=200m for Δy=600m),

-average slope in the eastern sector – 1:13 (Δd=200m for Δy=4000m).

The prepared models are designed to fall into the same steepness range.

5.2 General input parameters

The incoming swell wave parameters are based on the value obtained through the extreme wave statistics by Juliet Ngbeken (2016). The wave characteristics calculated for the winter season are used for the simplified cases analysis. Wind input is not taken into consideration.

Table 5-1 Extreme values for 100 year exceedance for winter and summer season. Ngbeken (2016)

	Significant wave height(m)	Peak period (s)	Wind speed(m/s)	Wind speed(m/s)	Wind direction
WINTER	12.4	17.1	14	14	288
SUMMER	7.58	13.18	26	26	324

5.3 Methodology for implementation of the simple cases and the simplified fjord model

Three groups of models described by the general principle schemes were created:

-ideal beach model with the varying depth value as the differentiating parameter,

-closed idealized fjord model with the varying side sloping as the differentiation,

-turn simulation model with the turn angle as the varying parameter.

5.4 Idealized beach model

5.4.1 Model description

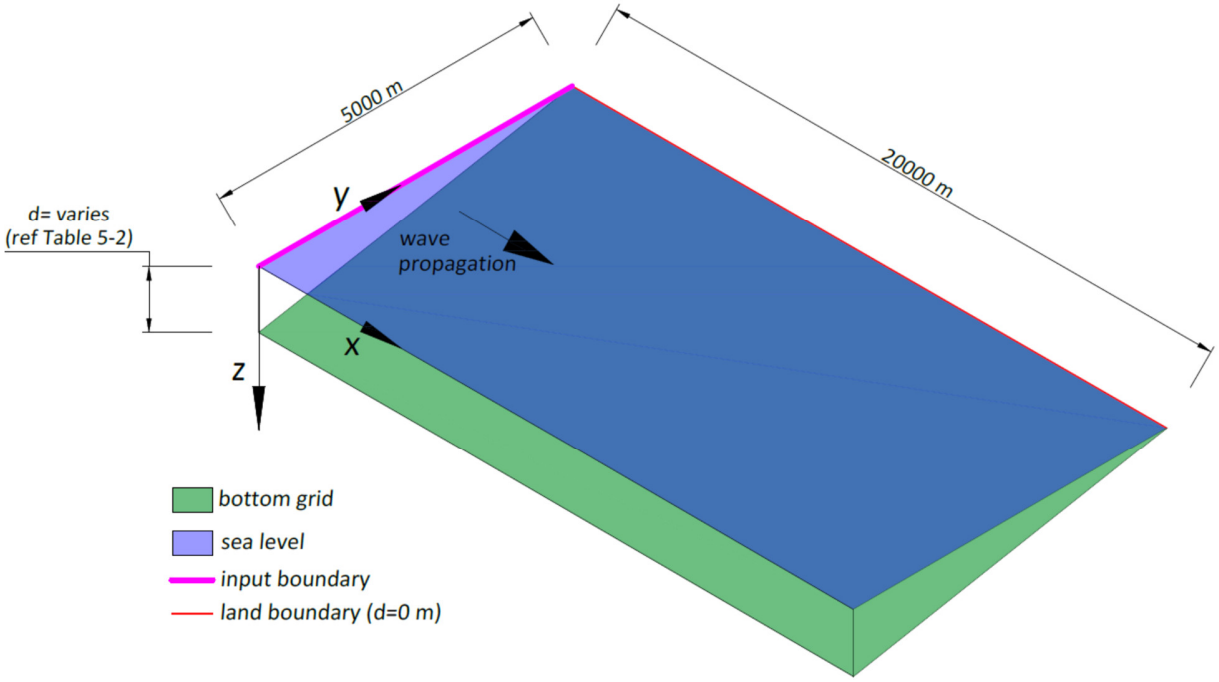

Figure 5-1 The principals for designing the ideal beach model group.

Table 5-2 List of the ideal beach models analysed

Depth	Gradient
25	1:200
50	1:100
75	3:200
100	1:50
200	1:25
300	3:50
400	2:25
500	1:10
600	3:25

The model is introduced to investigate the behaviour of a wave propagating parallel to the shoreline (along the x-axis).

The default processes activated for the analysis were: surf-breaking, white capping and diffraction. Refraction, bottom friction and triad wave-wave interactions where turned on and off for series of runs to analyse the influence of those processes on the spectra.

5.5 Results of the ideal beach analysis

The results obtained will be shown as H_s contour plots (with the direction of propagation indicated) for different processes active. (Figures 5-2 to 5-9). The following figures show the development of the wave profile. The situation described is an incident of the wave train, from deep water, into a beach with a constant slope. The contours profile therefore reflect a superposition of two main processes – development of refraction and an impact of a water mass stream into a linear obstacle parallel to the water velocity. An incident modelled like this is highly unlikely to occur in reality. In real bathymetry, there will be some sloping on the negative part of the x-asks towards the open ocean conditions. The waves will not hit a vertical triangular wall – and thus the wave dispersion will not be so abrupt as the one that can be seen in the high left corner of the contour plots. The sudden disruption off energy and the linear drop in the H_s value for **Figures 5-10 to 5-12** should be therefore neglected.

Nevertheless the incident modelled reflects, in a very overestimated way, the wave entering into the fjord from an ocean shelf. Similar disruptions can also be observed in the Bjørnafjord contour plots (refer **Chapter 6**).

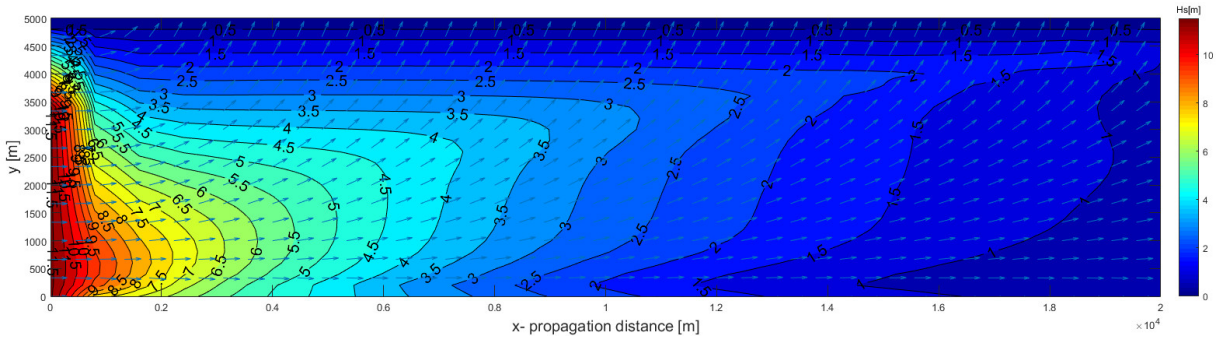

Figure 5-2 The Hs map over the beach area for the slope of 1:200 (maximum depth 25m). All default and investigated processes active.

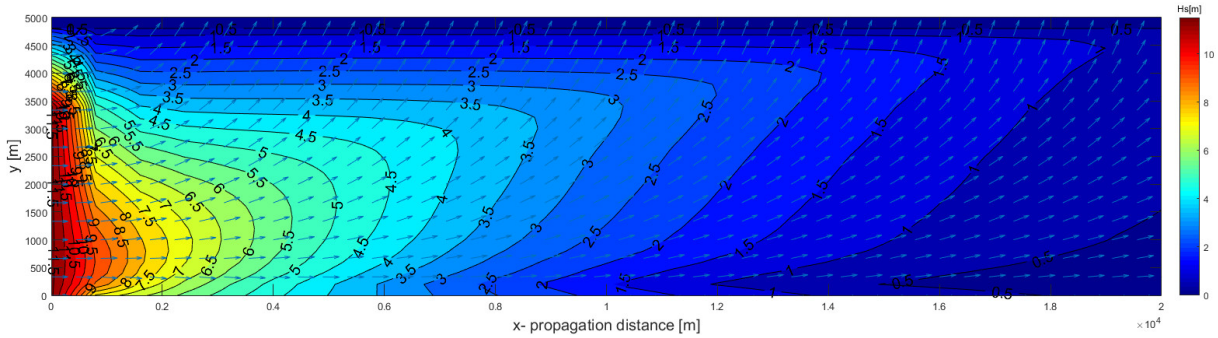

Figure 5-3 The Hs map over the beach area for the slope of 1:200 (maximum depth 25m). All default processes active. Bottom friction and triad interactions disabled.

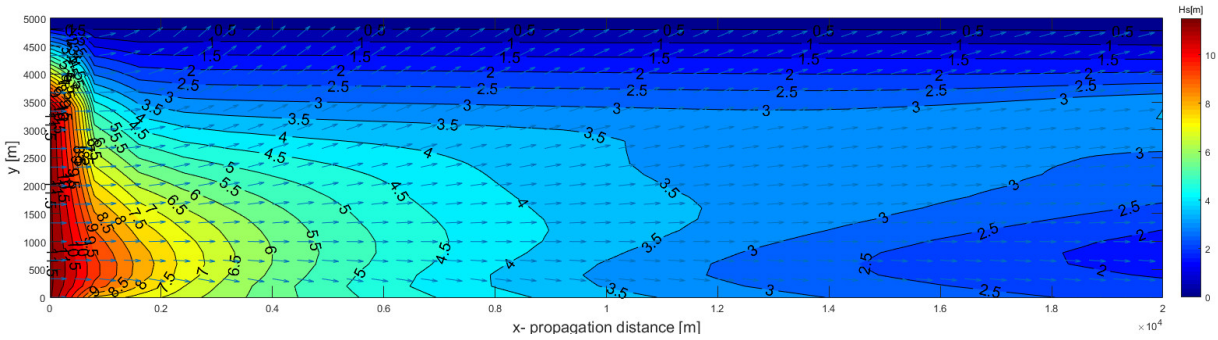

Figure 5-4 The Hs map over the beach area for the slope of 1:200 (maximum depth 25m). All default processes active. Refraction disabled.

Figures 5-2 to 5-4 describe the dissipation in near shallow water (in consideration to the linear wave theory) conditions. The visual assessment at once identifies refraction as the main dissipation mechanism.

The interesting part of **Figure 5-4** is the formation of a boundary layer near shore (due to effect of water depth variation) even thou refraction was not accounted for in the calculations (lack of directional shift).

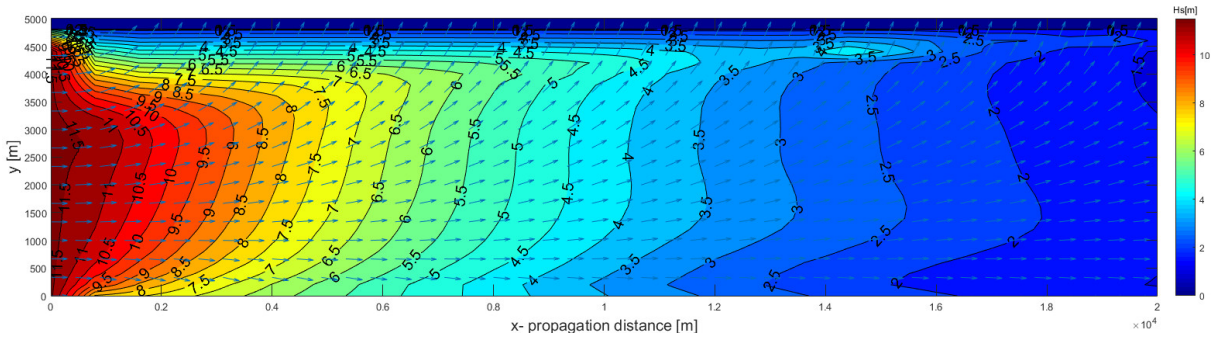

Figure 5-5 The Hs map over the beach area for the slope of 3:200 (maximum depth 75m). All default and investigated processes active.

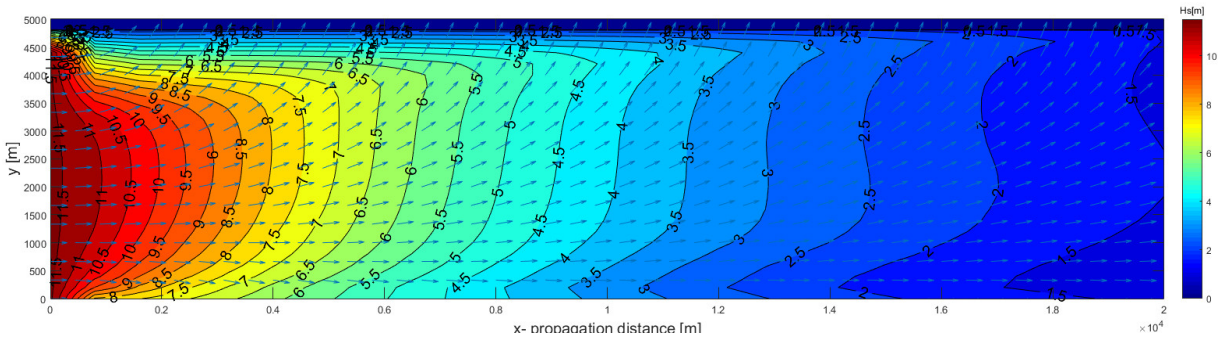

Figure 5-6 The Hs map over the beach area for the slope of 3:200 (maximum depth 75m). All default processes active. Bottom friction and triad interactions disabled.

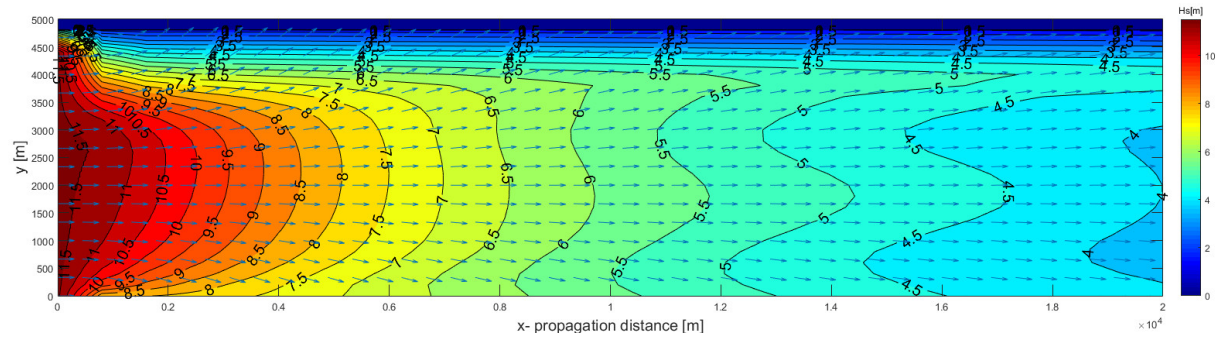

Figure 5-7 The Hs map over the beach area for the slope of 3:200 (maximum depth 75m). All default processes active. Refraction disabled.

Figures 5-5 to 5-6 show the finite water depth conditions for the investigated case. The refraction influence zone is clearly visible at **Figure 5-5** and can be estimated with a value of 3000m. Outside of this zone the refraction will still be present but the rate of directional shift will be smaller.

Influence of the introduced slope on the wave spectrum

The spectral sensitivity analysis was done in respect to two directions – parallel and normal to initial wave propagation (parallel to x and y axis respectively). The analysis was based on an intermediate case of sloping chosen from the modelled group - slope 3:50 (Δd=300m for Δy=5000m). Investigation was conducted for the case where all processes where active.

Figure 5-8 shows the evolution of the spectrum in the y direction. **Figure 5-9** shows the differentiation of energy in the x direction. The investigated positions lay on a line 5 km out from the input boundary. There difference in the observed spectra is the result of three phenomena:

- the developing wave profiles perpendicular to wave propagation direction due to refraction which is shifting into shoaling closer to land (and with the propagation direction shift),

-the difference in the depth along the investigated line,

-the development of the 'boundary layer' profiles parallel to the shoreline (it is a result of bottom depth gradient) – so close to the incident place the flow is not stabilized yet.

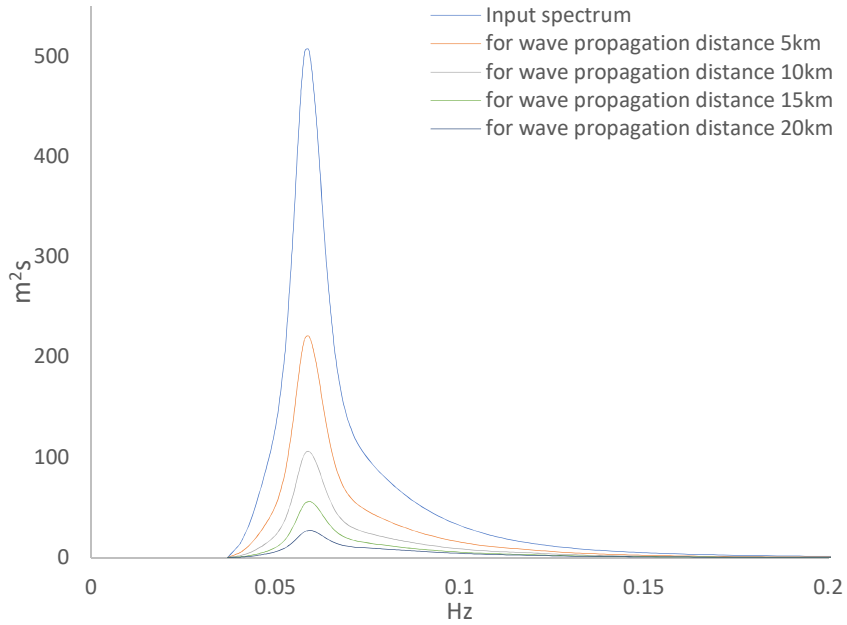

Figure 5-8 Wave spectrum evolution for d=120m (distance to shore 1000m) for slope 3:50 (Δd=300m for Δy=5000m) The investigation taken in the direction of the wave propagation, parallel to shore (constant depth).

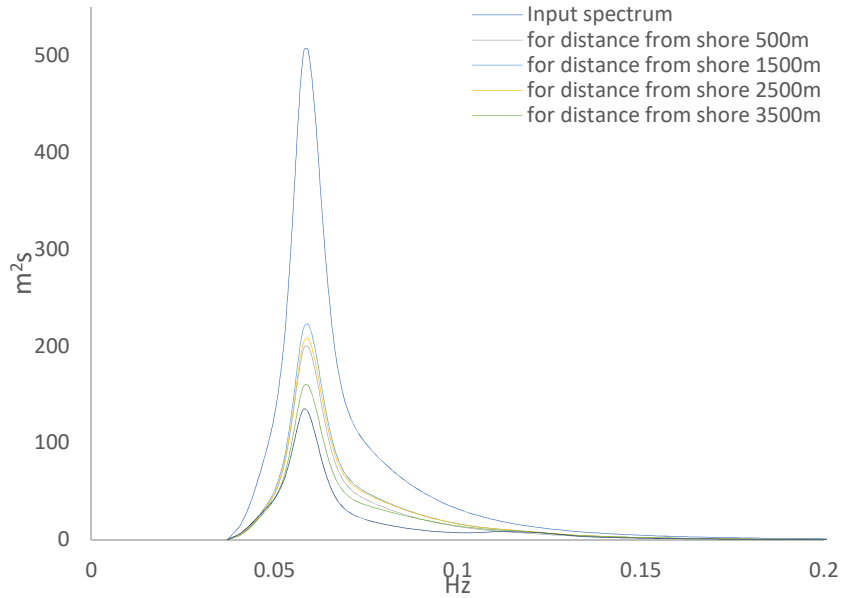

Figure 5-9 Wave spectrum evolution based on distance to shore propagation distance x=5000m. Slope 3:50 (Δd=300m for Δy=5000m). The investigation taken perpendicular to the wave propagation, normal to shore (varying depth)

The difference in the spectrum over a sloped shore is relevant for computation in SWAN when the input boundary is laying in the fjord, on a sloped bathymetry. The spectra should be then modelled to account for the difference in the depth. This influence is easy to have been omitted as engineers are used to calculate the input spectrum at a singular data gathering point.

SWAN can account for the mentioned problem in a number of ways:

- segmented or variable spectra along the input boundary are possible to be modelled,

- a nested series of runs can be used to transfer the characteristics from a less troubling location,

- a full unstructured input taken based on the calculations from a supporting program.

Sensitivity analysis to the slope gradient:

A number of water depths where chosen to investigate the influence of the beach inclination on the significant wave height. The compared results vary with consideration to the distance to shore for each slope value.

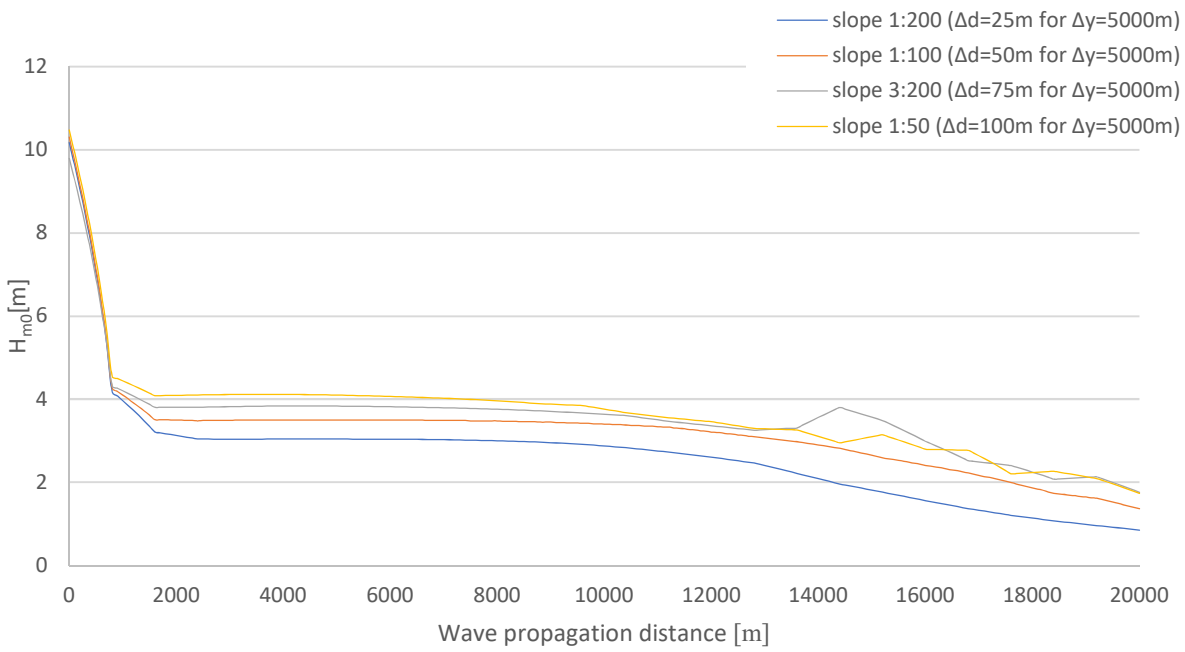

Figure 5-10 Significant wave height as function propagation distance for d=7m. All default and investigated processes active.

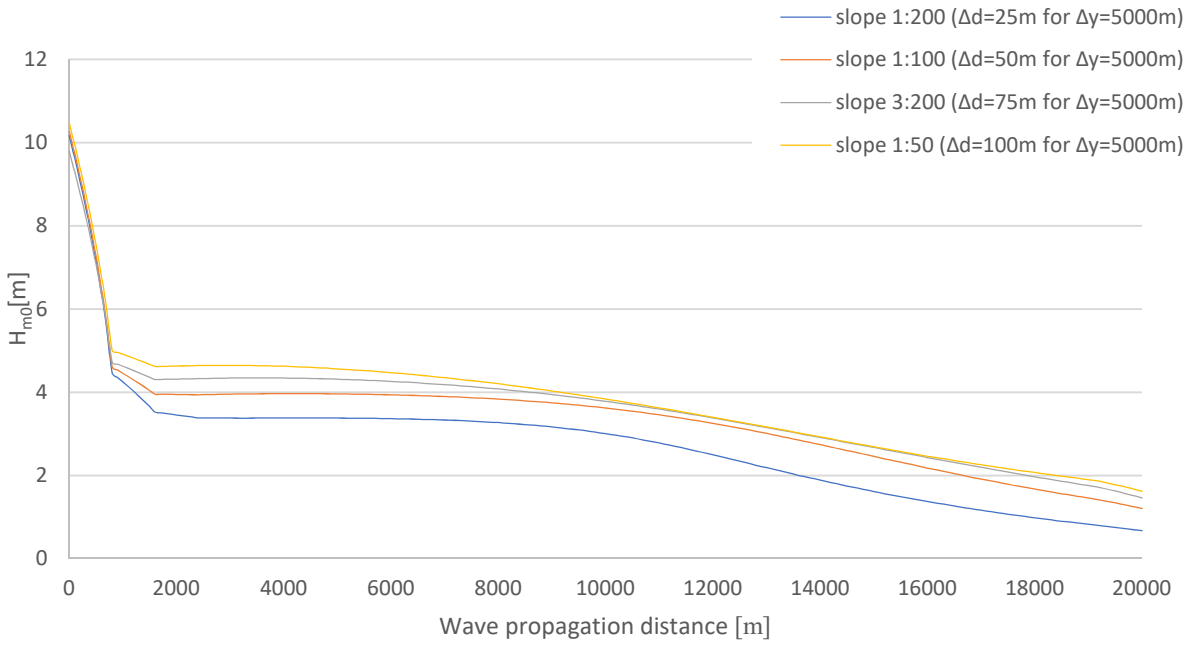

Figure 5-11 Significant wave height as function propagation distance for d=7m (bottom friction and triad wave-wave interaction calculation disabled in SWAN)

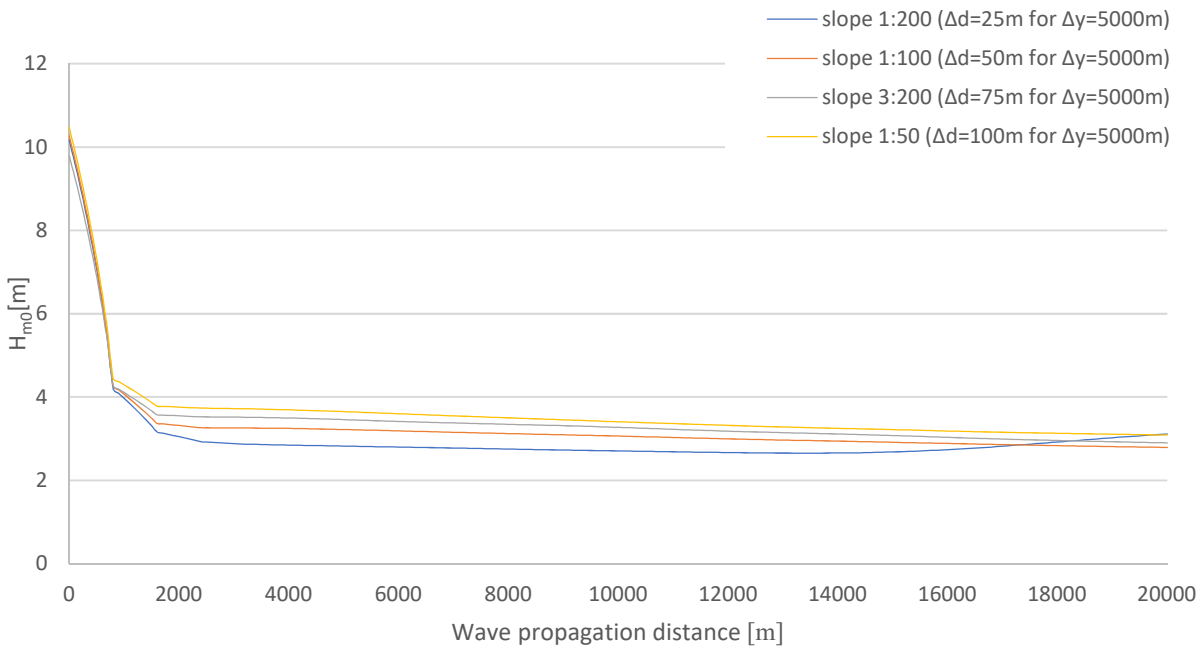

Figure 5-12 Significant wave height as function propagation distance for d=7m (refraction calculation disabled in SWAN

Figures 5-10 and 5-11 show the differences off the significant wave height due to refraction for shallow water case. After the initial turbulence effects dissipated and a typical flow is established (about 2km into the fjord) the refraction becomes the main mechanism for energy loss at the line (after the wave turns other processes take over). The sloping gradient influences the rate of refraction which is reflected in **Figure 5-10 and 5-11**. Once the significant wave height level differentiates in the more regular wave domain the rate of loss of energy seems constant.

In addition to the influence of sloping on refraction the influence of other mechanisms in the shallow waters was investigated. The difference between **Figures 5-11 and 5-10** shows that dissipation due to bottom friction and triad wave-wave interactions is not responsible for a significant energy loss in the wave field (which had to be controlled due to differences in the water depth for the plotted lines). Triad resonance is suspected to be responsible for the waving of value for the significant wave height after 14km of propagation distance in the case described in **Figure 5-10.**

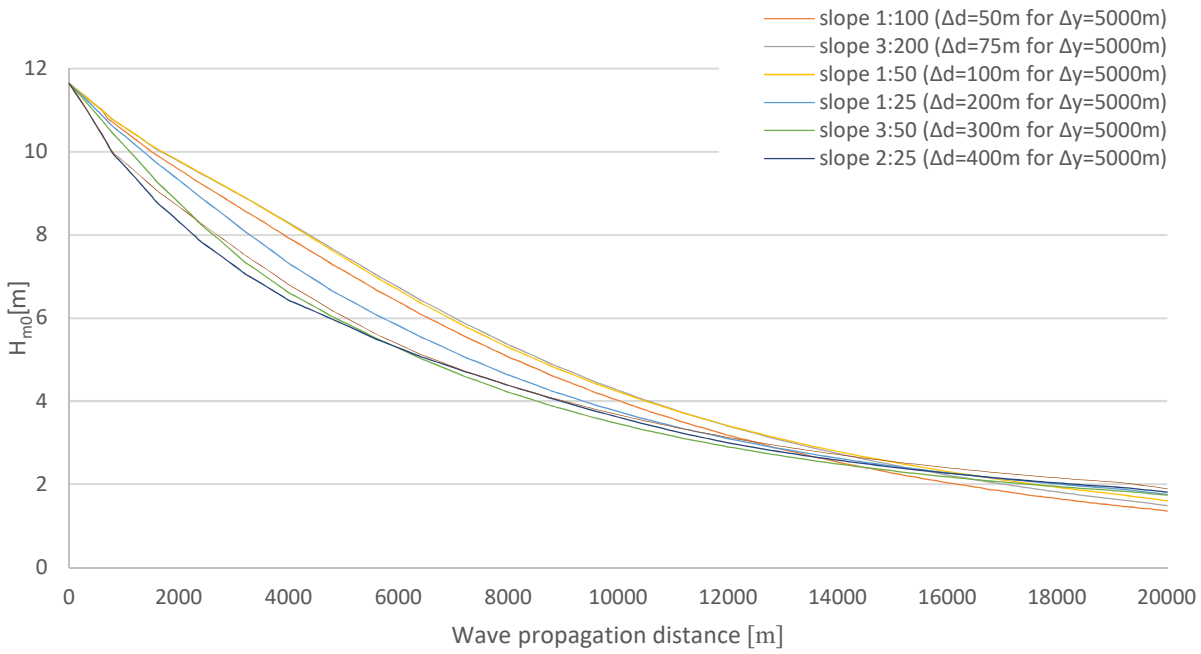

Figure 5-13 Significant wave height as function propagation distance for d=25m. All default and investigated processes active.

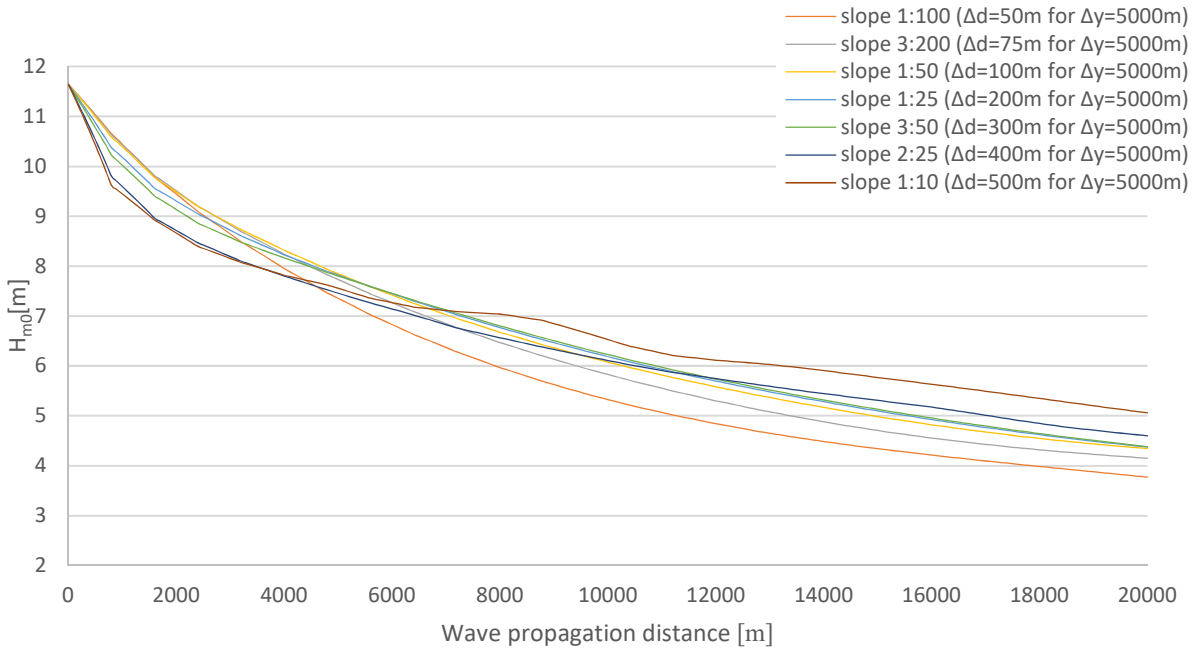

Figure 5-14 Significant wave height as function propagation distance for d=25m (refraction calculation disabled in SWAN)

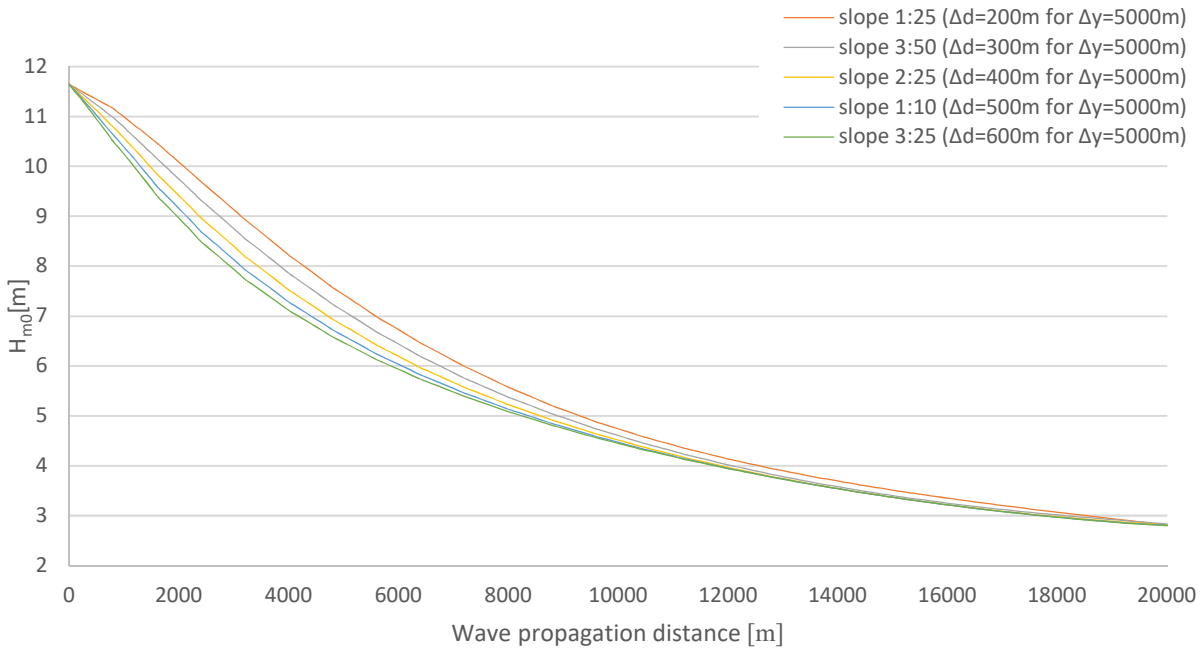

Figure 5-15 Significant wave height as function propagation distance for d=100m. All default and investigated processes active.

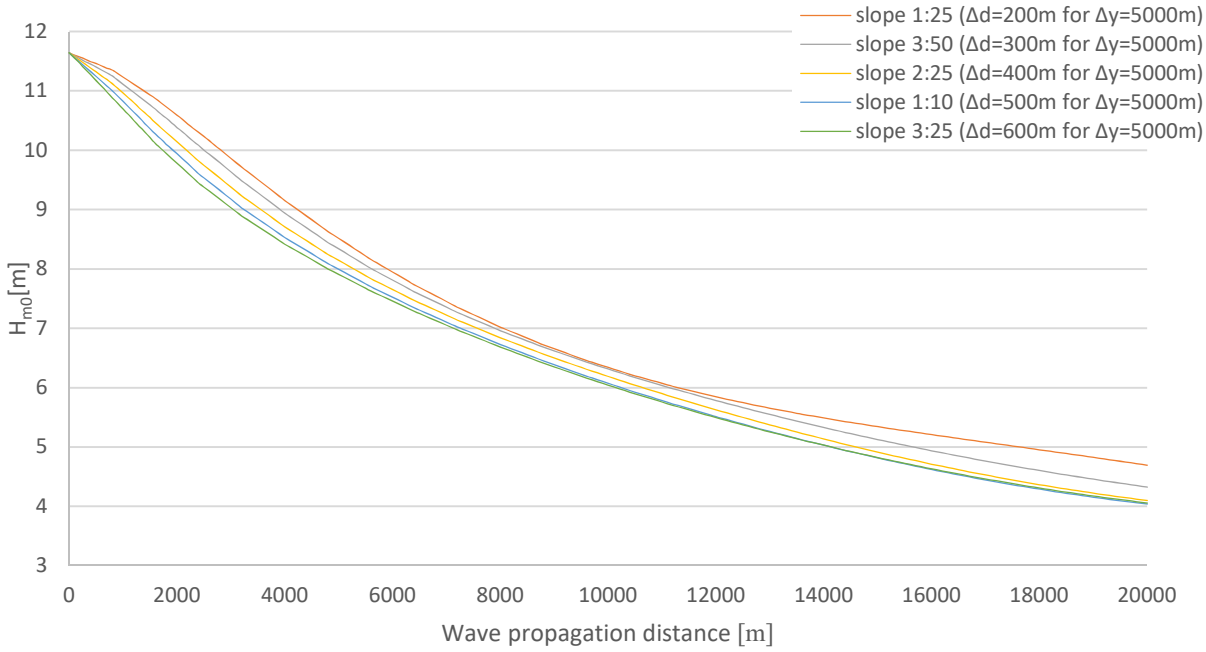

Figure 5-16 Significant wave height as function propagation distance for d=100m (refraction calculation disabled in SWAN)

For **Figures 5-13 to 5-15** (describing the influence of slope variations in finite water conditions) show that for deeper water the incident of a high energy wave (as the inputted spectrum) does not generate unnatural flows. The influence of the refraction is still clearly visible but the rate of dissipation dose not

differentiate the values based on the modelled slope. The wave at this water depth do not 'feel' the bottom which is the suspected cause for indifference of the wave height to the sloping conditions.

5.6 Closed idealized fjord model

The second model group is design to investigate the wave behaviour in a constricted area. The model group was designed in connection to the principals scheme shown in **Figure 5-17**.

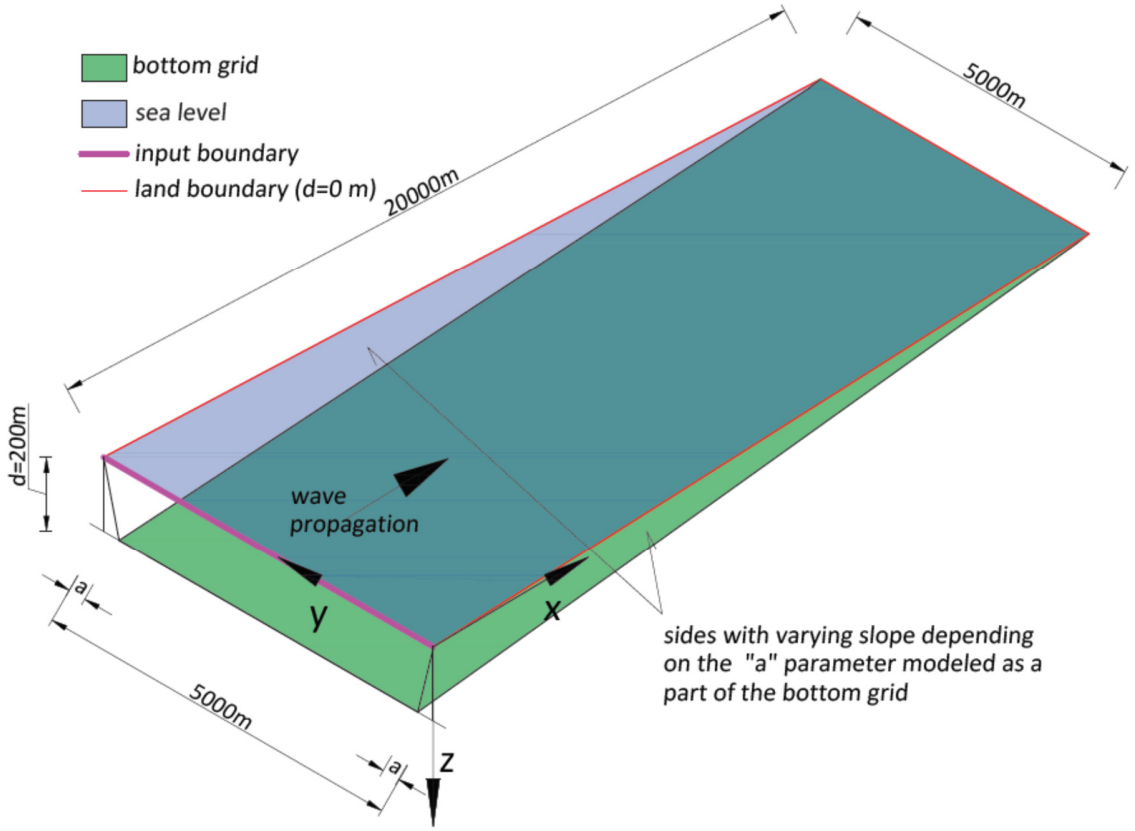

Figure 5-17 The principals for designing the closed ideal fjord model group.

To better visualize the problem analysed one of the bottom grids is shown in **Figure 5-18**.

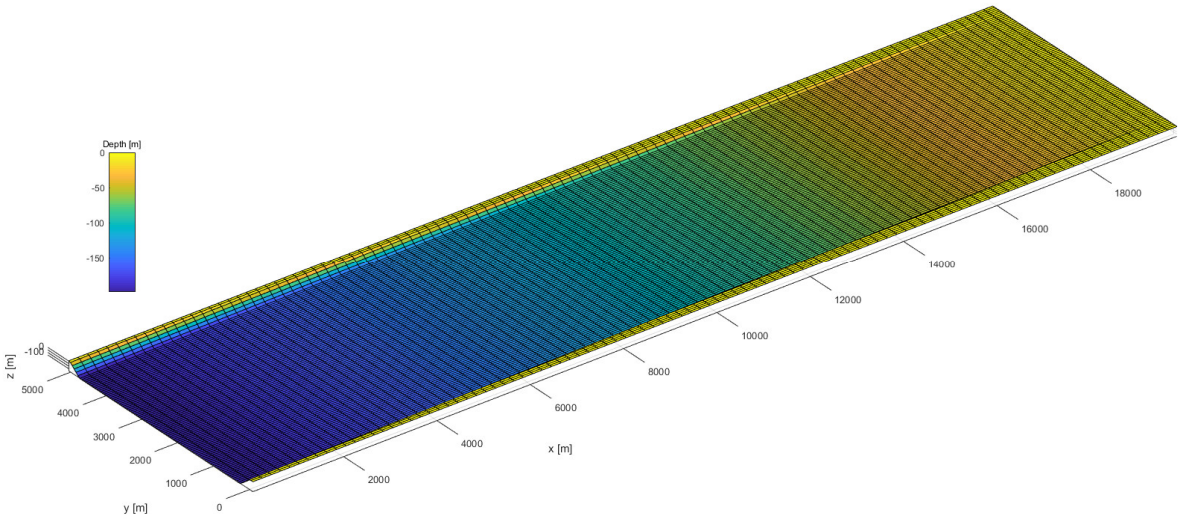

Figure 5-18 A model of the bathymetry grid (for 100m by 100m cells) of the closed ideal fjord. The side slope 8:5 (Δd=125m for Δy=200m).

The varying element for the group is the side slope gradient. With the constant bottom level of -200m for all cases the inclination was modified by the horizontal distance variation *Δy* marked as the ''a'' parameter on **Figure 5-17**. The inclination assumed for models is shown in **Table 5-4**

Table 5-3 List of the closed fjord models analyzed

depth	*Δy* variation	Slope
200	125	8:5
200	250	4:5
200	500	2:5
200	750	4:15
200	1000	1:5

The assumption of constant slope was made: in the longitudinal direction for the main bottom surface, and in the transverse direction for the sides. Two sloping surfaces meeting under these constrains provide that the shape of the models narrows toward the end. The contraction is equal the Δy variation value from **Table 5-2** for each side. This means, in example, that the case with the 1:5 slope (Δy equals 1000) the end will be shorter by 2000m (because of the two side slopes)- refer **Figure 5-20**.

Models due to geometric conditions have a different area cross-section at the input boundary. This results in a difference in total mass of water propagating into the model. The effect of this differences can be investigated with a study of geometry and be controlled with an extra series of models. Due to the time constrains for the report work this investigation was omitted.

The following analyses where conducted for the closed fjord model:

-investigation of the influence of the side inclination gradient (together with the narrowing) on the significant wave height,

-sensitivity analysis to the different dissipation processes for the 1:5 slope model (Δy equals 1000 for Δd=200m).

5.7 Results of the closed ideal fjord analysis

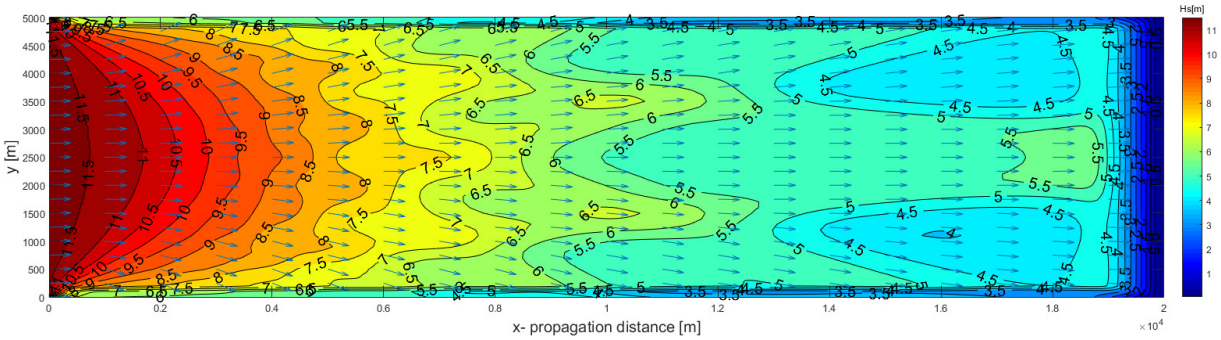

Figure 5-19 The H_s plot for the closed fjord model with the sides constant slope 1:5 (Δy=1000m for Δd=200m)

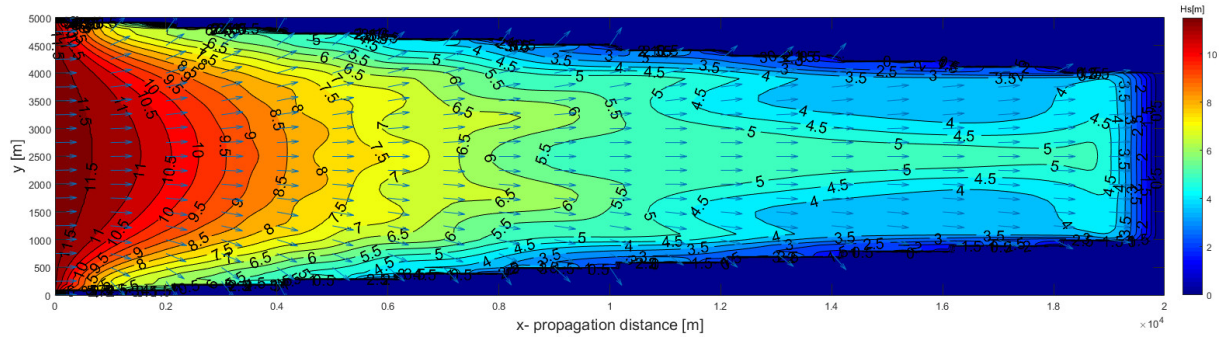

Figure 5-20 Figure 5-21 The Hs plot for the closed fjord model with the sides constant slope 8:5 (Δy=250m for Δd=200m)

Figures 5-19 and 5-20 show the qualitative difference in the sea state developed for the two cases - most differentiated in respect to the side inclination. A clear difference in the wave height is visible in the shallow water area on the right side of the model.

The edgy side line of the plot (between points [0,0] and [20000,1000]) in **Figure 5-20** is the result of the series of interpolations necessary to run for different grids. The results in SWAN are initially calculated only for the nodes of the computational grid based on the interpolated depth value (obtained based on nearest bottom grid nodes). The results are therefore interpolated twice. Those values are afterwards transformed to the locations requested in the output grid node series. The output plotted as a contour map is then redistributed by the calculations done in MATLAB.

In addition, regular cartesian grids where adopted to model a triangular-like shape which provides lacking information in the domain coverage by the mesh at the bathymetry grid boundaries.

The problem is constricted however to the edges of the bottom topography. The interpolation for the more regular bottom surface in the middle of the model provides reliable information.

The whole process of producing a contour plot can result in three level of data interpolation. A full investigation of the process and the uncertainty estimations is an demanding scientific problem. As the complication not entirely connected to this report's topic -it is omitted in the further analysis.

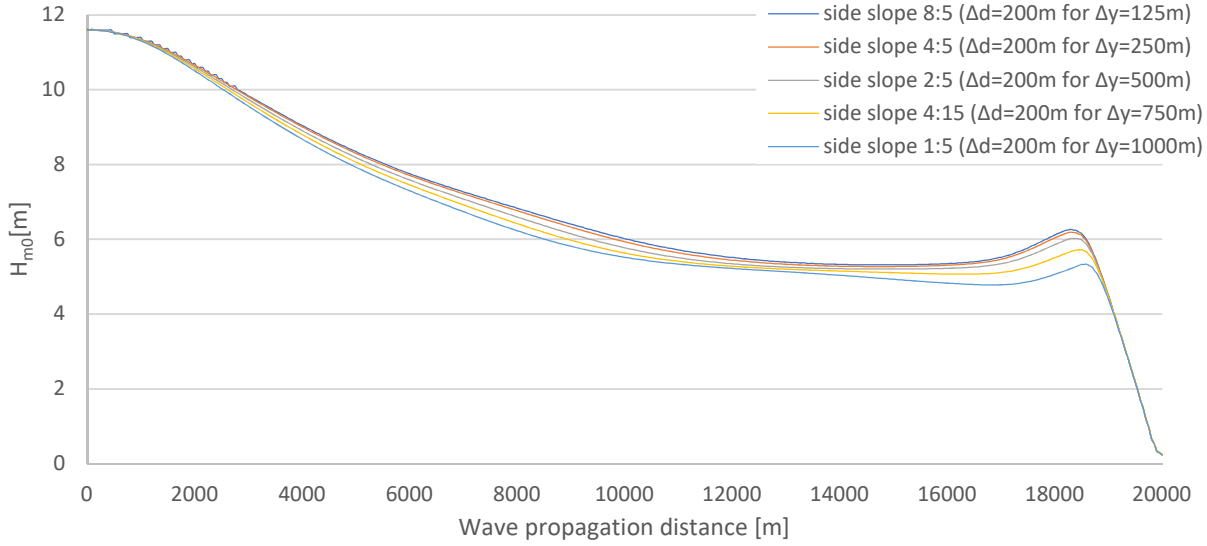

Figure 5-22 Significant wave height as a function of propagation distance for the different models of the closed ideal fjord group. The investigated points lay in the midline of the model in the longitudinal direction.

Sensitivity to slope inclination and fjord narrowing

Figure 5.12 Shows that the biggest influence of the side slope introduction (and narrowing) is shown when the wave approaches the shallow water. The range when wave has cover the distance between 17 and 18.5km is the point where most of the dissipation processes activate.

The bulge in the plot at the 18th km – the amplitude raise, shows the effect of shoaling followed with a rapid decrease of significant wave height due to breaking.

The intense loss of energy in that area begins quicker and is more excessive for more steep sides. The suspect ion is that the intense refraction provided by more narrowed cases prevents wave bunching and increase in the amplitude provided by shoaling.

The result shows that another study for the influence of side steepness should be conducted with a model series that does not introduce narrowing to research the true influence of side's inclinations. The effect of total water volume inputted into the model should be also investigated.

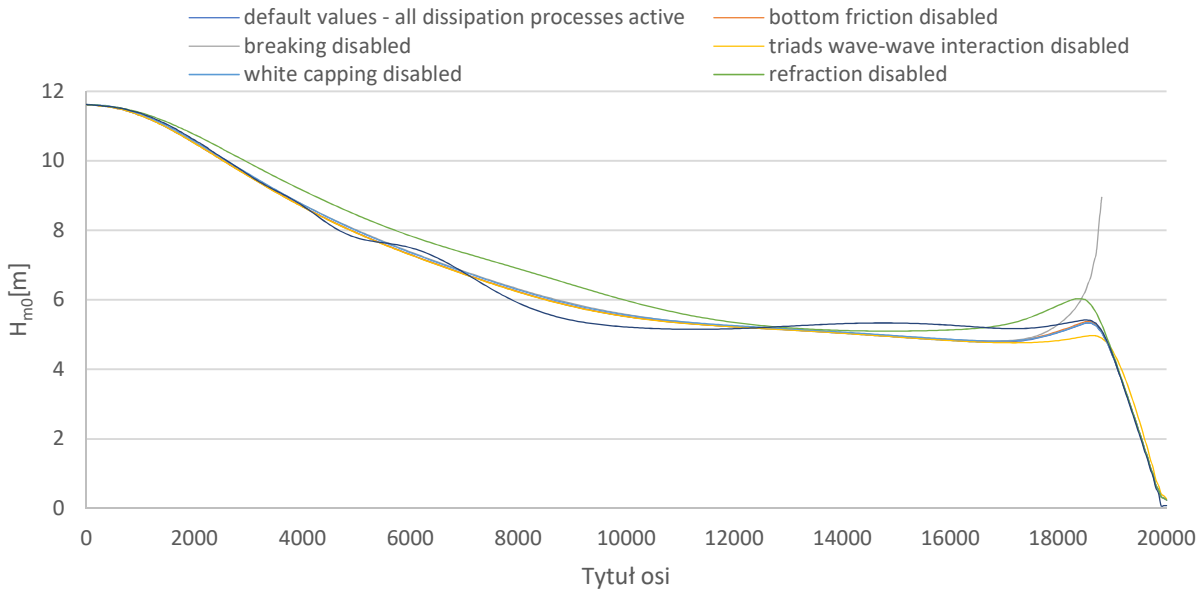

Figure 5-23 Sensitivity study for the influence of different processes for the significant wave height for the 1:5 slope model (Δy equals 1000 for Δd=200m).

Sensitivity to different dissipation mechanisms

Figure 5-22 shows the participation of different dissipation processes on the wave energy. It is shown that refraction is the main dissipation mechanism for the deep and intermediate water. This fact was expected because of the quick contraction of the fjord width. Approaching shallow water, as the waves hit the bottom the water level raises slightly. The energy raise due to shoaling increases the rate of refraction and breaking.

The breaking curve was intentionally stopped at 19km. Further propagation to the shore was increasing the significant wave height but the observations were excluded from the data set to maintain a proper scale for the plot. This was done because with the breaking calculation disabled SWAN has calculated the significant wave height equal to 42m at the shoreline. The value although is in accordance with the theory (for the ideal case of shoaling without breaking the wave amplitude reaches infinity asymptotically – refer **Figure 3-6**) it is highly unrealistic. The lack of breaking in such a case is not feasible in reality.

5.8 Curve introduced in the middle of the ideal fjord model

Bjørnafjord main connection to the open ocean waters is through to inlets (refer **Figure 6-1**). The northern inlet with the total length of ca. 20km has an over 90 degrees curve in the middle of the route. The radius for the curve is similar to the width of the inlet (2.5km). The analysis preformed in **Chapter 6.3** and the rapports by NORCONSULT (Lothe, 2015) and SINTEFF (Stefanakos, 2015) show that this turn stops the propagation of the swell into the fjord (wave crash onto the shore in the far end of the curve). This research show the enormous influence of route turning on the waves in the fjords. The investigations conducted in this chapter are focused on understanding this phenomena.

5.9 Turn of the fjord model description

A simplified model was introduced to investigate the influence of the angle of the turn on the wave field. The governing idea behind the bathymetric model is shown in **Figure 5-23**. The varying parameter for the model is the angle value for the fjord turn. There was a total of 6 bathymetric models prepared for calculations. The angles adopted were: 15°, 30°, 45°, 60°, 75° and 90° for each model respectively.

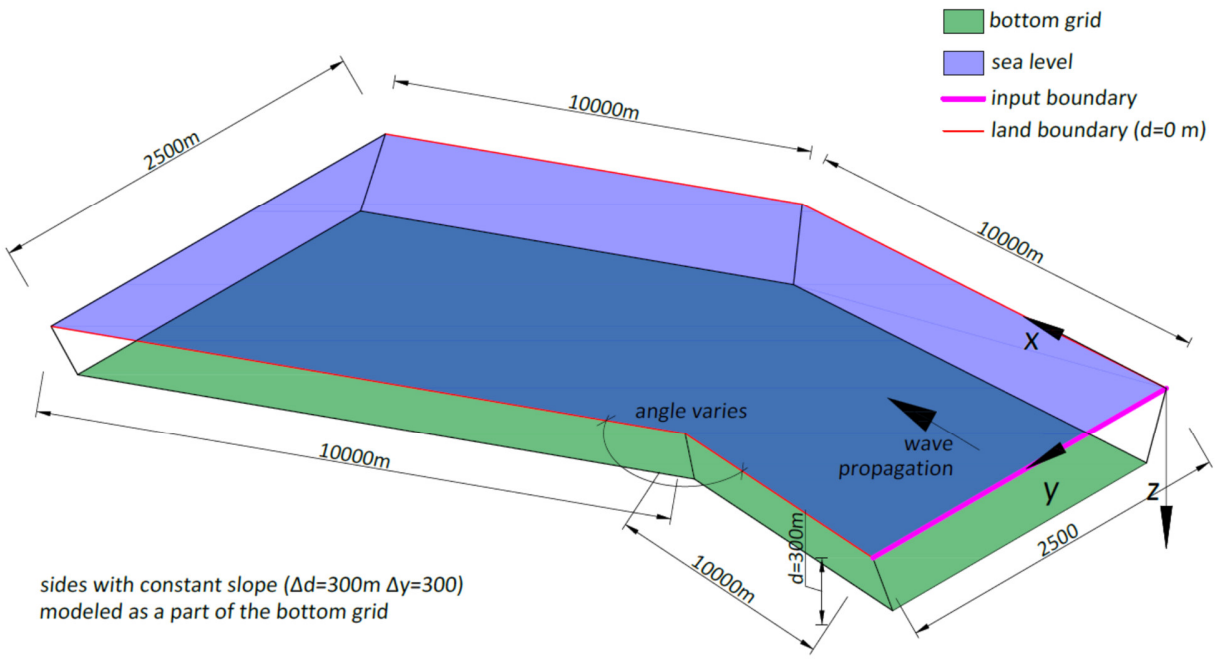

Figure 5-24 The principals for designing the turn of the fjord model group.

Some differences in comparison to the previous model need to mentioned. The depth has been set to 300m, with the assumption of the flat bottom in the middle of the fjord. The sides are modelled as a constant slope of 1:1 ratio (Δd=300m for Δy=300m). Those changes were introduceed to better reflect the conditions found in the Bjørnafjord northern route.

For better visualization of the problem, **Figure 5-24** shows a sample of the model group for the 30° angle.

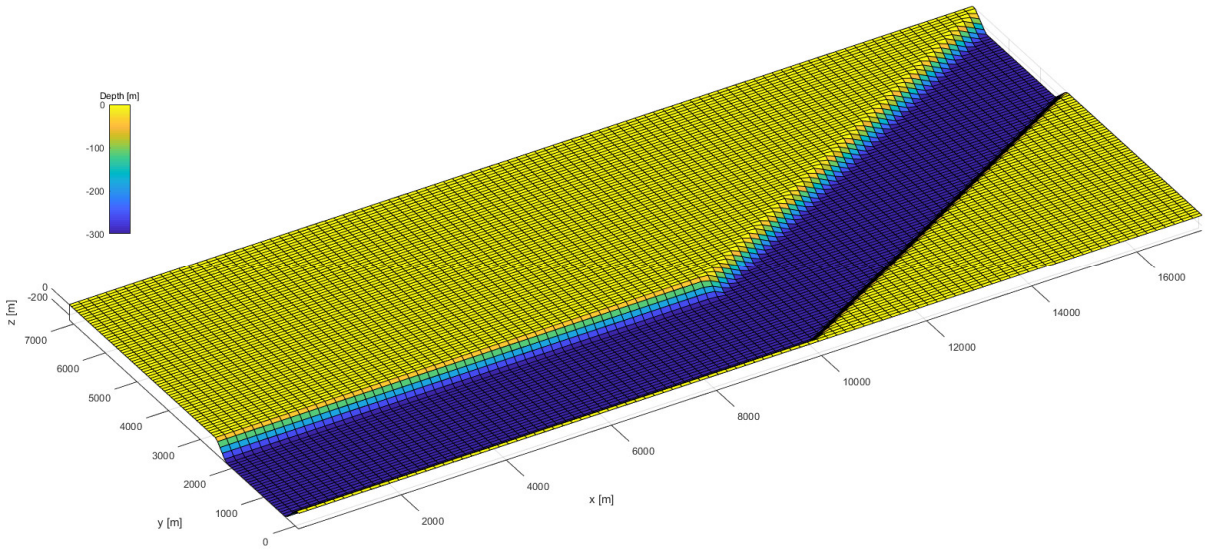

Figure 5-25 A model of the bathymetry grid (for 100m by 100m cells) of the turn of the fjord model for the 30° angle. The side slope are 1:1 (Δd=300m for Δy=300m).

The following analyses were conducted for the fjord turn model:

-investigation of the H_s contour plots in connection to the shape of the wave field,

-investigation of the significant wave height evolution due to propagation over the turn, in the fjord,

-sensitivity of the models to the diffraction and refraction mechanism modelled in SWAN.

5.10 Results of the analysis of the turn model.

Figure 5-25 to 5-27 describe the wave field propagating through the bathymetric curve. The plots were prepared for the default dissipation processes available in SWAN (with the refraction and diffraction calculations enabled).

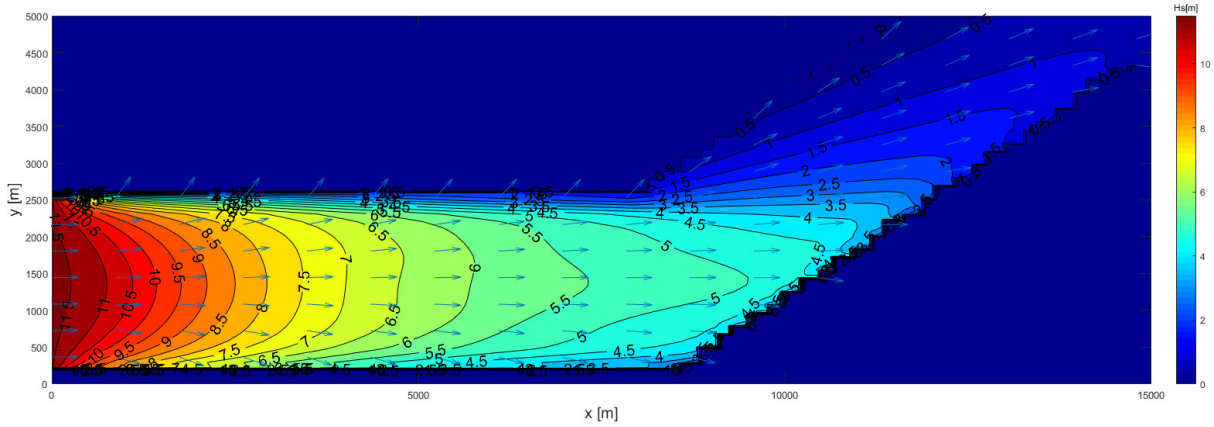

Figure 5-26 Contour plot of the Hs values for the wave field propagating through a 30° angled curve in the ideal fjord.

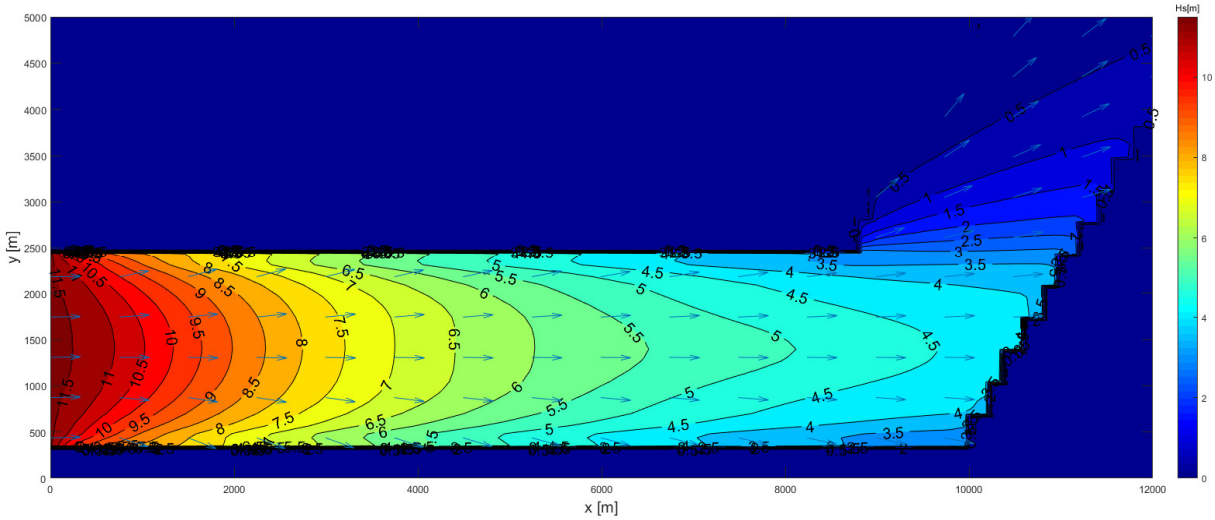

Figure 5-27 Contour plot of the Hs values for the wave field propagating through a 60° angled curve in the ideal fjord.

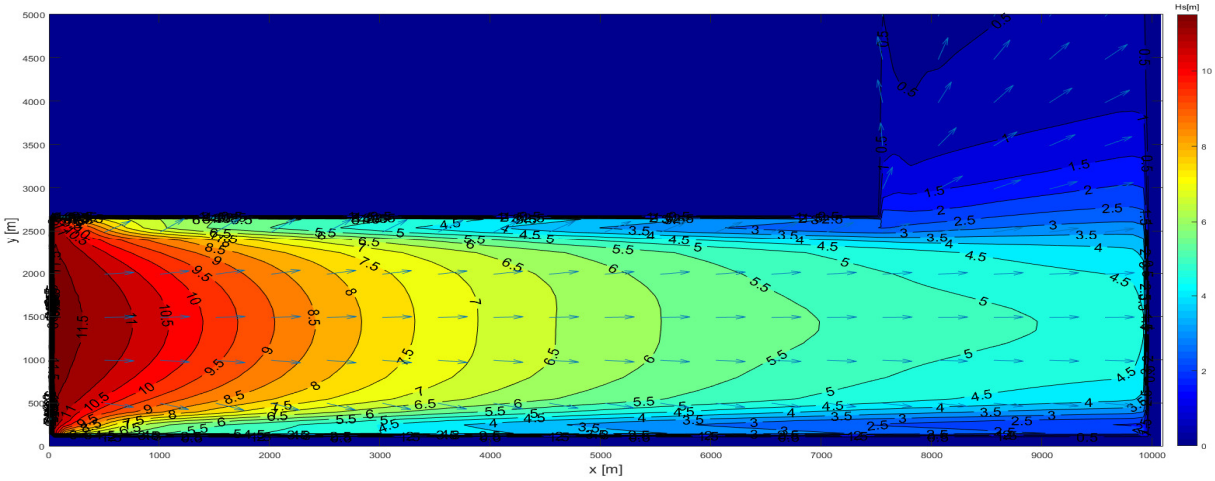

Figure 5-28 Contour plot of the Hs values for the wave field propagating through a 90° angled curve in the ideal fjord.

Figure 5-25 shows the considerable decrease in the wave height due to influence of the curve. The wave field before the turn shows a typical development for a symmetric channel, with the highest wave energy in the middle (at the deepest area) and the waves refracting towards the sides. The directional field shows that after the turn the rate of refraction dose not manage to induce waves propagation towards the left side of the model. The highest waves energy tend to propagate on the right side. There is suspected a local, slight increase in water level on the right side that produces a surge further towards the end of the model. The participation of refraction, diffraction and surging water volumes on the wave field requires further investigation. The element of reflection that may be crucial for this case was not analysed due to complex modelling requirements in SWAN for this mechanism.

Figure 5-26 shows the evolution of the contour. With the increasing angle the range for the influence of the input spectrum decreases.

Figure 5-27 shows that for the incident with a straight angled curve with a radius small (2500m) in relation to the wave length, almost all wave energy is absorbed by the shore. The waves with the significant height of 1 -1.5m range propagating after the curve are assumed to be the effect of resonance of the surge water.

Incidents in **Figures 5-25 to 5-26** are of a turbulent nature. The significant wave height being a characteristic of a statistical spectrum of the total incoming waves dose not illustrate this properly. The lack of reflection provides to a high uncertainty in the results obtained.

Sensitivity to the turn with the angle as the governing parameter.

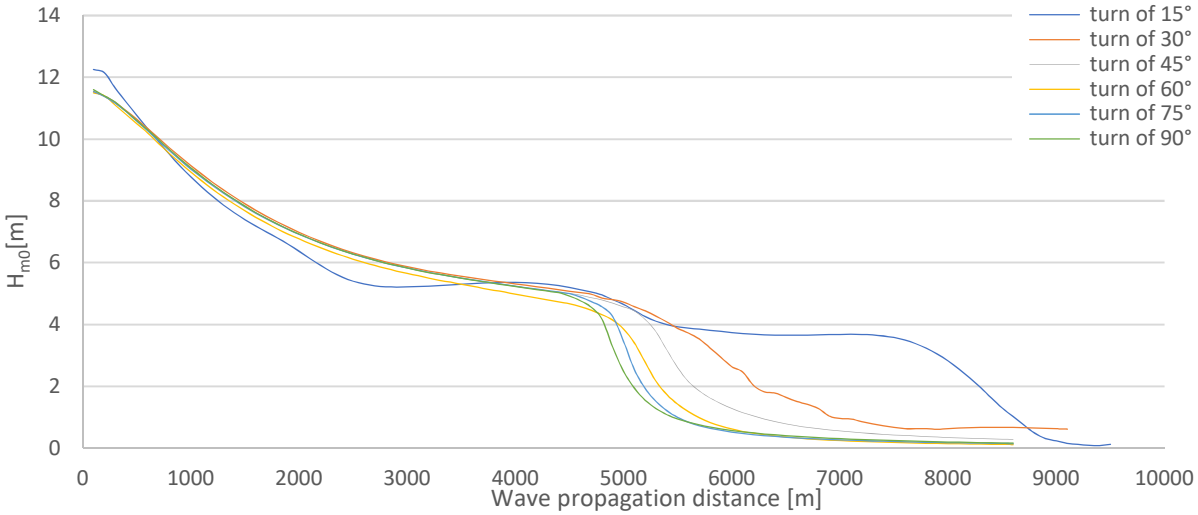

Figure 5-29 Significant wave height as function of propagation distance for the different values of the angle governing the turn. All dissipation processes are active in SWAN.

Figure 5-29 shows that the input wave do not manage to travel through a curve introduce for such a narrow width. A correlation between the angle of the turn and the distance the wave travels is visible. The drop in the significant wave is most abrupt in the case of angles wider than 60 degree. For smaller angles some energy seems to propagate through the curve but dissipates afterwards due to refraction as the waves are forced to travel along the right side - near shore.

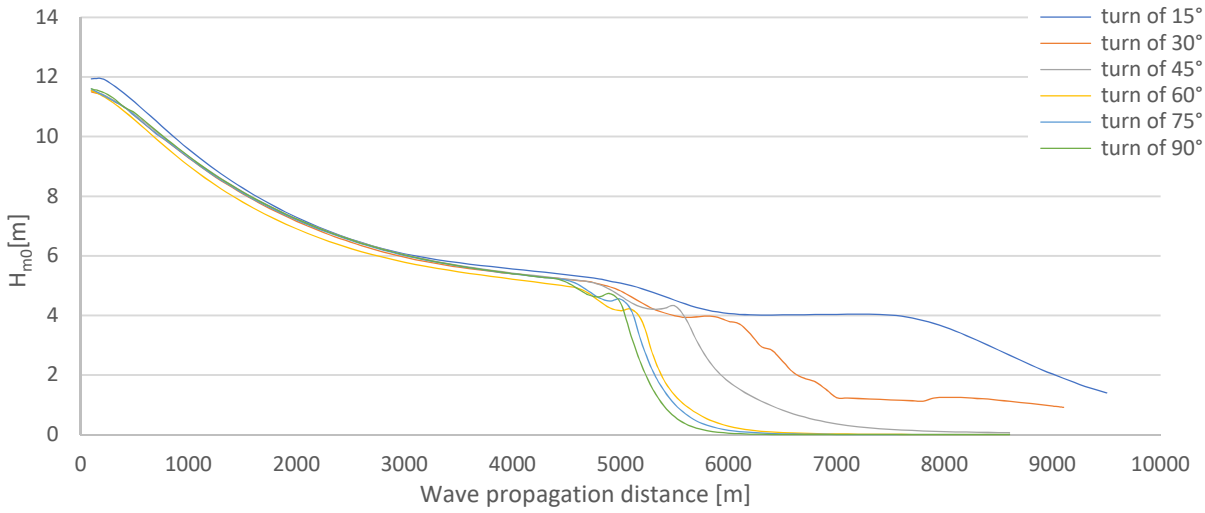

Figure 5-30 Significant wave height as function of propagation distance for the different values of the angle governing the turn. All default dissipation processes are active while refraction is disabled in SWAN.

With the loss of rarefaction influence (shown in **Figure 5-30**) the model loses less energy in the first part of the channel increasing the significant wave height at the swing location. The comparison between **Figure 5-30 and 5-29** shows that refraction is the main dissipation mechanism after propagation over the turning point.

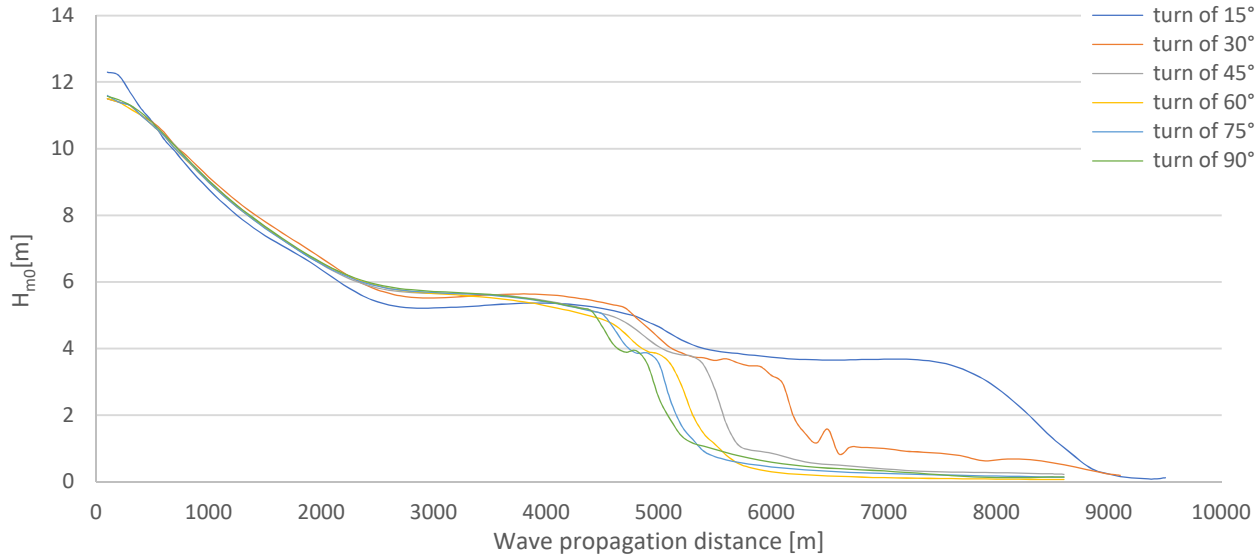

Figure 5-31 Significant wave height as function of propagation distance for the different values of the angle governing the turn. All default dissipation processes are active while diffraction is disabled in SWAN.

Figure shows that diffraction plays a negligible role in the wave directional shift in this case. The diffraction calculation according to SWAN (2015) are also only an estimation. Diffraction is not enabled in the default set up of processes in SWAN.

6 The Bjørnafjord bathymetry simulation in SWAN

6.1 Introduction

Bjørnafjord located near Bergen is one of the fjord mentioned in the ferry free E39 motorway connection project. Obtaining a proper estimate of the design wave conditions is therefore crucial for the design of the future bridge.

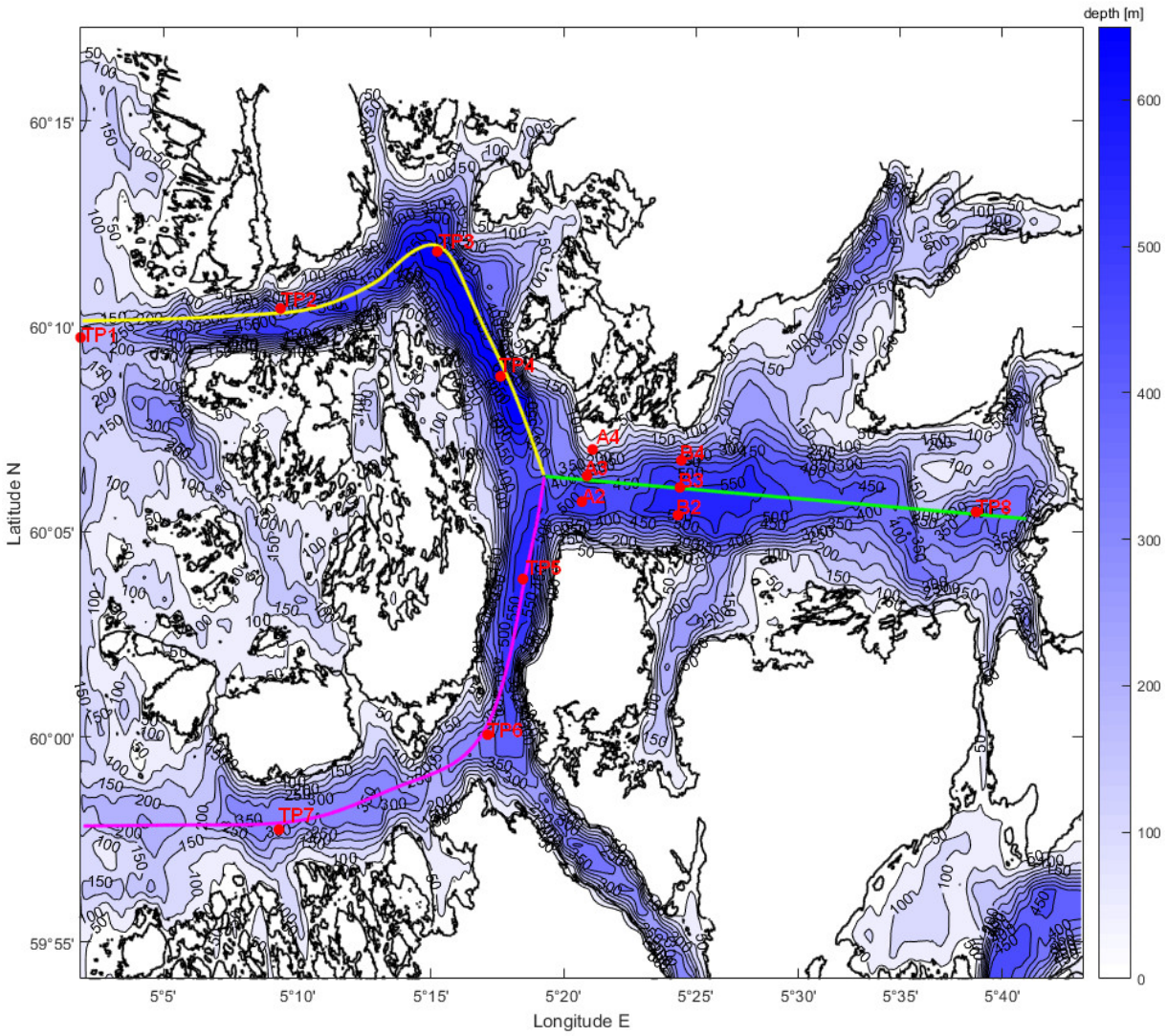

Figure 6-1 Bathymetry of the computational grid for the Bjørnafjord calculations with target points and routes adopted for calculations

For such a complex basin precise bottom input is required for estimation. Bathymetry maps were acquired from Kystverket (in the WGS-84 UTM 33N coordinate system). Maps obtained in the form of GIS data (shapefiles together with the coordinate system data) where discretised in MATLAB to obtain a regular grid.

The goal of the analysis is to obtain wave characteristics at the planed bridge locations -target points. Overview of the target locations can be found in the table 6-1 - after Stefanakos (2015).

Beside of the values in the bridge location contour maps of the significant wave height were created for each analysed case.

A sensitivity analysis of the influence of different dissipation process was conducted for three curves (refer **Figure 6-1**). The lines describe the northern (yellow), southern (purple) and eastern (green) routes. The division of the investigated curve is based on the different forcing mechanism that are dominant for the respective areas: forcing from the southern or northern fjord inlet or wave generation by wind for the eastern sector.

Table 6-1 Target point locations for the Bjørnafjord analysis

Target point	Latitude [deg]	Longitude [deg]
TP1 (input point)	60° 08’ 00’’ N	4° 57’ 00’’ E
TP2	60° 09’ 25’’ N	5° 06’ 20’’ E
TP3	60° 11’ 20’’ N	5° 13’ 25’’ E
TP4	60° 08’ 35’’ N	5° 17’ 20’’ E
TP5	60° 03’ 50’’ N	5° 19’ 50’’ E
TP6	60° 00’ 00’’ N	5° 19’ 15’’ E
TP7	59° 57’ 00’’ N	5° 10’ 00’’ E
TP8	60° 07’ 00’’ N	5° 41’ 00’’ E
A2 (first proposed bridge position)	60° 05’ 53’’ N	5° 22’ 06’’ E
A3 (first proposed bridge position)	60° 06’ 31’’ N	5° 22’ 10’’ E
A4 (first proposed bridge position)	60° 07’ 10’’ N	5° 22’ 15’’ E
B2 (second proposed bridge position)	60° 05’ 54’’ N	5° 26’ 47’’ E
B3 (second proposed bridge position)	60° 06’ 34’’ N	5° 26’ 41’’ E
B4 (second proposed bridge position)	60° 07’ 13’’ N	5° 26’ 34’’ E

6.1.1 Input parameters

Input boundary was designed at the TP1 position. The values of the wave characteristics were taken from SINTEF rapport by Stefanakos (2015). The additional reason for assuming those values is the possibility to compare the output values for the preformed analysis. The differences in the modelling technique in SWAN will be commented on in the second part of this chapter.

Table 6-2 Input parameters for the incoming swells based on (Stefanakos, 2015)

Target point	H_s [m]	T_p [s]	θ_{wave} [deg]
TP1	12.85	14.08	269

6.1.2 Sensitivity studies

Two sensitivity studies were conducted in regard to the computational and the bottom grid resolution to help obtain the most economic (in regard to computational efforts) combination of parameters. The sensitivity to the computational grid was conducted for constant of 75m by 75m bottom grid whereas the bottom grid sensitivity adopted a 75m by 75m computational grid.

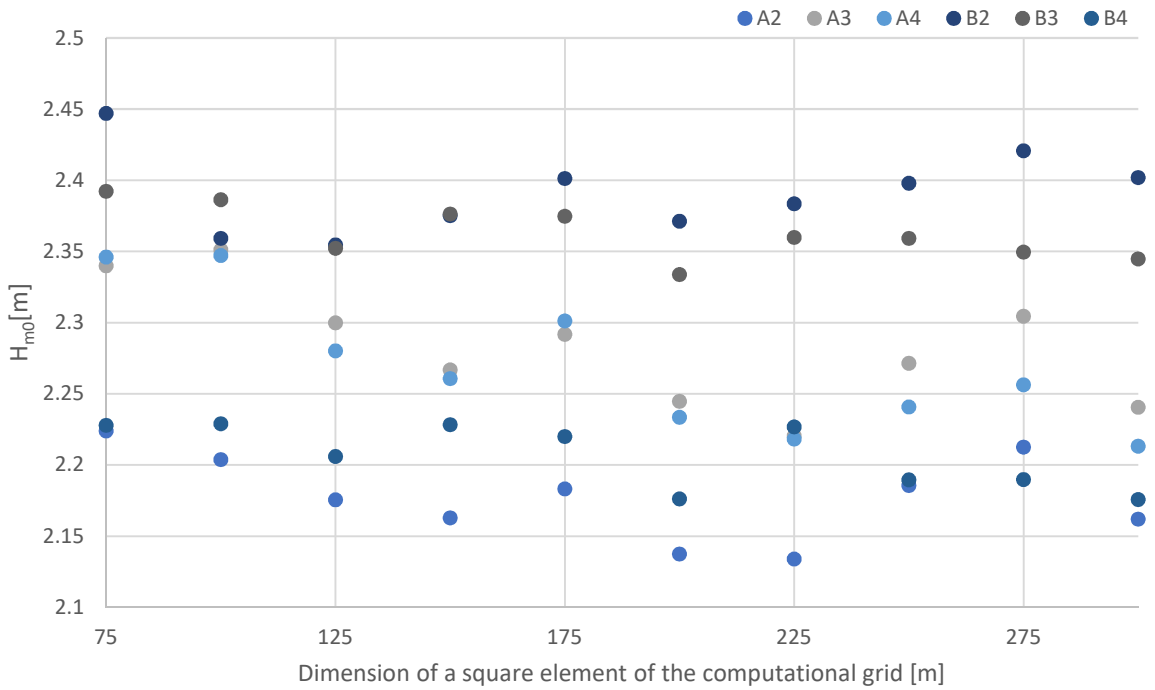

Figure 6-2 Sensitivity analysis of the computational grid resolution for Bjørnafjord modelling.

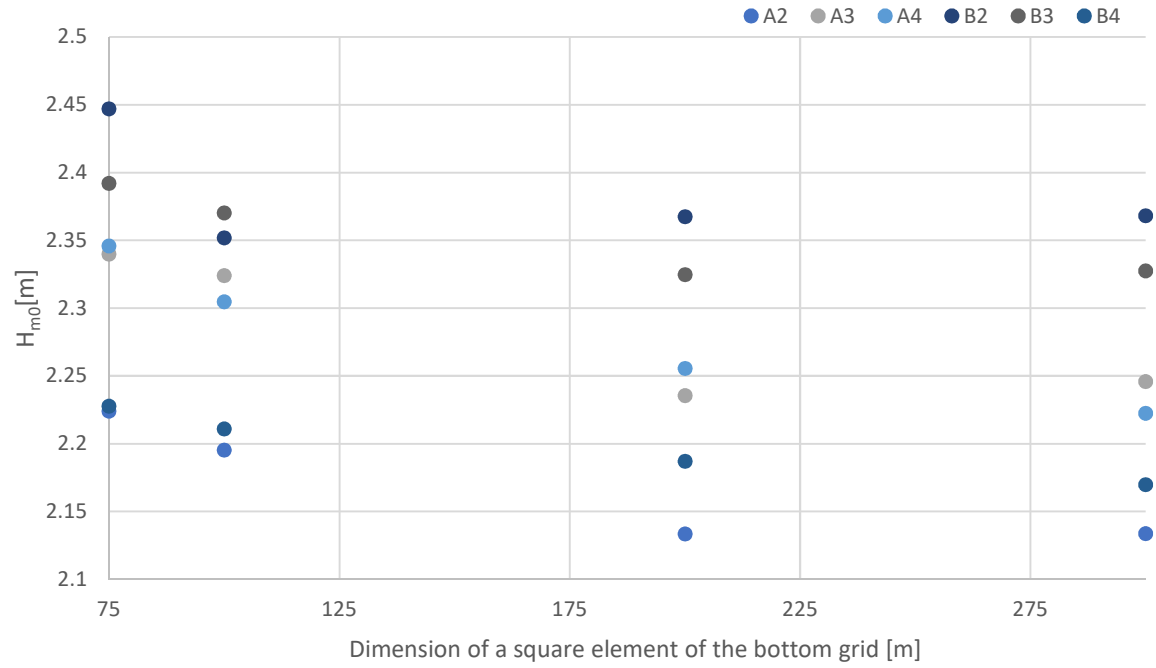

Figure 6-3 Sensitivity analysis of the bottom grid resolution for Bjørnafjord modelling.

The models analysis results seem to show moderate sensitivity to grid resolution. The maximal differences of 0.2 m (around 10% of the value of obtained H_s at investigated locations) significant wave

height at the target locations can be neglected for rough estimations but a higher density should be assumed for final analysis. The trends in both studies showed to the identical bottom and computational resolution (cell of 75m by 75m) as the best solution for modelling the problem at hand.

With the 2 hours as the longest time needed for one run, this grid resolution was acceptable both for the computational grid and the bottom grid. The resolution was further adopted as the basic output grid used as the basis for plotting the contour maps for H_s. The additional advantage resulting from the fact of identical grid resolutions is omitting the internal interpolation of data in SWAN for the bottom level or the requested output parameters. This helps to reduce the uncertainty level. The only interpolation step was conducted in MATLAB for the contour plotting command.

Higher resolutions were tested but calculations resulted in a non-acceptable number of errors that prematurely ended the initial computations.

The computational grid and the bottom grid were taken between [59° 52’ 00’’N and 60° 18’ 00’’ X 4° 57’ 00’’E and 5° 50’ 00’’ E]. Due to topography and bathymetry conditions no relevant (effect of the boundaries in the north- and south- west corners is negligible) water boundaries without wave input were present thus no possibility of leakage of energy due to refraction to open ocean. The area covered by those grids is shown in **Figure 6-1** and all the other maps.

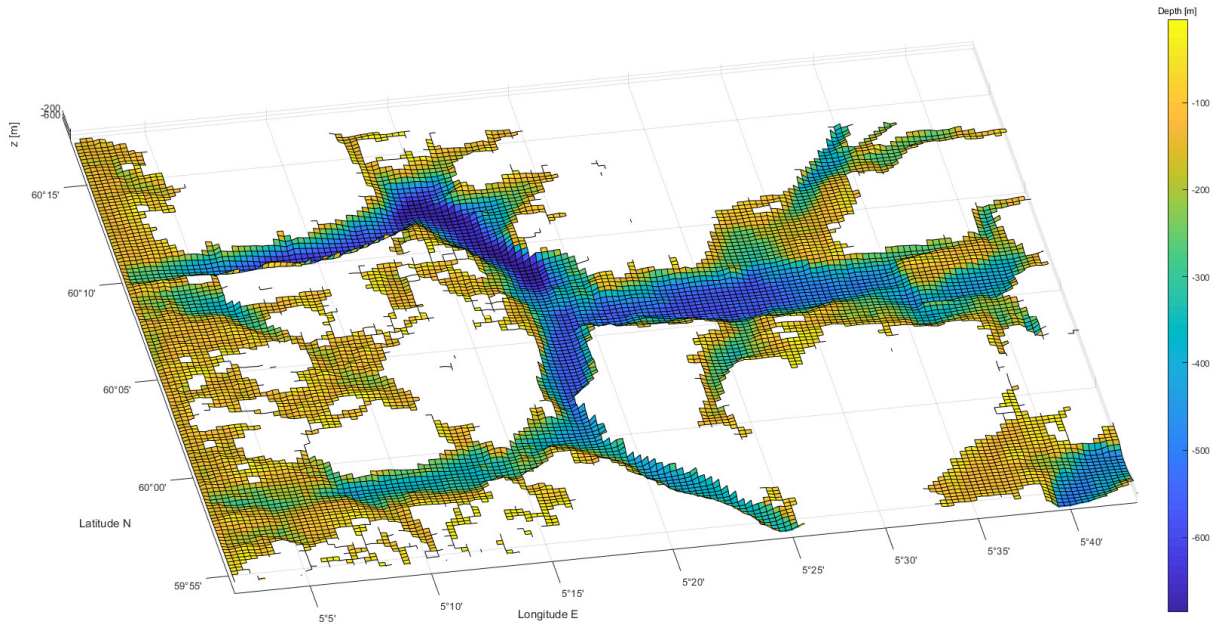

Figure 6-4 Bottom topography input grid with a cell size equal to x=300m and y=300m.

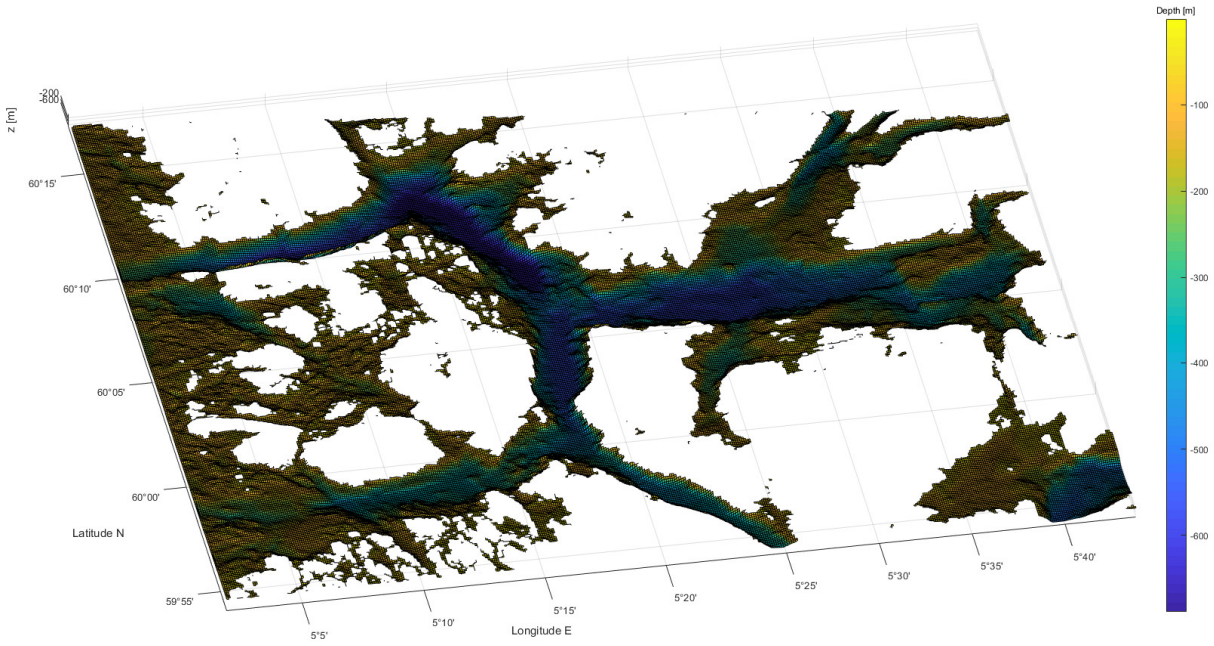

Figure 6-5 Bottom topography input grid with a cell size equal to x=100m and y=100m.

Figures 6-4 and 6-5 show the difference in the precision of reproducing the bottom topography for different mesh sizes. The visual assessment and the initial analysis indicates that the additional roughness in the case of the second grid would have a strong influence on the obtained results. **Figure 6-3** shows that the real differences at the bridge positions are lesser than expected – this is due the fact that most of the wave energy is transferred in the deep water areas. The areas with deep water conditions have low sensitivity to bottom topography. This indicates that smaller bottom grid resolution can be used for obtaining reliable results (for deep water conditions at the incoming waves route and investigated locations).

Due to the variety of data sources and the differences in the coordinate system descriptions in the software used a unified coordinate system has been applied for the following description- refer **Figure 6-6.** The system is adopted from the Cartesian coordinate system notation for the SWAN application.

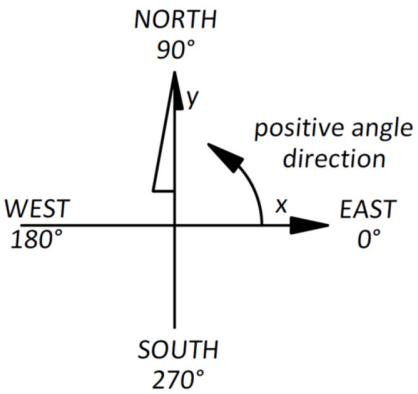

Figure 6-6 Coordinate system adopted for Bjørnafjord model description.

6.2 Modelled cases

Modelling followed all the basic assumptions used for the simplified models (refer **Chapter 5.1**)

The list over analysis (not including the sensitivity cases) is shown in **Table 6-3**

Table 6-3 Input for the analysed cases for Bjørnafjord

Name	Wave input				Wind input	
	Input boundary	HS [m]	T_p [s]	Direction [deg]	Velocity [m/s]	Direction [deg]
Swell waves *	West	12.45	14.08	1	-	-
Wind sea *	West	-	-	-	33	1
Total sea *	West	12.45	14.08	1	33	1
Eastern region *	-	-	-	-	35	180
Eastern region *	Initial condition	0.20	4.00	180	35	180
Eastern region *	-	-	-	-	35	180
Eastern region *	Initial condition	0.20	4.00	180	35	180
Case 1**	West	5.00	12.00	0	25	300
Case 2**	West	5.00	12.00	0	25	60
Case 3**	West	5.00	12.00	0	-	-

* - based on Stefanakos (2015)

** - modelled after Lothe (2015)

6.3 Bjørnafjord analysis -result and discussion

6.3.1 Swell waves

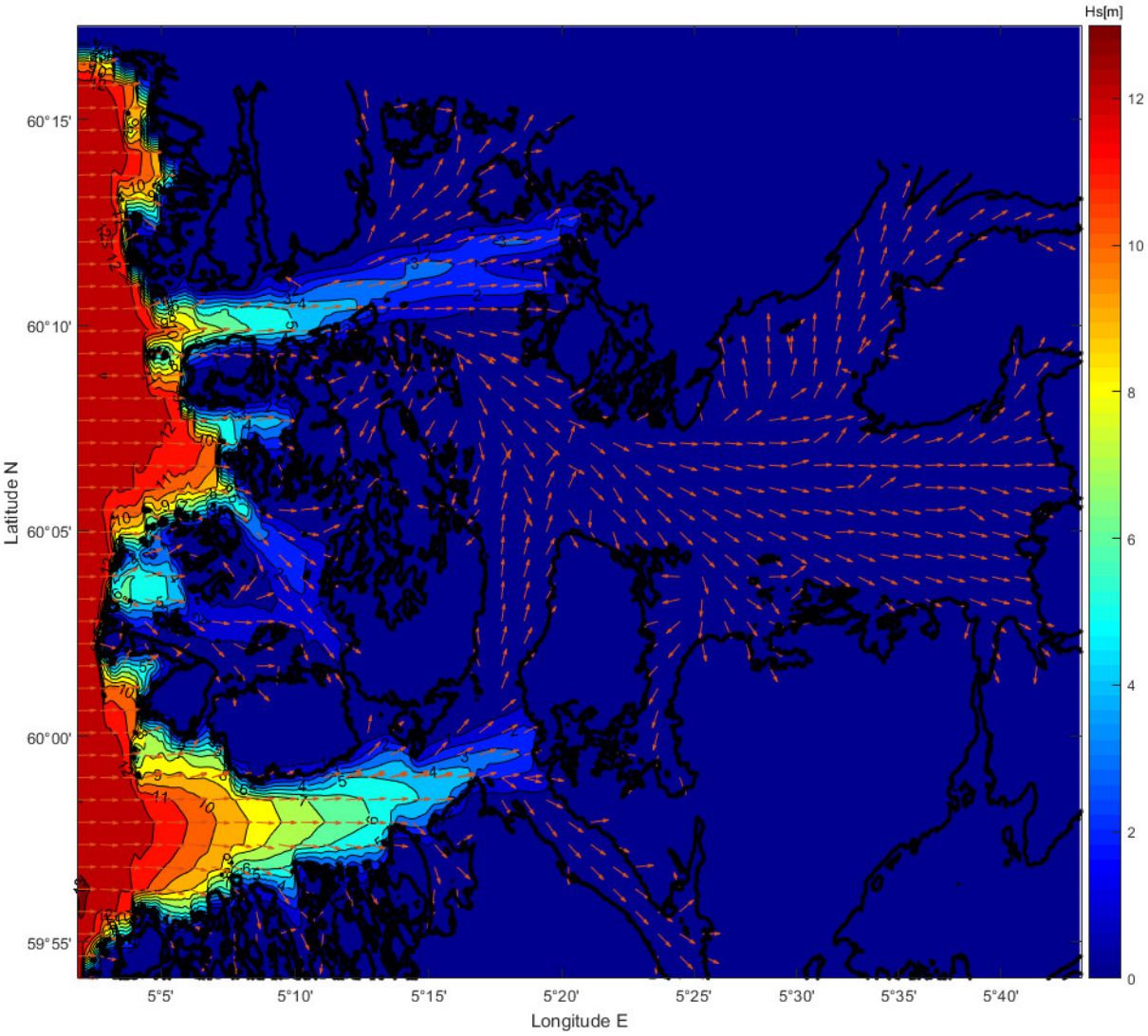

Figure 6-7 Bjørnafjord- Hs map for wave input if Hs=12.48m and Tp=14.08s DIR= 1° with no wind input.

The incoming swell waves for the winter season are presented on **Figure 6-8**. In accordance with the results obtained in **Chapter 5.9** the incoming waves do not manage to shift the propagation direction at the turns of the inlets. The energy is lost due to the waves coming ashore, both in the southern and the norther route. Due to that fact we can see that the offshore conditions have little influence on the wave regime in the isolated estuaries refer **Table 6-4**.

The analysis conducted in Stefanakos (2015) and Lothe (2015), discuss widely the case of the dominant forcing inlet for the incoming waves in the bridge position. The quiver plot describing the mean direction of propagation (**Figure 6-8**), together with the direction obtained for the

bridge position (**Table 6-4**), in this scale are not conclusive in regard to the topic of governing forcing wave direction. Based on the basis of all conducted analyses it was established that the norther route delivers a greater input for the bridge positions in regard to the wave energy transferred.

Table 6-4 Results for the wave characteristics obtained for the bridge positions for the incoming swell case.

Target point	A2	A3	A4	B2	B3	B4
H_s [m]	0.009	0.169	0.236	0.09	0.086	0.053
T_p [s]	17.15	14.09	13.93	13.79	14.03	13.99
θ [deg]	263	315	323	323	335	347

The significant wave pattern analysed from the western direction shows that the main dissipation mechanism in the norther and southern approaches are refraction and the development of the boundary conditions at the side of the channels. The wave field evolution is in accordance with the findings described for the ideal beach case of the closed fjord analyses (refer **Chapters 5.8 and 5.7**).

6.3.2 Wind sea

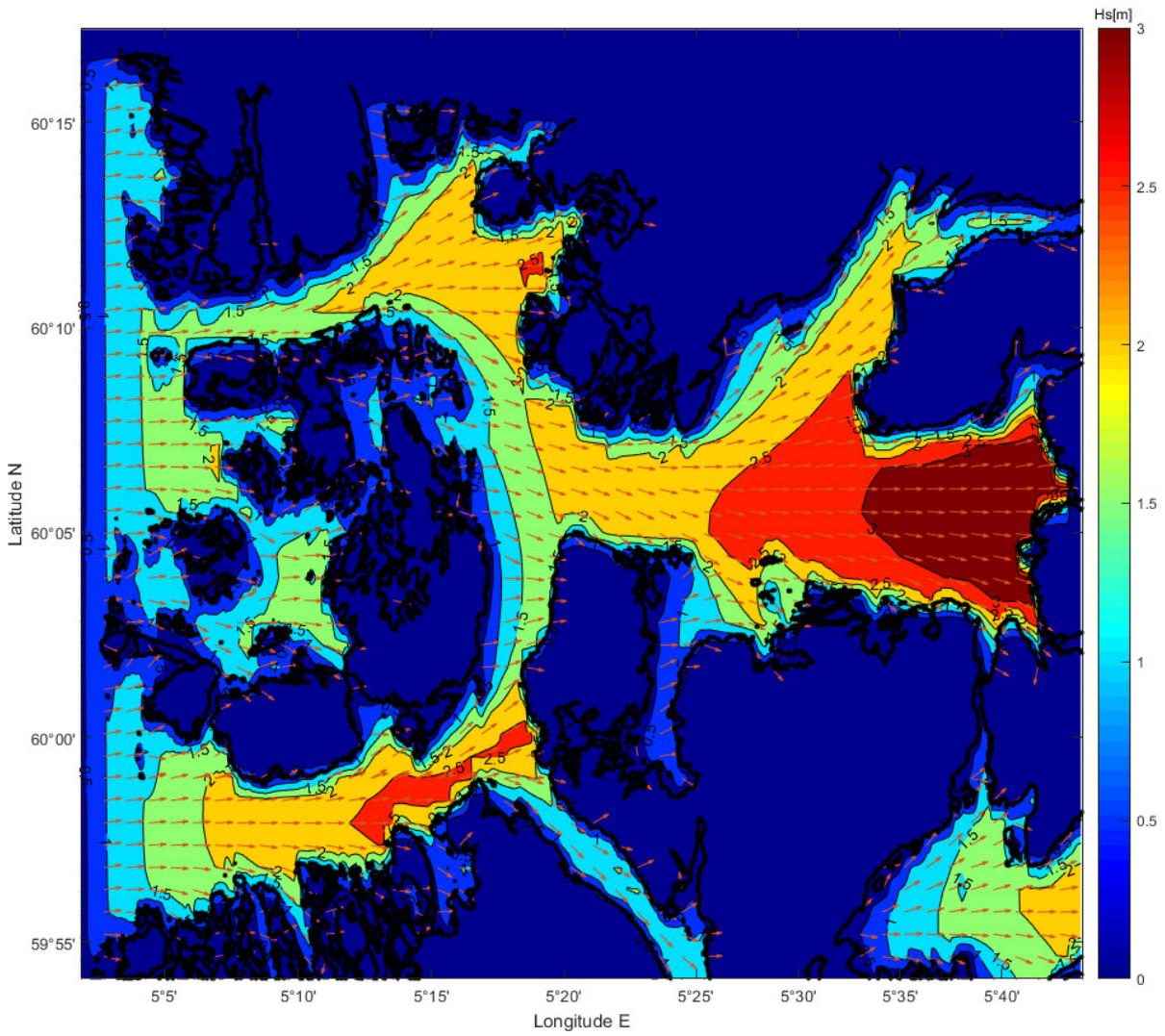

Figure 6-8 Bjørnafjord- Hs map for constant wind of 33 m/s input over the total area. Wind direction DIR= 1°.

The wind generation is the dominant forcing mechanism responsible for the waves at the bridge locations. This fact inspires necessity for more extensive analysis of wind input directions and values. Due to a constricted geometry an analysis assuming most probable wind directions in the long fetch routes were conducted (**Chapter 6.5** and the additional cases).

Figure 6-9 show the results obtained for the pure wind sea developed due to wind blowing form the wester direction.

6.3.3 Total sea

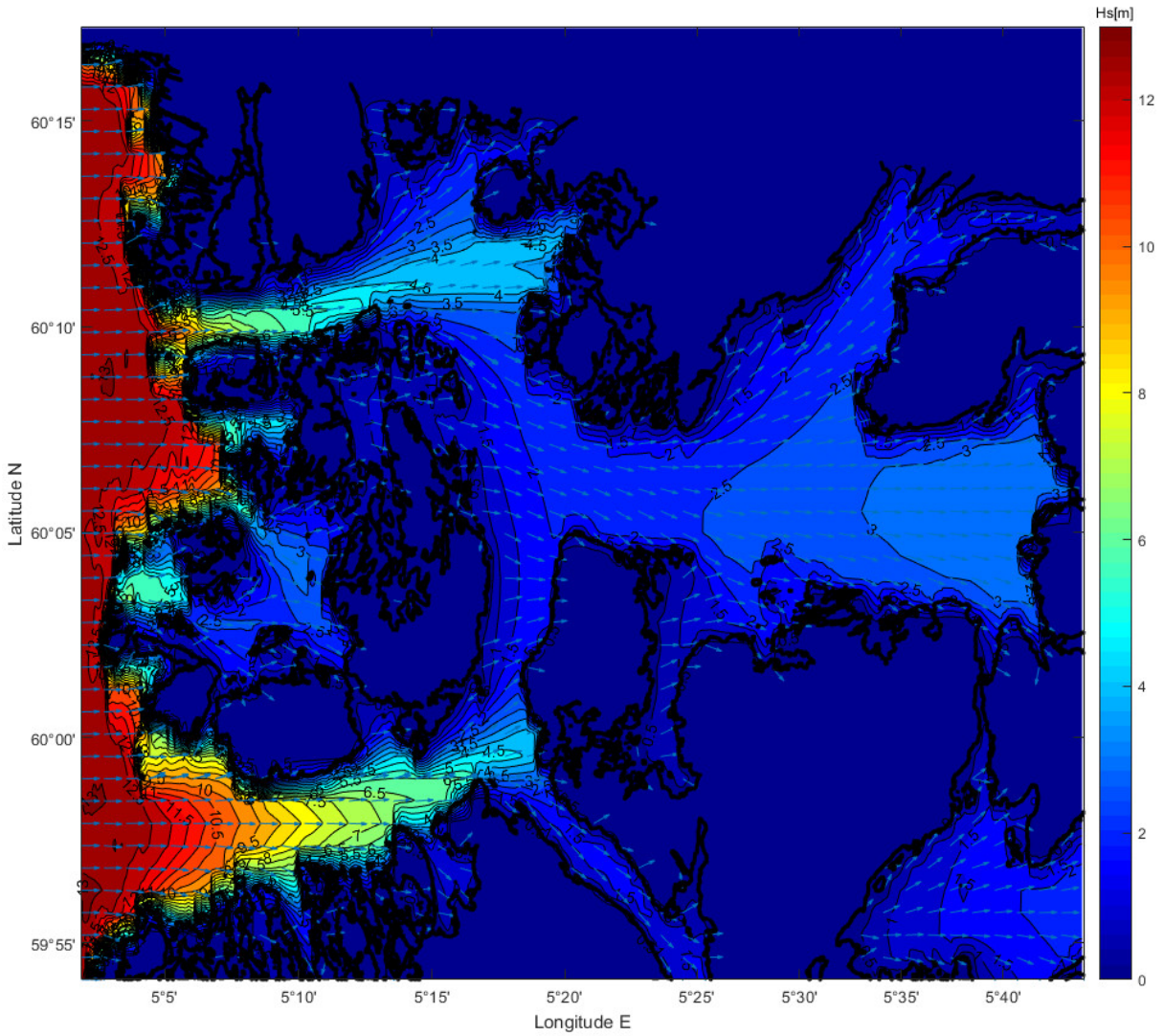

Figure 6-9 Bjørnafjord- Hs map for wave input if Hs=12.48m and Tp=14.08s DIR= 1° with constant wind of 33 m/s input over the total area. Wind direction DIR= 1°.

The incoming wave swells together with the wind generated waves provide the total sea conditions. The swell input is marginal for the condition of no wind input. The co-dependency described in **Chapter 3.1.1** however states that the initial roughness of the sea surface provided by swells will increase the wave generation at the eastern sector. The case shown in **Figure 6-10** is the most severe case of loading coming from the western sector and has been chosen as a basis for further analysis.

A comparison of the results obtained by Stefanakos (2015) and in this thesis are shown in **Table 6-5.**

The directions of propagation from SINTEFF report where transformed to the adopted coordinate system.

Table 6-5 Comparison of results obtained in the thesis with the results by Stefanakos (2015)

Target points		A2	A3	A4	B2	B3	B4
Results obtained by SINTEFF	H_s [m]	2.5	2.52	2.46	2.87	2.83	3.07
	T_p [s]	4.88	4.88	4.88	5.65	5.26	5.65
	θ [deg]	364	359	360	1	358	359
Results obtained in the thesis	H_s [m]	2.22	2.34	2.35	2.45	2.39	2.23
	T_p [s]	5.00	5.03	5.02	5.49	5.39	5.09
	θ [deg]	336	342	350	339	350	4
Relative difference	H_s [m]	-11.0%	-7.1%	-4.6%	-14.7%	-15.5%	-27.4%
	T_p [s]	2.5%	3.1%	2.9%	-2.9%	2.5%	-9.9%
	θ [deg]	-7.7%	-4.8%	-2.9%	-6.2%	-2.2%	1.4%

The comparison shows that the results obtained during the thesis preparation are lower than the ones obtained by Stefanakos. The difference may be a result of modelling parameters:
-different set of dissipation mechanism activated during SWAN computations or different values adopted for the governing parameters like for example the value assumed for bottom friction coefficient,
- the difference in the spreading coefficient assumed - the difference in the wave crest length,
- the difference in the precision of adopted grids (SINTEFF grid size varies for different runs between 230m and 90m whereas the final results obtained in the thesis adopt the mesh size of 75m by 75m for the computational, bottom and output grid).
The biggest difference between Stefanakos approach and the one realized in this thesis is the modelling methodology. In the SINTEFF report the model was executed as a number of nested runs (3 different steps with a different grid for each step). The information about the nesting realization, control of the transfer of information, between the runs – especially in regard to the 2D spectra input/output as well as the sensitivity analysis for changing grid resolutions was not available to the thesis author.

The realization of the model in this thesis was done as a single model with the coverage of the whole fjord area. This solutions provides (private assumption of the author) a better coverage and transfer of information in the side-ends of the directional spectra.

Further analysis and more data concerning the input parameters needs to be gathered for full comparison of models and the modelling methodology.

6.3.4 Analysis of the influence of the energy dissipation processes on the total sea

An analysis of the influence of different dissipation mechanics was done for the three routes specified in **Figure 6-1.**

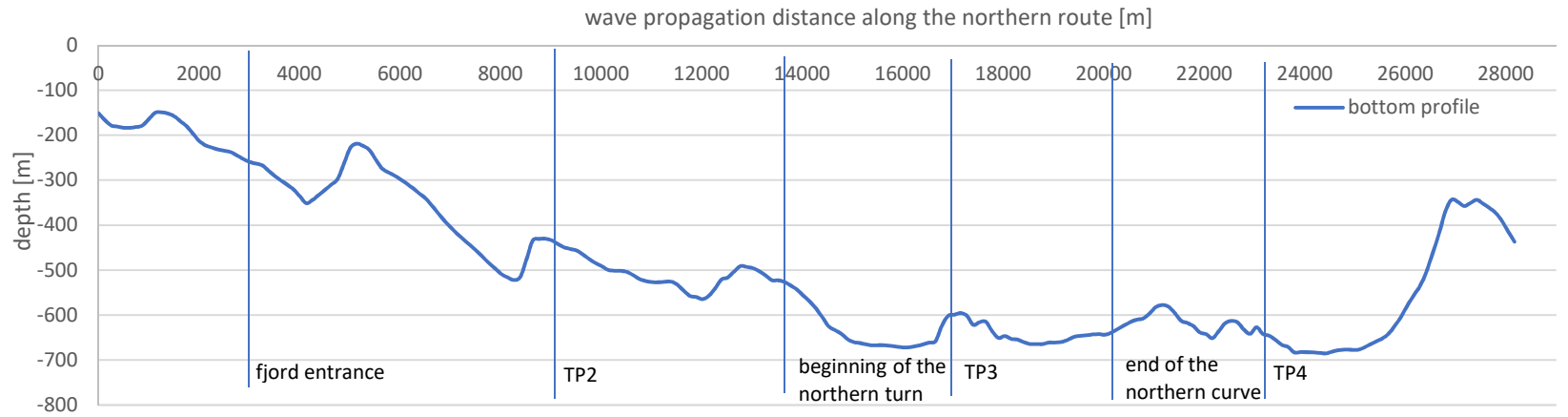

Figure 6-10 Depth profile of the northern route – inlet to the Bjørnafjord (yellow curve on Figure 6-1).

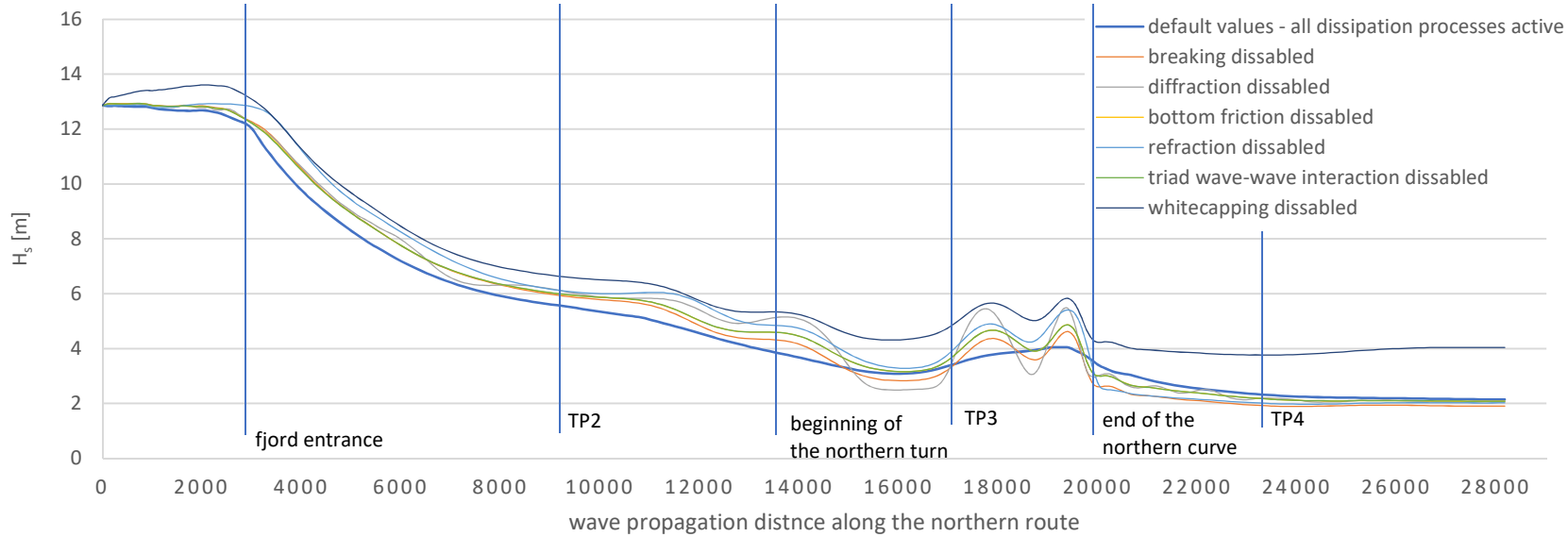

Figure 6-11 Significant wave height development along the northern route in respect to the dissipation processes

Figures 6-12 and 6-13 show the bottom profile and the evolution of significant wave height along the northern route. The most prominent dissipation mechanism throughout the route is white capping. This is due the high wind input blowing over the domain.

The figure illustrates the steady wave propagation from the offshore sector towards the fjord entrance. The significant wave height is constant due to wind generation in the deep water conditions and the white capping mechanism staying in balance. The influence of all other dissipation mechanisms is constant and laying in a similar range.

At the fjord entrance the refractions influence increases. This is due to introduction of the sides of the channel. Near the 12th kilometre the participation of single mechanism in total energy dissipation begins to shift as the wave field begins to 'feel' the incoming turn.

At the curve beginning we see a high impact of diffraction. The diffraction term is both negative and positive as it is responsible mainly for the directional shift. The investigation is conducted in the midline of the fjord which means that the line of investigation is also bending. The effect of diffraction – the dispersion of the wave rays first result in the lower amplitude and with the dispersed wave rays crossing the line of investigation again, they produce a positive influence on the wave amplitude. The investigation line crossing the wave field two times at a different angle of income seems to be the main reason for the turbulence visible in the section of the plot corresponding to the turn.

At the end of the northern route with the situation returns to the wind sea generated state. The influence of refraction is smaller than in the fjord entrance due to bigger width of the fjord cross section.

Figure 6-13 and 6-14 show the situation at the southern route. Due to a big radius of the turn, the arcing of the route does not have such an abrupt effect on the dissipation. The problem of the turbulences in the observations caused by the investigation line crossing wave rays twice is not present

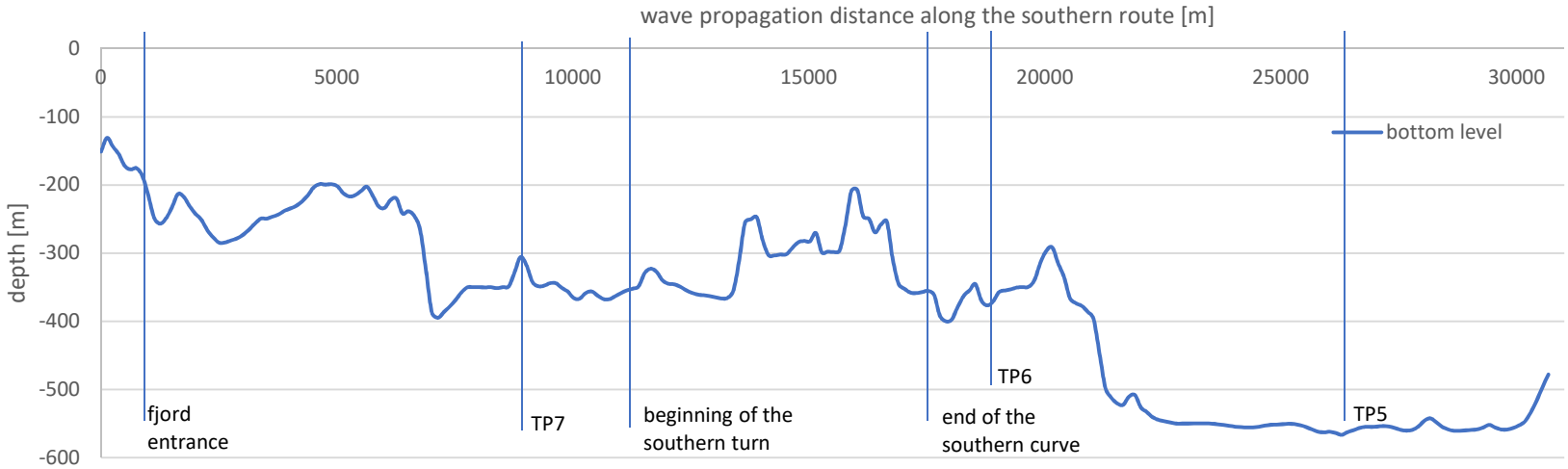

Figure 6-12 Depth profile of the southern route – inlet to the Bjørnafjord (purple curve on Figure 6-1).

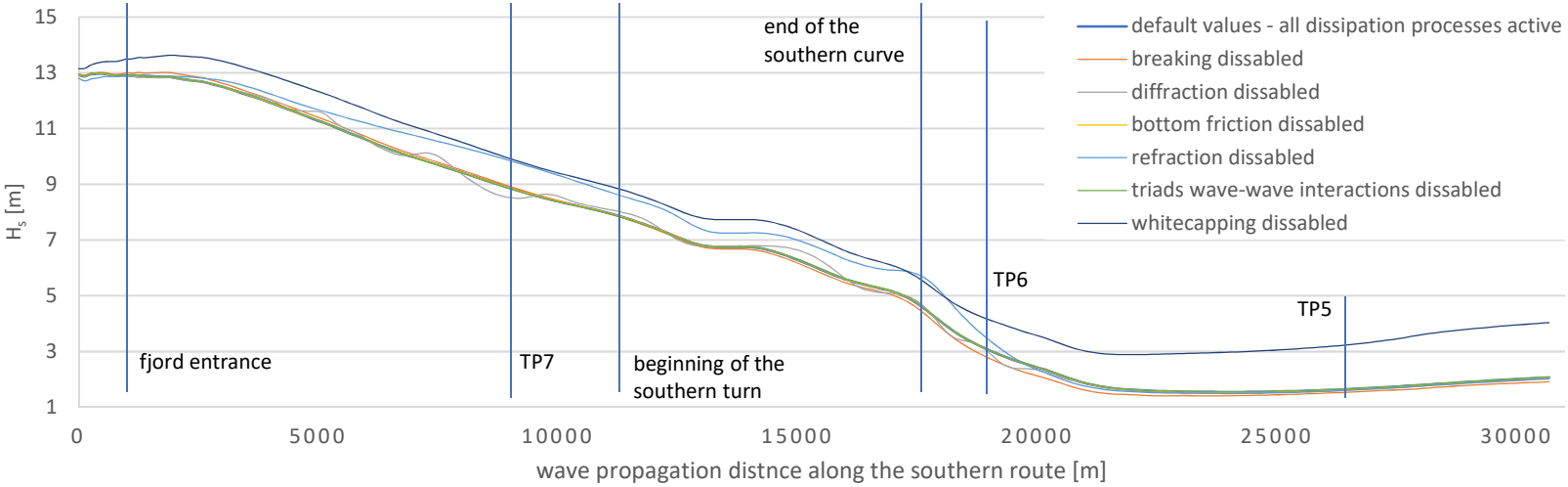

Figure 6-13 Significant wave height development along the southern route in respect to the dissipation processes

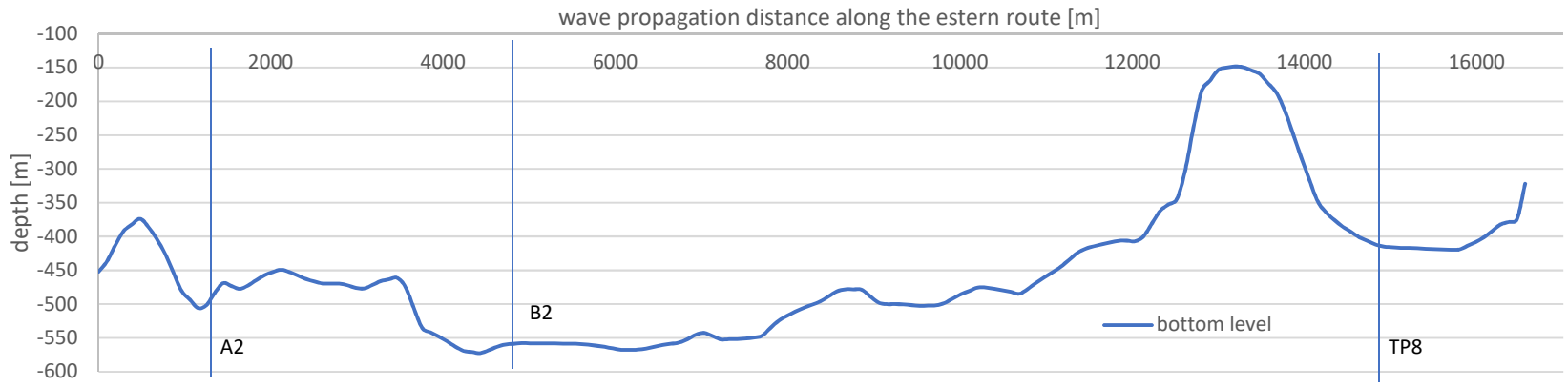

Figure 6-14 Depth profile of the eastern route – eastern sector of Bjørnafjord (green line on Figure 6-1).

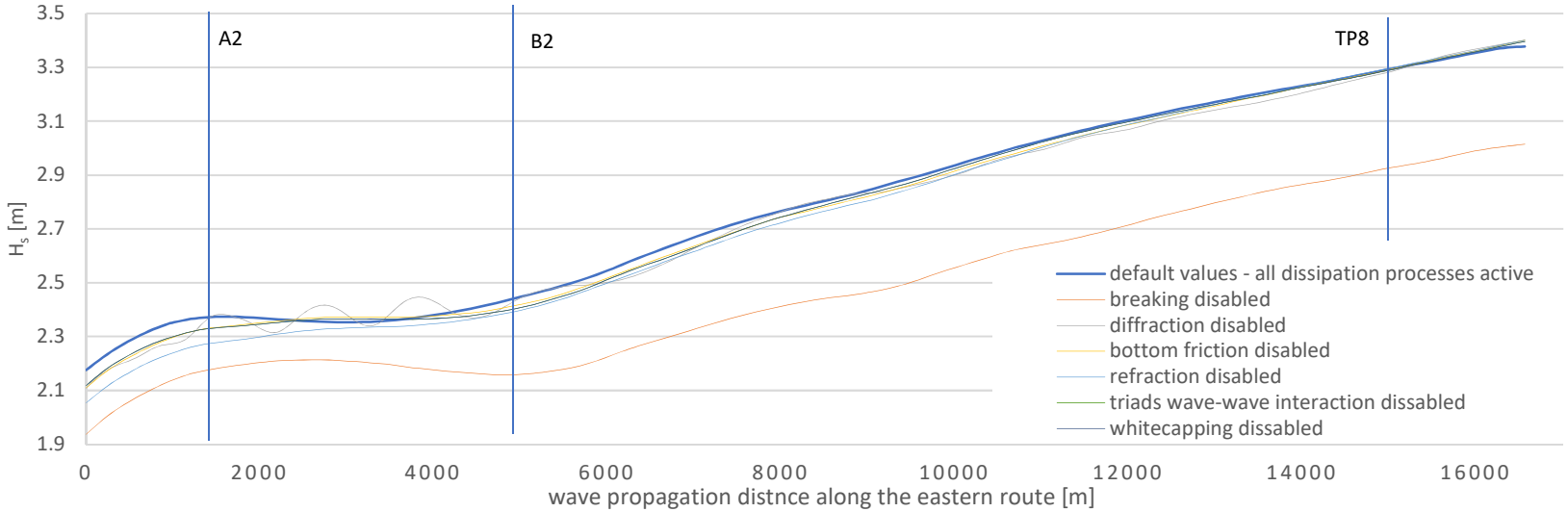

Figure 6-15 Significant wave height development along the eastern route in respect to the dissipation process

Figures 6-15 and 6-16 showing the eastern route show the development of the wind sea in deep water. The near shore dissipation effects show little influence on the midline of a 5 kilometre width and 400 meters deep basin.

The deactivation of breaking mechanism in SWAN resulted in an unrealistic situation where breaking generates wave energy. The obtained data is surprising as all three routes were analysed based on the same run in SWAN and the results seem reasonable for the norther and southern approach. The occurrence of this result needs to be further investigated and the probable error eliminated.

6.3.5 Wind sea analysis for the fjord from the eastern direction

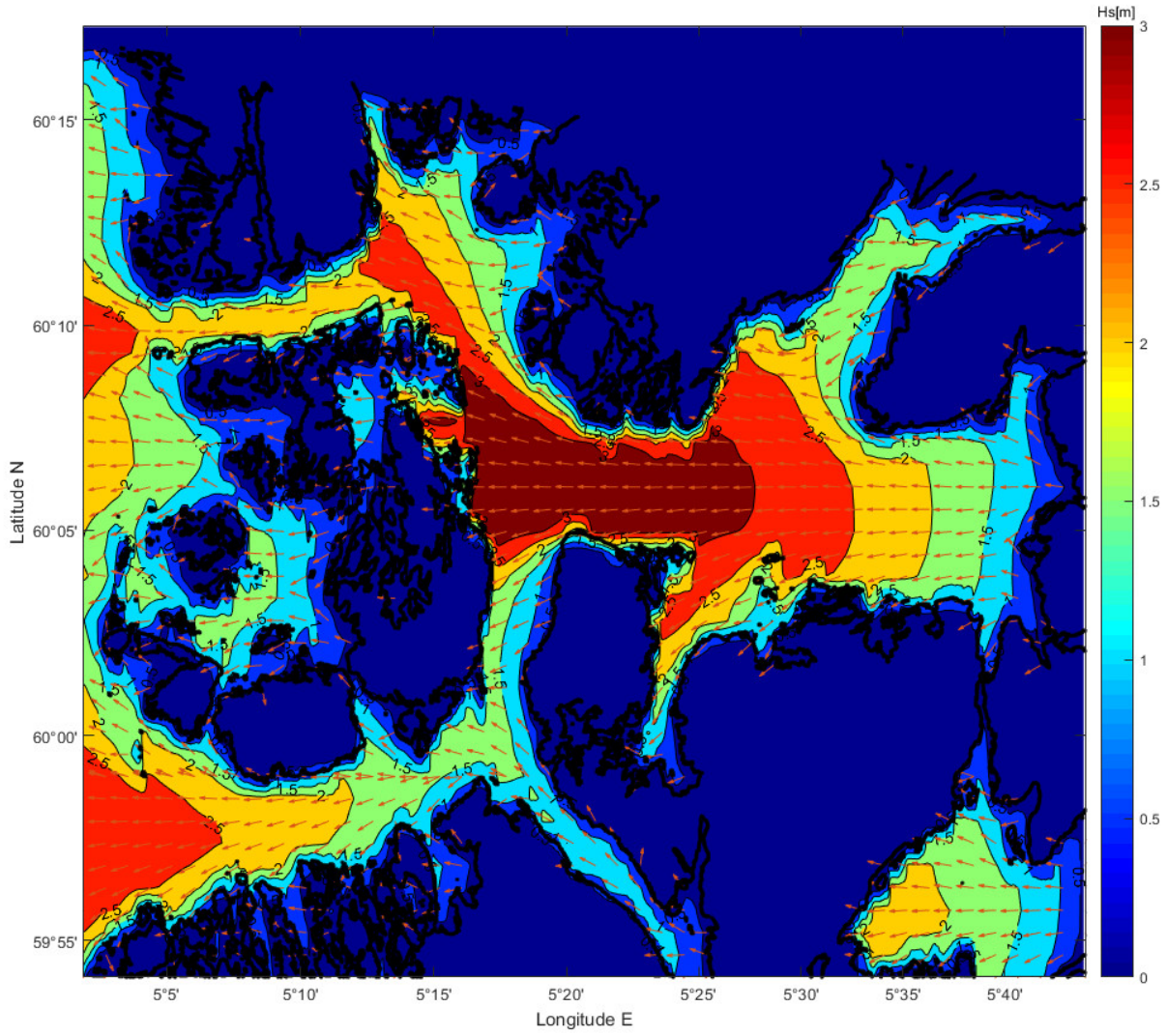

Figure 6-16 Bjørnafjord- assessment of the eastern sector. Wind velocity 35 m/s DIR=180° blowing over the whole area.

An analysis after Stefanakos (2015) were adopted to investigate the influence of wind incoming from the eastern sector. The fetch is longer in this situation (with regard to the bridge position) and thus the developed wind sea can produce higher values for the significant wave height. The problem connected

to such an analysis is to properly assume the sea state when the highest winds begin to blow. The assumption is that there is an pre-existing wave field at the beginning of the highest wind weather although modelling of such a situation and adopting proper values for wave characteristics is a task connected to high uncertainty.

The approach taken by Stefanakos in the SINTEFF report is based on an arbitrary chosen values (based on authors experience) of Hs=0.2 m for a Tp=4.0s forcing at point TP8 form the eastern direction. This approach needs to 'cut' the model at the TP8 line to introduce a water boundary for input of waves. The data on the depth and wind history from the area laying eastwards from TP8 is lost and replaced with the approximation of incoming significant wave height modelled. The assumptions seems reasonable but still show a number of uncertainties and show that the problem at hand need further research.

The approach adopted in this thesis is slightly different. The analysis of the eastern sector wind input was done separately under two (seemingly conflicting assumptions):

1) that the wind generation process in SWAN can calculate the proper fully developed wind sea state in an stationary run, based on the total information about the bathymetry and the fetch range for the closed basin (the time period for which the generation effects is being calculated needs to be controlled for stationary and nonstationary runs and a sensitivity analysis needs to be conducted).

2)that some wave field is existing when high wind approaches. The assumption is that it exist over whole area of the basin. This situation is modelled by introducing the initial sea state over the whole sea surface. This simplification here have been done with an unrealistic input of a constant wave condition for each point of the bathymetry. Such a situation will never occur due to a number of effects varying from water depth to wave propagation character. The assumption to overcome this uncertainty is that the sea state of Hs=0.2 m and for a Tp=4.0s is feasible for every point over the bathymetry greed which is quite reasonable.

Figures 6-19 and 6-17 show the results for the first assumption for wind speed 25 m/s and 35 m/s respectively. **Figures 6-18 and 6-20** show the realisation of the second set of assumptions for wind speed 25 m/s and 35 m/s respectively.

Result comparison of the different approaches is show in **Table 6-5**.

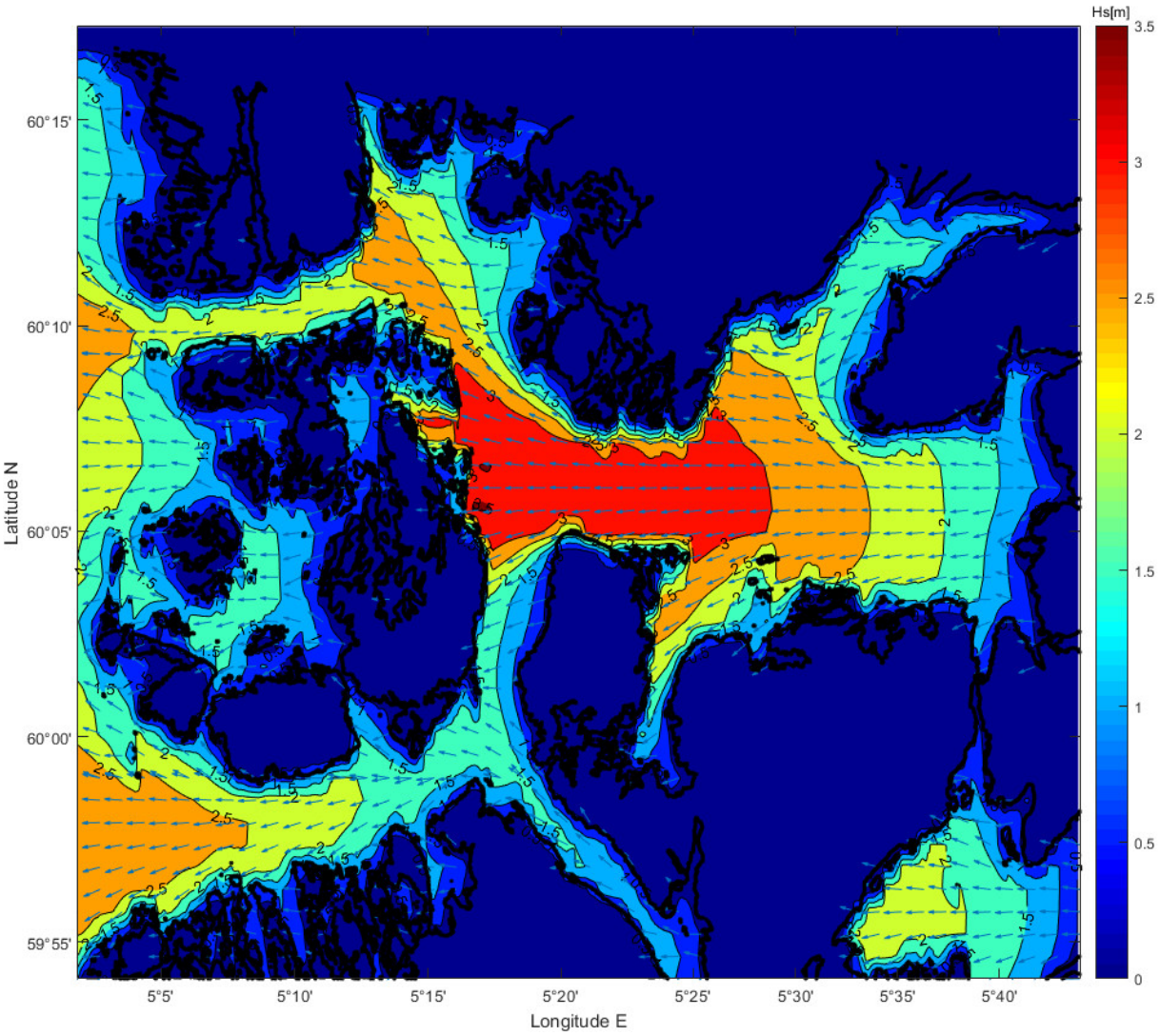

Figure 6-17 Bjørnafjord- assessment of the eastern sector. Wind velocity 35 m/s DIR=180° blowing over the whole area, initial wave input Hs=0.2 m Tp=4 s DIR=180° over the whole area.

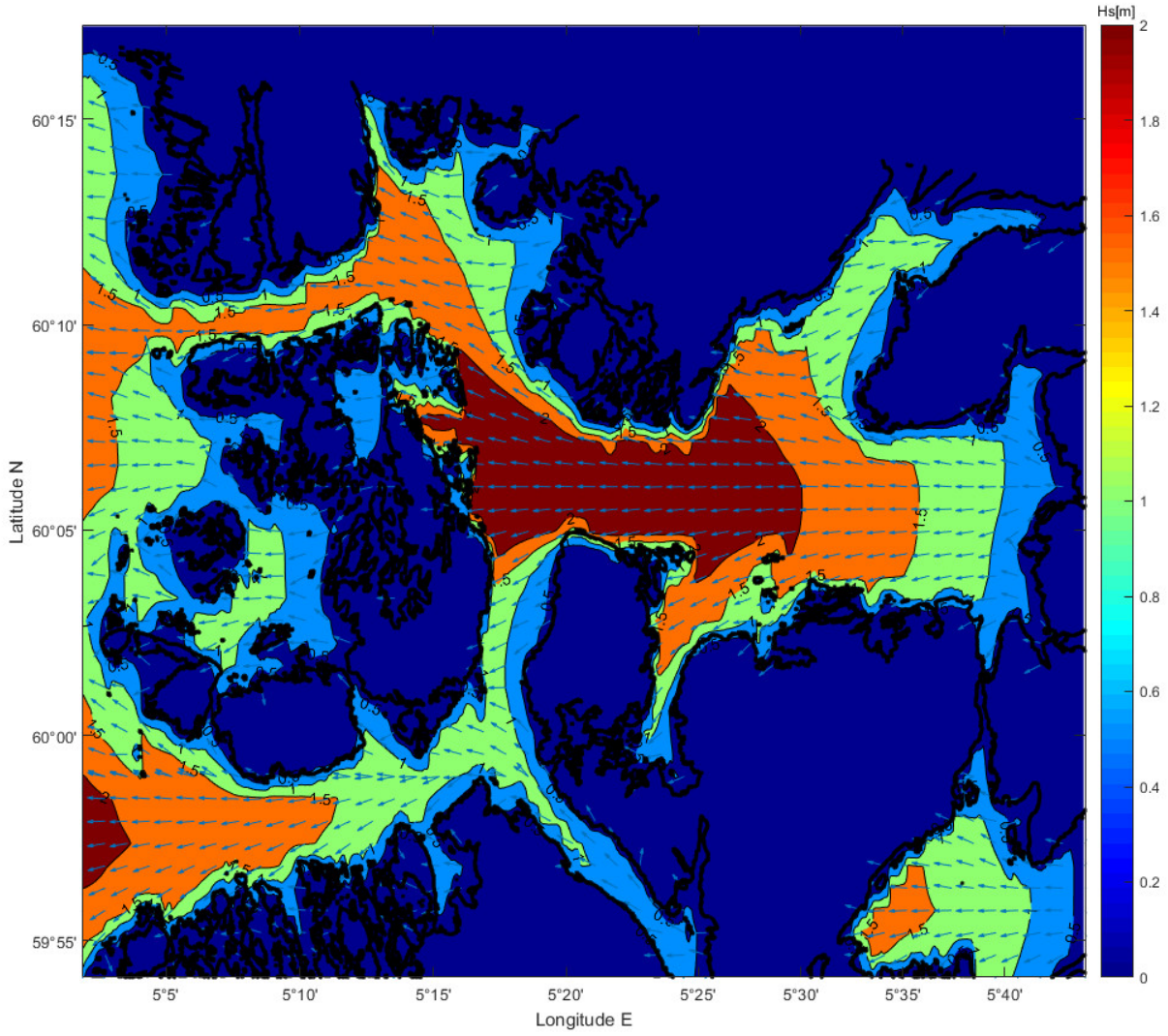

Figure 6-18 Bjørnafjord- assessment of the eastern sector. Wind velocity 25 m/s DIR=180° blowing over the whole area.

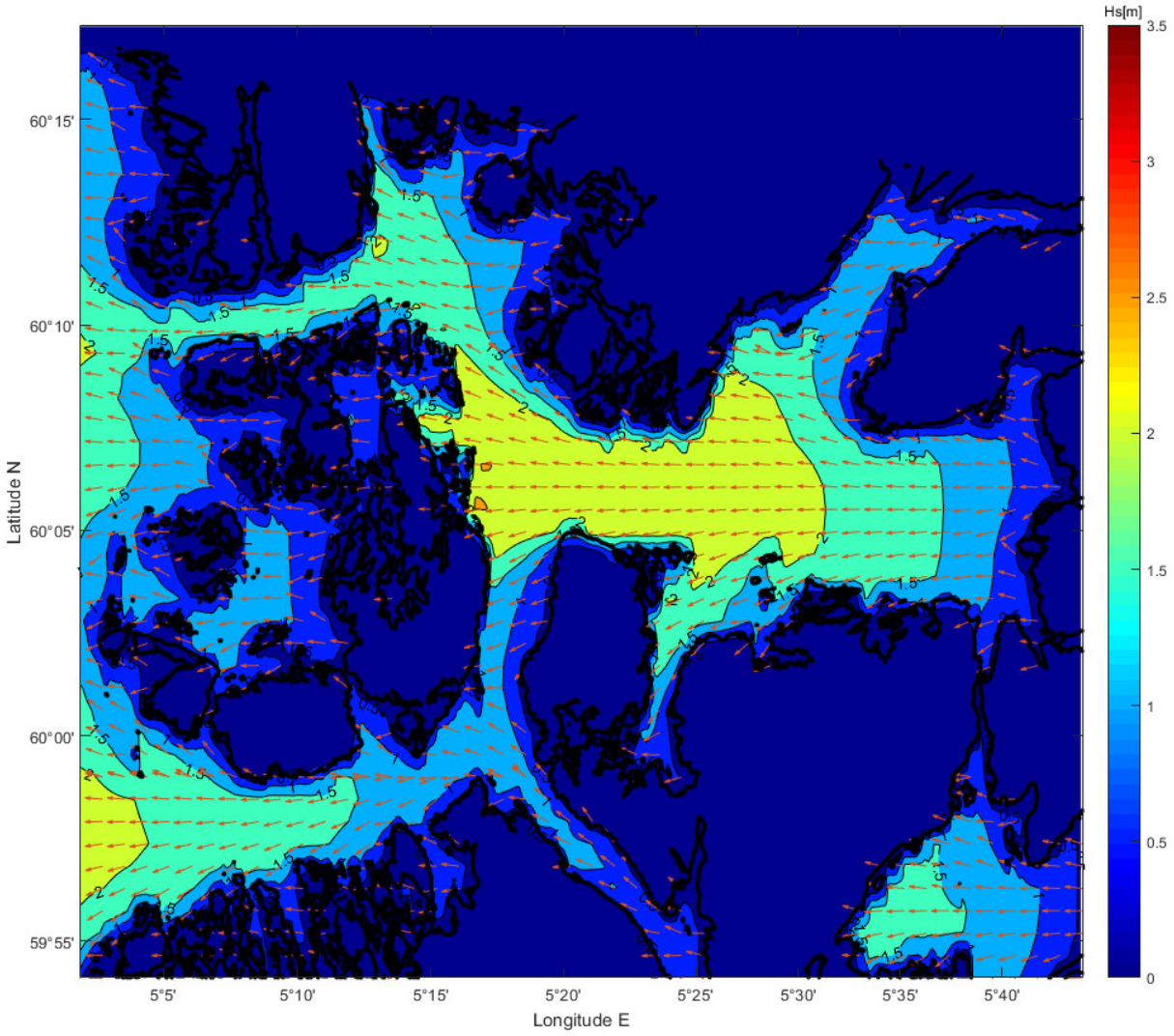

Figure 6-19 Bjørnafjord- assessment of the eastern sector. Wind velocity 25 m/s DIR=180° blowing over the whole area, initial wave input Hs=0.2 m Tp=4 s DIR=180° over the whole area.

Table 6-6 Comparison of the results obtained in the SINTEF REPORT (by Stafanakos,2015) and in the investigated runs for 25m/s wind.

Target point		A2	A3	A4	B2	B3	B4
Results obtained by SINTEFF for wave input at TP8	H_s [m]	2.02	2.01	2.03	1.91	2.03	2.01
	T_p [s]	5.08	5.43	5.43	4.67	5.08	5.08
	θ [deg]	174	180	185	177	182	184
Results with only wind over the whole fetch	H_s [m]	2.27	2.40	2.22	2.29	2.29	2.27
	T_p [s]	5.69	5.68	5.67	5.48	5.39	5.33
	θ [deg]	182	175	164	187	180	176
Results for the initial wave input over the whole area	H_s [m]	3.40	3.41	3.18	3.29	3.26	3.25
	T_p [s]	6.67	6.67	6.65	6.29	6.21	6.14
	θ [deg]	182	175	164	187	180	177

Results from table 6-5 show that the first assumption is false – SWAN dose not generate a fully developed wind sea in a stationary run. Possibilities for obtaining such results should be checked as this sea state will be probably the most extreme loading situation and thus a basis for the structural design.

Small differences between SINTEFF's results and the pure wind sea (second series of results) shows that both the methodology and the values assumed by Stefanakos are reasonable.

The increase in the Hs and Tp values with the initial wave excitation (the third series of results) show that wave conditions can assume higher values at the bridge position than the ones calculated in the runs with different input manner. However the quantitative values are very uncertain due to the amount of energy introduced to the model in the somewhat artificial way (the initial state input). The way for proper modelling of initial wave input should be further researched in connection to SWAN technical documentation and discussed at lengths with model developers.

6.3.6 Additional cases analysis.

Three additional cases where included based on the report of Lothe (2015). This analysis was introduced to compare STWAVE based results with the ones produced in SWAN. The analysis is also beneficial because it investigates other fetch generated wind conditions and allows to research wave conditions at bridge positions for forcing from the southern direction.

The cases assume the situation where the wind is blowing from the longest fetch distance in the north direction (Case 1- **Figure 6-22**) and the southern direction (Case 2 – **Figure 6-23**). The last case is adopted as a control case for the situation without wind.

The original results are shown in **Figure 6-24** and the results obtained during the thesis work are shown in **Table 6-7.**

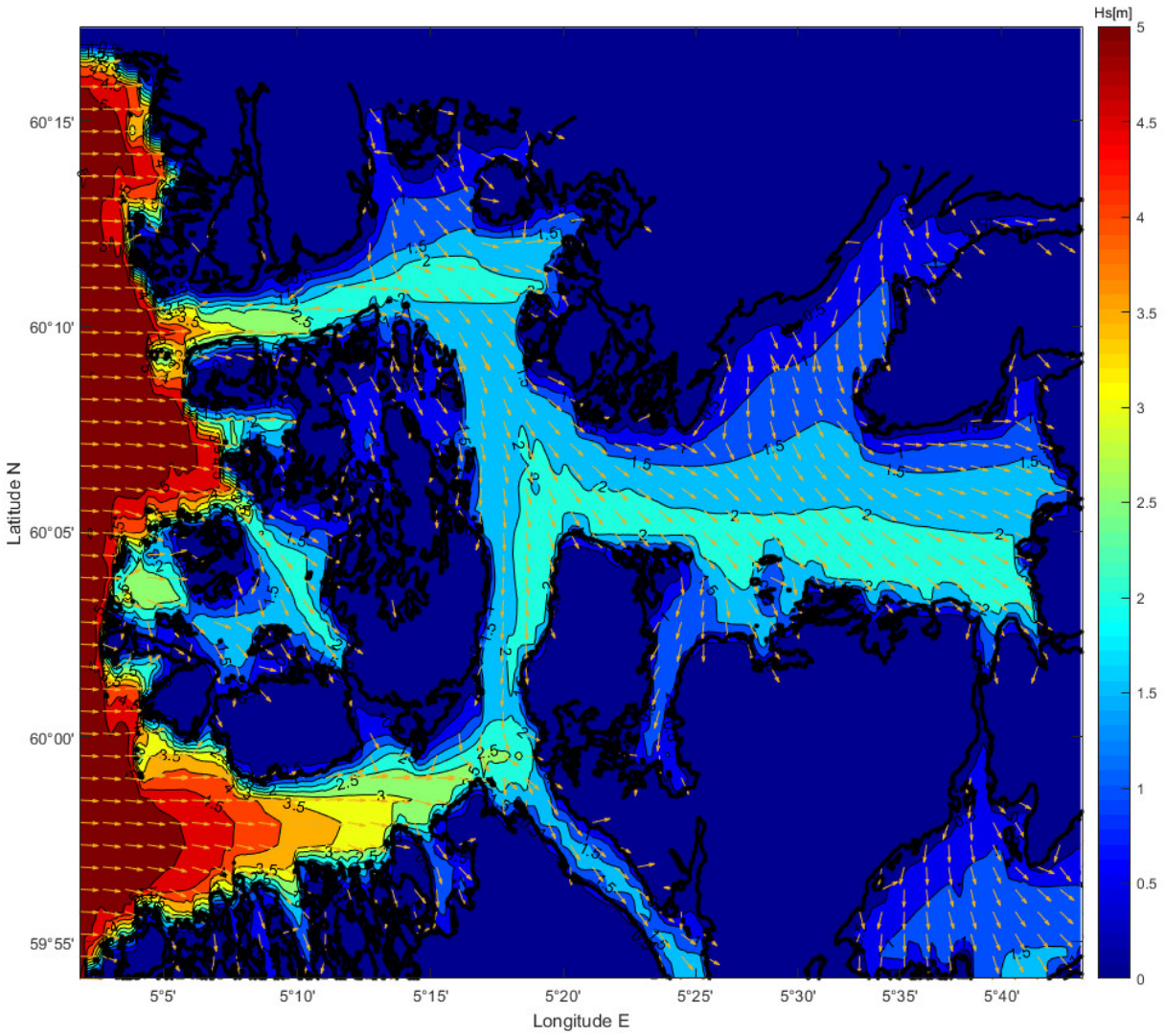

Figure 6-20 Case 1. Bjørnafjord- assessment of refraction. Wind velocity 25 m/s DIR=300° blowing over the whole area, wave input Hs=5.0 m Tp=12 s DIR=0° at the western boundary.

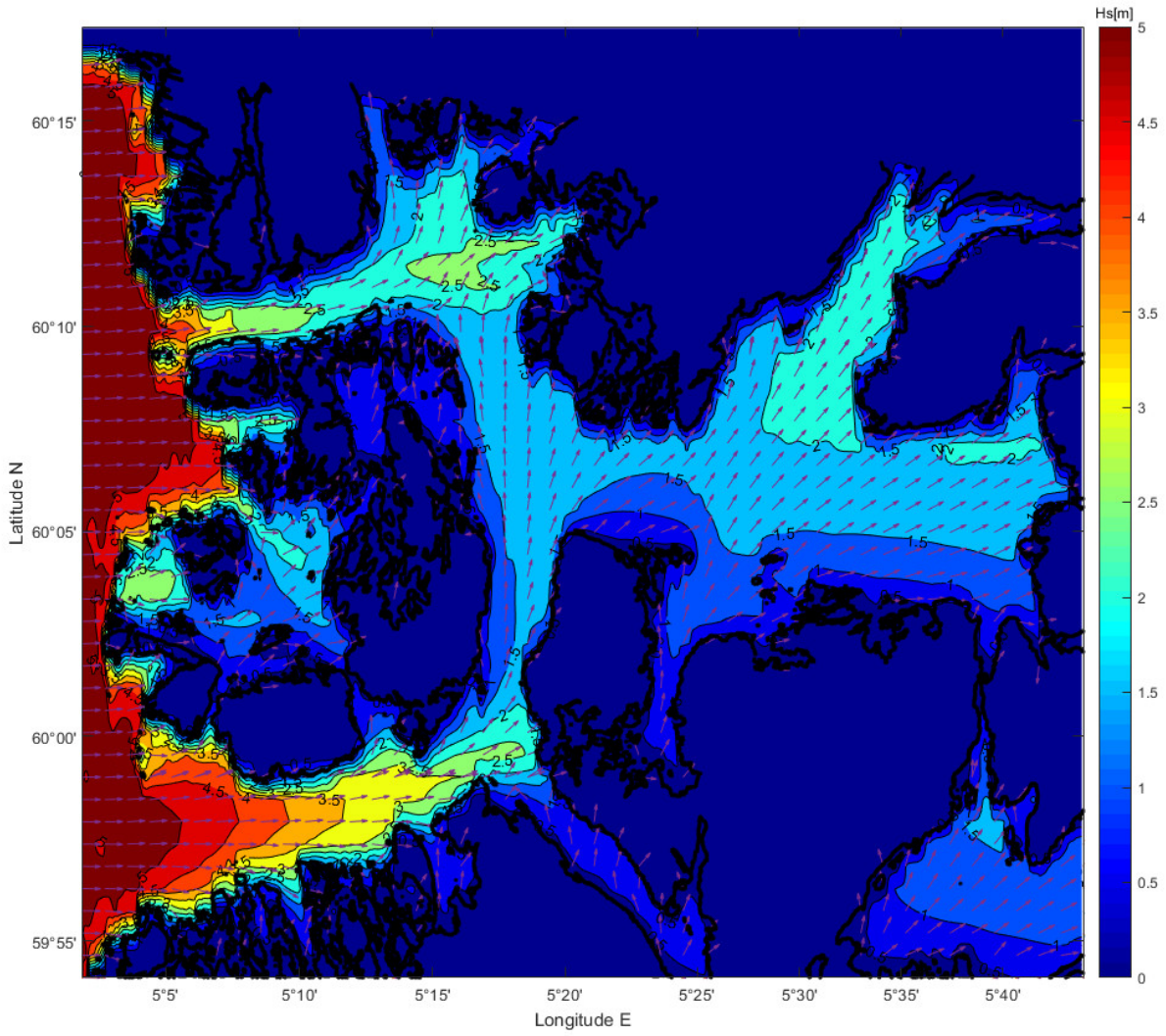

Figure 6-21 Case 2. Bjørnafjord- assessment of refraction. Wind velocity 25 m/s DIR=60° blowing over the whole area, wave input Hs=5.0 m Tp=12 s DIR=0° at the western boundary.

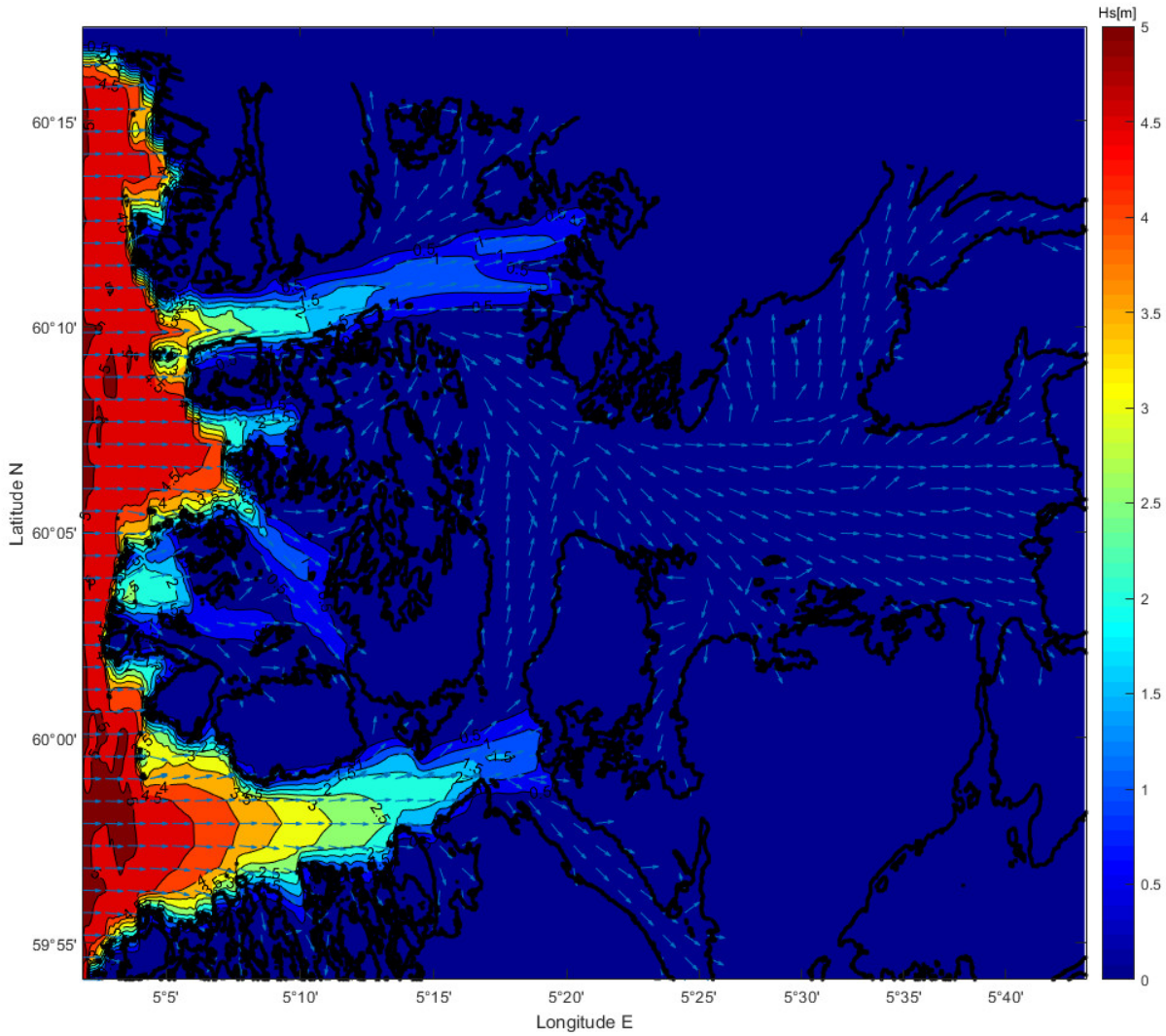

Figure 6-22 Case 3.Bjørnafjord- assessment of refraction. Wave input Hs=5.0 m Tp=12 s DIR=0° at the western boundary.

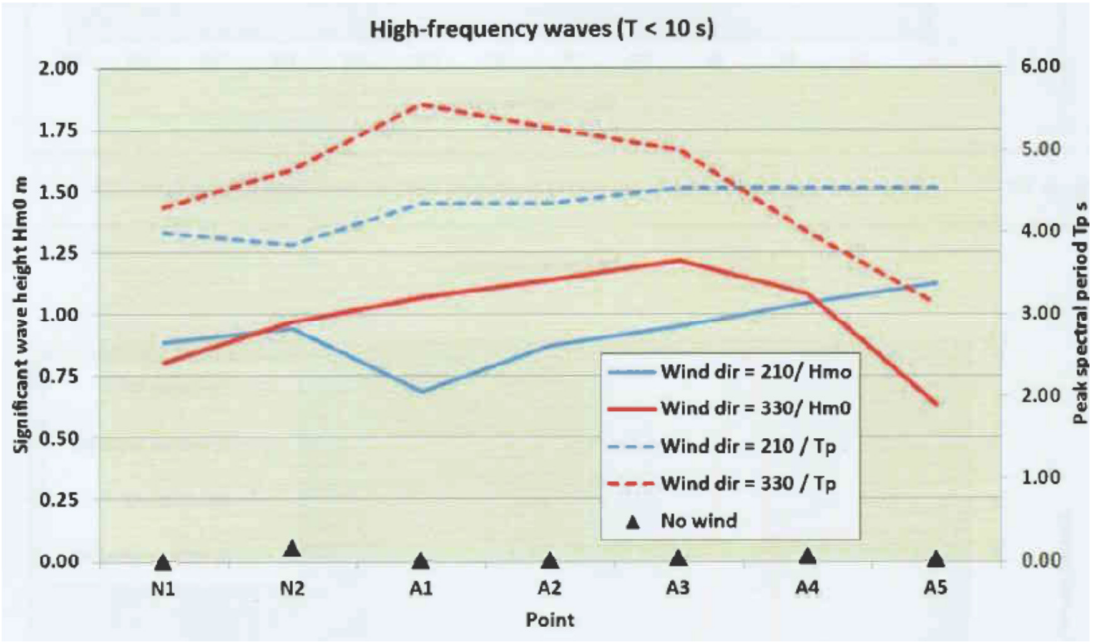

Figure 6-23 Results of the analysis performed by NORCONSULT Lothe (2015) p 46. The wind directions in the figure correspond: 210=60 in the thesis coordinate system and 330=300 in the thesis coordinate system.

Table 6-7 Results for cases 1 to 3 for the A bridge location.

Target location		A2	A3	A4
Case 1	H_s [m]	2.08	1.97	1.84
	T_p [s]	5.39	5.33	5.32
	θ [deg]	304	314	325
Case 2	H_s [m]	1.52	1.72	1.82
	T_p [s]	4.63	4.79	4.95
	θ [deg]	50.9	54.9	57.6
Case 3	H_s [m]	0.002	0.055	0.090
	T_p [s]	15.34	11.96	11.83
	θ [deg]	258	315	324

The result comparison is difficult to perform due to the division of the results in the original report to high and low frequency waves and data presentation. A preliminary assessment shows that results obtained in SWAN are higher than the ones obtained in STWAVE. The Full comparison of models would also require data on other parameters connected to the generation and dissipation processes and the realisation of the theories in the STWAVE software suite.

7 Discussion and propositions for future work

Research done shows that the correlation between the different generation an dissipation mechanisms is of a complex nature. Further investigations are required for a full comprehension of:
-wave field in a side constrained constant slope beach,
-influence of the inclination angle on the wave field while an oblique incident of wave towards a constant slope beach,
-physical processes influencing wave behaviour in a turning channel.
-reflection in a turning channel.

Furthermore an investigation of the best possible solution for bypassing an unnecessary number of interpolations while preparing calculations and visualizations of the wave field parameters based on modelling in SWAN.

The obstacles in the form of the terrain have also an influence on the wind field over the fjord. The estimations of the design wave conditions calculated in this paper where concluded with the assumption of a constant wind velocity propagating in a constant direction over the whole field which can be unrealistic.

The real situation at the fjord location can also differ from the wind calculated at the offshore position. The wind directions and velocities should be measured (with a proper size of the dataset) with the measuring points placing resolution sufficient for calculating input for the wave calculations. A model of the wind field can be prepared and included as an input in SWAN calculations.

Bottom friction coefficient and vegetation influence on the wave conditions research should be conducted. The assumed bottom friction for the Bjørnafjord case with the value of $c_f = 0.019\ m^2 s^{-3}$ is the advised value for non-sandy bottoms. The value taken for the calculations could be an underestimate in regard to the total friction generated by the underwater vegetation and bottom material roughness – vegetation can have a significant role in the Bjørnafjord area due to influence warm of the Gulf Stream current.

Bathymetry data with higher resolution should be gathered for the northern and the southern turn of the fjord inlets. A study of the wave field should be conducted for the mentioned places with programs that fully supports reflection calculations.

Further investigation of the initial sea state conditions set for the analysis of the east wind for the eastern sector should be conducted. An analysis should be conducted to discover the realistic assessment for the maximum wave height and its steepness possible for the eastern sector. A fetch based calculation of the wave field could be concluded to obtain this data. The investigation of the non-stationary and long-time analyses in swan should be done in respect to the mentioned problem.

Influence of the tide can produce local high velocity currents at some throating positions in the semi-enclosed basins. Such currents can have an influence the amplitude, frequency and direction change of a harmonic wave. The existence of such currents should be investigated and properly incorporated in the model.

Bibliography

DNV (2014). DNV-RP-C205. *Environmental conditions and environmental loads.*

Ellevset, O., (2014). *Norwegian coastal highway route E39.*Norwegian Public Roads administration.

Engebretsen, E.A, (2012).*Wave conditions for offshore wind turbine foundations in intermediate water depths.* Master thesis. Norwegian University of Science and Technology.

Holthuijsen, L.H., (2007). *Waves in oceanic and coastal waters.* Cambridge University Press.

Lothe,A. and Musch,O., (2015). *Bjørnafjord submerged floating tube bridge (No 12149-01).*Norconsult AS:Trondheim.

Lothe,A. and Musch,O., (2015). *E39 Bjørnafjord Crossing – Design wave data (No 5146702-01).*Norconsult AS:Trondheim.

Ngbeken, J. E,. (2016) *Assessing wave conditions in a Norwegian fjord*. Master thesis. University of Stavanger

Stefanokos,.C (2015). *Bridge across Bjørnafjorden. Metocean analyses*. (SINTEF F26636). SINTEF.

Svangstu, E. (2011). An investigation of wave conditions and wave induced loads for design of wind turbine foundations at 15 40m depth., Technical report, NTNU.

Svendsen, I. A. (2006). Introduction to Nearshore Hydrodynamics, World Scientific.

SWAN (2015). SWAN User Manual for SWAN Cycle III version 41.10AB, The SWAN team.

SWAN (2011). SWAN Scientifc and Technical Documentation for SWAN Cycle III version 40.85, The SWAN team.

Vegdirektoratet (2015). Statusrapport Ferjefri E39. Technical report Norwegian public roads administration.

Vennetti, D., (2012). Wave and tidal energy technology survey for ferry free E39 project (No.109). Norwegian public roads administration.